



THE HONG KONG
POLYTECHNIC UNIVERSITY

香港理工大學

Pao Yue-kong Library

包玉剛圖書館

Copyright Undertaking

This thesis is protected by copyright, with all rights reserved.

By reading and using the thesis, the reader understands and agrees to the following terms:

1. The reader will abide by the rules and legal ordinances governing copyright regarding the use of the thesis.
2. The reader will use the thesis for the purpose of research or private study only and not for distribution or further reproduction or any other purpose.
3. The reader agrees to indemnify and hold the University harmless from and against any loss, damage, cost, liability or expenses arising from copyright infringement or unauthorized usage.

If you have reasons to believe that any materials in this thesis are deemed not suitable to be distributed in this form, or a copyright owner having difficulty with the material being included in our database, please contact lbsys@polyu.edu.hk providing details. The Library will look into your claim and consider taking remedial action upon receipt of the written requests.

**FIBER RING LASERS AND ALL-OPTICAL SIGNAL
PROCESSING DEVICES FOR
WAVELENGTH-DIVISION MULTIPLEXING SYSTEMS**

QURESHI Khurram Karim

A thesis submitted in partial fulfillment of the requirements for the
Degree of Doctor of Philosophy

Department of Electrical Engineering,
The Hong Kong Polytechnic University

March, 2006



Pao Yue-kong Library
PolyU • Hong Kong

CERTIFICATE OF ORIGINALITY

I hereby declare that this thesis is my own work and that, to the best of my knowledge and belief, it reproduces no material previously published or written, nor material which has been accepted for the award of any other degree or diploma, except where due acknowledgement has been made in the text.

_____ (Signed)

QURESHI Khurram Karim (Name of student)

Dedicated to my parents

Abstract

The wavelength division multiplexing (WDM) optical fiber system is an important enabling technology to satisfy the requirements of bandwidth of today's information age. The main objective of this research project is to develop novel devices with the potential applications in WDM systems. In particular, novel semiconductor fiber ring lasers based on a recently introduced linear optical amplifier (LOA) and all-optical signal processing devices based on an entirely new type of highly nonlinear fiber as well as devices based on injection-locking in Fabry Pérot laser diodes are investigated.

We proposed and demonstrated a simple configuration of a widely tunable single wavelength semiconductor fiber ring laser and a multiwavelength semiconductor fiber ring laser based on a linear optical amplifier (LOA). In an LOA, a vertical-cavity surface-emitting laser is integrated, perpendicularly, along the entire length of the amplifier, serves as a ballast to provide a constant gain to the amplifier and helps to clamp the gain competition in a laser cavity. In case of a single wavelength laser, ultra-wide continuous wavelength tuning range of over 90 nm was achieved using a scanning Fabry Pérot filter. In addition a stable multiwavelength semiconductor fiber ring laser was also realized using F-P etalon. Thirty eight lasing lines were obtained with a fixed channel spacing of 0.8 nm, which is defined by the free-spectral range of the F-P etalon. Power stability of less than 0.15 dB during a 3-hour test for a single channel of the multiwavelength laser demonstrated the stability of this laser. A gain clamped SOA scheme is also realized using optical feedback. Using this scheme a stable multiwavelength semiconductor fiber laser was demonstrated.

In the second part of this research project, all-optical signal processing devices were investigated. An all-optical switch is a key component in high capacity optical fiber communication networks such as optical time division multiplexed and wavelength division multiplexed systems. In this study an all optical on-off switch based on FWM in only 1.9-m long Bismuth Oxide Highly Non Linear Fiber ($\text{Bi}_2\text{O}_3\text{-HNLF}$) was demonstrated. The principle of the switch is that in the presence of the control signal, i.e., when the control signal is ON, the data will be transmitted, whereas when the control signal is OFF, the data signal will be blocked. The switch has a fast response time and high ON/OFF switching ratio.

Robust optical pulse trains sources, capable of producing width-tunable pulses with high repetition rate and high extinction ratio are important sources for many applications, such as all optical sampling, ultrafast spectroscopy, all-optical reshaping and high speed optical communication. In this project width tunable train pulses were generated by employing FWM effect in 1.9-m of $\text{Bi}_2\text{O}_3\text{-HNLF}$. The scheme involves generating two optical pulse trains at different wavelengths, combining them in a short length HNLF to generate FWM and then varying the delay between the pulse trains. Due to FWM process the product term carries an optical pulse whose width depends on the overlap time between the two original pulses. The high nonlinearity of the fiber also compresses the pulsewidth of the generated pulse.

The all-optical AND operation is one of the fundamental logic gates because it provides on-the-fly bit level functions such as address recognition or packet header

modification, binary adders and binary counters. In this study an all-optical AND gate working at 10 Gb/s was implemented using the FWM effect in 1.9-m of Bi₂O₃-HNLFF for NRZ signals. No additional input beam such as clock signal or continuous wave light other than input signals is used which is required in other schemes.

All-optical signal quality monitoring system (SQMS) is crucial for fault management, quality of service, optical layer protection and eye monitoring for adaptive polarization-mode dispersion (PMD) compensation in high capacity transport and access networks. Typical error monitoring schemes require expensive optical–electrical conversions and high speed large-scale integration chips. Real-time all-optical signal quality monitoring is useful for future all-optical networks as the generated optical error signals can be forwarded to the corresponding network node for processing using the same network. It is, however, difficult to implement a real-time error-monitoring system all-optically because of the limited signal processing capabilities of current all-optical devices. In this study we proposed an all-optical signal quality monitoring system at 10 Gb/s using two multi-wavelength mutual injection-locked Fabry P rot laser diodes (FP-LDs) without employing any high speed electronics. Relatively complex logic operations, two threshold, one NOT, and one NOR, functions are realized. The proposed SQMS uses two threshold levels to determine the error bits. The resulting optical indicator signal, sometimes known as the “pseudo-error” signal, identifies both the positions and the durations of the error bits.

ACKNOWLEDGMENTS

I would like to express my sincere gratitude to my chief supervisor, Prof. Hwa-Yaw Tam, for his invaluable guidance and encouragement throughout this project. I am also very grateful to my co-supervisor, Prof. P. K. A. Wai, for his useful advice and encouragement during my research at The Hong Kong Polytechnic University.

I would also like to take this opportunity to thank my colleagues, and especially Dr. W. H. Chung and Dr L. Y. Chan for their collaboration and technical support. I would also like to thank Dr Liu Heliang, Dr. Xu Lixin, Mr Wang Shaohao, Mr Fu Hongyan, Dr Hoi, Mr Ju Jian, Dr Y. L. Hoo, Mr L. F. K. Lui for their support and suggestions.

I also wish to thank my parents from the core of my heart, for providing me the moral support during all these years.

Finally, I greatly appreciate the Hong Kong Polytechnic University for awarding the International postgraduate scholarship and the Asahi Glass Corporation Ltd., Japan for providing the bismuth-based highly nonlinear fibers.

Contents

Certificate of originality	i
Dedication	ii
Abstract	iii
Acknowledgments	vi
1. Introduction	
1.1 Motivation for the Project	1
1.2 Original Contributions	4
1.3 Organization of thesis	5
1.4 Flow chart of thesis	8
1.5 Publications	9
2. Literature review of semiconductor fiber ring lasers	
2.1 Background review of single frequency SFRL technologies	13
2.2 Background review of multiwavelength FRL technologies	15
2.3 Chapter Summary	24
References	25

3. Semiconductor fiber ring lasers	
3.1 Linear optical amplifier	27
3.2 Widely tunable single frequency semiconductor fiber ring laser	32
3.2.1 Experimental results	33
3.3 Stability conditions for multiwavelength generation	37
3.4 Multiwavelength semiconductor fiber ring laser using LOA	41
3.4.1 Experimental results and discussions	42
3.5 Gain clamped SOAs	49
3.5.1 Gain clamping techniques	50
3.5.1.1 Gain control using current injection	50
3.5.1.2 Gain control by optical feedback	54
3.5.1.2.1 Using CWDM couplers	54
3.5.1.2.2 Using circulators	62
3.5.2 Switching transients in a multiwavelength scenario	66
3.5.2.1 Experiments and discussions	66
3.6 Multiwavelength generation using a gain clamped SOA	73
3.7 Chapter summary	77
References	78
4. Overview of optical signal processing technologies	
4.1 SOA nonlinearities	82
4.1.2 Cross gain modulation (XGM)	82
4.1.3 Cross phase modulation (XPM)	84

4.1.4	Four wave mixing (FWM)	86
4.2	Fiber nonlinearities	86
4.2.1	Self phase modulation (SPM)	88
4.2.2	Cross phase modulation (XPM)	89
4.2.3	Four wave mixing (FWM)	90
4.2.4	Stimulated scattering effects	93
	References	95
5.	Highly nonlinear Bismuth oxide fiber based devices	
5.1	Introduction	97
5.2	Bismuth oxide based highly nonlinear fibers	99
5.3	All-optical on-off switch	103
5.3.1	Experiments and discussions	106
5.4	Tunable pulsewidth generator	114
5.4.1	Theory	116
5.4.1.1	Model	116
5.4.1.1.1	Effect of initial pulse shape parameters on evaluation results	119
5.4.1.1.2	Tunable pulse generation at 40 GHz	121
5.4.2	Experiments and discussions	125
5.5	All-optical AND gate	129
5.5.1	Experiments and discussions	131
5.6	Chapter summary	138

References	139
6. Injection locking in Fabry Perot laser diodes	
6.1 Introduction	143
6.2 Applications of injection locking	147
6.3 Semiconductor laser diodes	148
6.4 Characterization of a Fabry Perot laser diode	152
6.4.1 Light(L)~Current (I) relationship of a semiconductor laser	152
6.4.2 Effect of operating current on FP-LD	154
6.5 Single mode injection locking in FP-LD	156
6.5.1 Effect of wavelength detune on injection locking threshold power	164
6.6 Optical bistability and hysteresis	166
6.7 Chapter summary	171
References	172
7. All-optical logic gates and a signal quality monitoring system	
7.1 Introduction	177
7.2 Two mode injection locking	182
7.3 All-optical NOT gate with variable threshold	183
7.3.1 Experimental results and discussions	187
7.4 All-optical NOR gate	190
7.4.1 Experimental results and discussions	192

7.5	All-optical signal quality monitoring system	195
7.5.1	Operation principle	196
7.5.2	Experimental results and discussions	198
7.6	Chapter summary	207
	References	208
8.	Research summary and future work	
8.1	Research summary	217
8.2	Future work	220

Chapter 1

Introduction

1.1 Project motivation

Our present world appears to be shrinking day-by-day due to rapid developments in communications and information technology. In the past, telecommunication networks carried voice signals rather than data signals. Today is a digital era and many people are interested in browsing the Internet with broadband services. At the same time, other bandwidth-demanding services such as IP phone, video-on-demand and real-time streaming are burgeoning rapidly. The combination of more users and more services creates the need for transmission technology to carry more information to further distances at a higher bit-rate. The telecommunications network previously optimized for voice traffic cannot handle the explosion of such data traffic. In addition to this explosion in consumer demand for bandwidth, the nature of the traffic itself is becoming more complex. Traffic carried on a network can be circuit based (TDM voice and fax), packet based (IP), or cell based (ATM and Frame Relay).

Consequently, there is an increasing proportion of delay sensitive data, such as voice over IP and streaming video. Therefore, other than coping with enormous bandwidth demand, service providers must provide flexible systems which can serve the diverse requirements of different new services as well as being compatible with different protocols.

In order to fulfill the increasing demand for bandwidth, a wavelength division multiplexing (WDM) optical system is an attractive key technology to invariably reduce the cost of bandwidth. Furthermore, the WDM system provides an economical means to upgrade its capacity to handle higher bit-rates. Recently, the number of wavelength channels in a WDM system has increased significantly. Large inventory of laser sources operating at ITU wavelengths are stored to ensure minimal down time of the service. The most secure WDM system is “one-to-one” protection, which means that a spare laser is kept for each channel wavelength. This is not practical due to the overwhelming cost and large inventory volume.

An economical and practical approach is to stock broad wavelength-tunable lasers instead of fixed wavelength DFB lasers. A wavelength tunable laser source is now recognized as being essential for use in WDM systems. A single tunable laser can be used as spare for several wavelength channels thereby reducing system cost and simplifying the inventory management.

The multiwavelength laser sources are capable of providing multiple channels at once and each of them could be separately modulated. One device could replace a complete array of discrete lasers, thereby reducing the packaging cost and the management overhead considerably.

As the switching nodes in the optical networks acquire more optical functions, it becomes desirable to achieve all-optical signal processing operations. The all-optical processing is especially attractive in the high speed core networks where opto-electronic conversion is avoided. The requirements are not for massive processing, but rather the possibility of simple optical processing at bit rates close to or beyond the bandwidth of the presently available electronics.

This thesis reports the results of an investigation of semiconductor fiber ring lasers (SFRLs) and multiwavelength laser sources to address the aforementioned problems faced by the current WDM systems. The objectives of this study include the broad wavelength tunability, multiwavelength operation at room temperature, and power stability of SFRLs. Experimental results showed that SFRLs should find potential applications in WDM systems. The second objective of this research study was to investigate various kinds of all-optical signal processing devices for the future all-optical networks. In this thesis, studies and experimental results on tunable pulsewidth generators, all optical on-off switches, all optical logic gates, and an

all-optical signal quality monitoring system (SQMS) are reported. The SQMS aimed to monitor amplitude jitters, has been developed with a view to improving the security and reliability of WDM systems and the future all optical networks.

1.2 Original Contributions

The major contributions of this research project are summarized below:

1. Development of a broad wavelength tunable semiconductor fiber ring laser using a linear optical amplifier as a gain medium. Over 90 nm of wavelength tuning range was achieved via a scanning Fabry-Pérot filter in the cavity.
2. Development of a multiwavelength semiconductor fiber ring laser using a linear optical amplifier as a gain medium. More than 38 lasing lines were observed with a channel spacing of 0.8 nm. By varying the loss in the cavity the laser could be tuned within 22 nm.
3. Development of all-optical devices based on a newly introduced bismuth oxide highly nonlinear fiber. An all-optical on-off switch, a tunable pulsewidth generator, and an all-optical AND gate were proposed and demonstrated based on FWM in only 1.9 m long Bi-HNLF.

4. Development of all-optical logic devices based on injection locking in a Fabry P erot laser diode. An all-optical NOT and NOR gates were proposed and experimentally realized using respectively, the dual and multimode injection locking principle in a dc biased Fabry P erot laser diode. An all-optical signal quality monitoring system was proposed and experimentally demonstrated using cascaded optical NOT and NOR gates.

1.3 Organization of thesis

The thesis documents the research that was performed during the investigation of all optical semiconductor fiber ring lasers, and all optical signal processing devices. It delineates the various phases of the experimental work, in addition to reviewing relevant literature that was acquired during the course of study. The thesis is organized as follows:

Chapter 2 covers the background literature review of single frequency tunable fiber ring laser and multiwavelength fiber ring lasers.

Chapter 3 introduces the linear optical amplifier (LOA) as an inhomogeneous gain medium and also proposes a widely tunable semiconductor fiber ring laser using LOA as a gain medium. Next a theoretical analysis regarding the stability conditions for stable multiwavelength generation is delineated. The experimental configuration

of the proposed semiconductor multiwavelength fiber laser is explained and the experimental results are discussed.

Chapter 4 reviews the all-optical signal processing technologies utilizing nonlinearities in semiconductor and fiber based devices.

Chapter 5 introduces a new type of nonlinear fiber called Bismuth based highly nonlinear fiber. The characteristics of this fiber are described. The design of an all-optical on-off switch, an all-optical tunable pulsewidth generator, and an all-optical AND gate is presented and the experimental results are discussed.

Chapter 6 introduces the injection locking technique in semiconductor lasers. The properties of a Fabry P erot laser diode under single mode injection locking are discussed and experimentally studied.

Chapter 7 presents the experimental work on the realization of all-optical logic gates, namely NOT and NOR gate. Later, these gates are utilized to implement an all-optical real time Signal Quality Monitoring System (BEMS).

Chapter 8 is dedicated to general conclusions and recommendations for further research works.

Since fiber ring lasers and all-optical signal processing devices are distinct topics, there research backgrounds and technology are dealt with in separate chapters instead of a single background introductory chapter. The background review of fiber ring

lasers is delineated in chapter 2 and the work done in this project is presented in chapter 3. The research backgrounds of all-optical logic devices are reported in chapter 4 whereas the works done in this project are described in chapter 5, chapter 6, and chapter 7. The flow chart depicting the organization of the thesis is shown in Fig.

1.1.

1.4 Flow chart

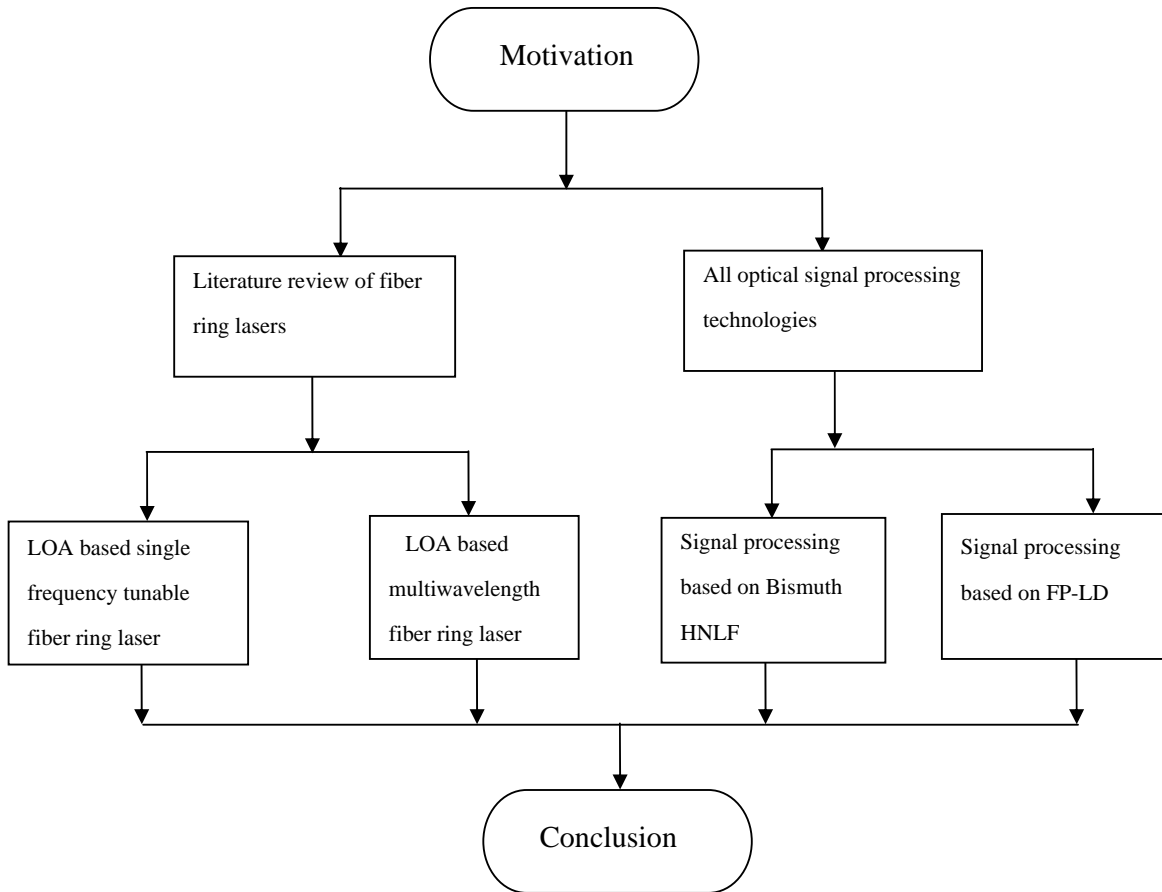


Fig 1.1 Flow chart of the thesis

1.5 Publications

The following publications arose during the period of this research study.

- (1) K. K. Qureshi, S. H. Wang, P. K. A. Wai, H. Y. Tam, N. Sugimoto, and L. Chao, "Tunable pulse generation using four-wave mixing in bismuth based highly nonlinear fiber," submitted to *Optics Comm.*
- (2) K. K. Qureshi, P. K. A. Wai, H. Y. Tam, L. Chao, and N. Sugimoto, "All-optical on-off switch based on bismuth based highly nonlinear fiber," submitted to *Microwave and Opt Technol Lett.*
- (3) K. K. Qureshi, H. Y. Tam, W. H. Chung, and P. K. A. Wai, and N. Sugimoto, "All optical on-ff switching using bismuth-based highly nonlinear fiber," *CLEO' 2006*, CMAA2, California, USA.
- (4) K. K. Qureshi, H. Y. Tam, W. H. Chung, and P. K. A. Wai, and N. Sugimoto, "Generation of optical pulses with tunable pulsewidth using 1.9 meter bismuth based highly nonlinear fiber," *CLEO' 2006*, CMEE3, California, USA.
- (5) K. K. Qureshi, H. Y. Tam, W. H. Chung, and P. K. A. Wai, "Multiwavelength laser source using linear optical amplifier," *IEEE Photon. Technol. Lett.* **17**, 1611-1613 (2005).
- (6) "Linear optical amplifier generates multiple wavelengths simultaneously" *Photonics Spectra*, 33-34, Oct 2005.
- (7) K. K. Qureshi, H. Y. Tam, W. H. Chung, and P. K. A. Wai, "LOA based multiwavelength laser source," *CLEO' 2005*, CTuF1, Maryland, USA.
- (8) K. K. Qureshi, H. Y. Tam, W. H. Chung and P. K. A. Wai, "Multiwavelength C+L band laser source using Linear Optical Amplifier," *ICOON'2004*, 333-336, Hong Kong.
- (9) K. K. Qureshi, W. H. Chung, H. Y. Tam, L. Y. Chan, and P. K. A. Wai, "Implementation of all-optical bit error monitoring system using cascaded optical logic gates," *CLEO' 2003*, CThJ7, Baltimore, USA.

- (10) L. Y. Chan, K. K. Qureshi, P. K. A. Wai, B. Moses, L. F. K. Lui, H. Y. Tam and M. S. Demokan, "All optical bit error monitoring system using an inverted wavelength converter and optical NOR gate," *IEEE Photon. Technol. Lett.* **15**, 593-595 (2003).

- (11) K. K. Qureshi, L. Y. Chan, L. F. K. Lui, P. K. A. Wai, and H. Y. Tam, "Real-time bit error monitoring system (BEMS) for optical communication by use of high speed logic gates," *CEOS'2003*, 169-171, Hong Kong.

- (12) K. K. Qureshi, W. H. Chung, H. Y. Tam, L. Y. Chan, P. K. A. Wai, and L. F. K. Lui, "An all-optical NOT gate with variable threshold using dual wavelength injection locking," *CLEO/Europe'2003*, CJ11038, Munich, Germany.

- (13) K. K. Qureshi, L. Y. Chan, P. K. A. Wai, L. F. K. Lui, W. H. Chung, and H. Y. Tam, "Implementation of all-optical NOR gate using multi-wavelength injection-locked laser diode," *OECC' 2003*, 397-398, Shanghai, China.

Chapter 2

Literature Review of semiconductor fiber ring lasers

The studies on wavelength division multiplexing (WDM) systems began in the late 1980s. These systems used widely spaced wavelengths in the 1310 nm and 1550 nm windows, because these wavelengths experienced minimum attenuation in optical fiber. These types of systems can be used to realize high-capacity optical fiber communication systems demanded by the recent explosive growth in the Internet traffic [1]. An important component of these systems is the laser source. These sources can be classified into three types;

Discrete lasers with fixed wavelength: this is the option that is currently used. High performance devices are available. However, if the number of wavelength channels increases, the management overhead may become complex.

Tunable lasers: can be used as backup lasers to replace a complete set of discrete backup lasers.

Multiwavelength lasers: single devices which are able to provide multiple channels at once, all of them are separately modulated. One device may replace a complete array of discrete lasers, thereby reducing the packaging cost and the

management overhead considerably.

Although each transmitter source in a WDM system does not represent a major cost on its own, however it is impractical to stock one or two lasers for each wavelength channel, particularly for WDM systems with high channel-count due to the overwhelming cost and large inventory, which could be many hundreds of lasers. These issues could be circumvented by stocking much lower number of tunable laser sources whose wavelengths cover the entire operating wavelength range of the WDM systems. A single tunable laser can serve as backup for multiple channels, so that fewer lasers need to be stocked as spares. Tunable lasers also provide flexibility in management of optical networks by facilitating the switching to alternative channels without swapping hardware or reconfiguring the network resources and hence play a key role as an enabling technology in these systems [2]. Since fiber ring lasers (FRLs) exhibit a wide tunable range, narrow linewidth and could be tuned at high speed, allowing fast component characterization. Hence a great deal of research has been carried out on fiber ring lasers in the last few decades [3-6,10-17].

Fiber ring laser has a ring structure whereby some of the output light is fed back to its input. The gain media in a ring laser can be provided by a section of excited rare-earth ions doped fiber or a current-driven semiconductor optical amplifier (SOA) or a combination of both [17]. Different rare-earth ions, such as erbium, neodymium, ytterbium, and thulim can be used to realize FRLs capable of operating over a wide wavelength range. For optical fiber communication systems, semiconductor fiber ring lasers (SFRLs) and erbium doped fiber ring lasers (EDFRLs) are of interest because they

operate in the 1.55 μm spectral region, which coincides with the low-loss region of silica fibers [3-6,10-17]. However, it is to be noted that the SFRL can be realized both at 1.3 or 1.55 μm wavelength regimes due to the availability of SOAs at these wavelengths. Fiber ring lasers can be broadly divided into two classes; continuous wavelength output fiber ring lasers and pulsed output fiber ring lasers. In this thesis, we focused on the continuous wavelength output FRLs using semiconductor based gain medium.

2.1 Background review of single frequency SFRL technologies

Chawki et al. [3] demonstrated the first all fiber tunable semiconductor ring laser working at 1550 nm regime as shown in Fig. 2.1. Broad tuning over 50 nm was electronically achieved by using a fiber Fabry P rot filter as a wavelength selective element. Single wavelength operation was demonstrated with a side mode suppression ratio (SMSR) of around 35dB. However, the drawback of this scheme is very high coupling loss (~ 12 dB) at the facets of the semiconductor amplifier.

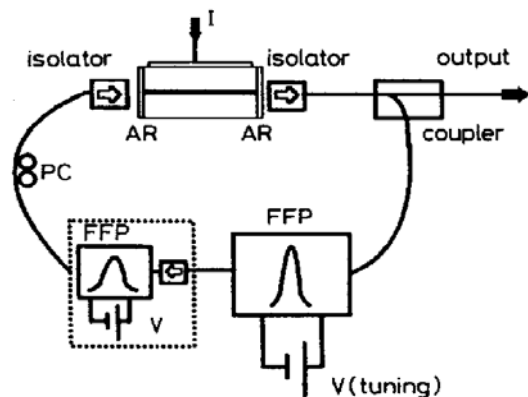


Fig. 2.1 Experimental setup of the tunable semiconductor fiber ring laser using electronically controlled FFP-filter [3].

Porte et al. [4] reported a FRL that includes a semiconductor near-travelling wave amplifier at 1300 nm tuned by an intra-cavity electrooptic birefringent filter as depicted in Fig. 2.2. The tuning range thus obtained was 20 nm and the tuning rate was 0.05 nm/V. The measured output power is improved by the use of an intra-cavity polarization element. The fiber configuration improves the stability of the laser compared with previous extended-cavity lasers with an external mirror. The major drawback of this scheme is the small reflectivity from the facet of the amplifier chip, yielding a multimode lasing emission and wavelength tuning by mode hopping.

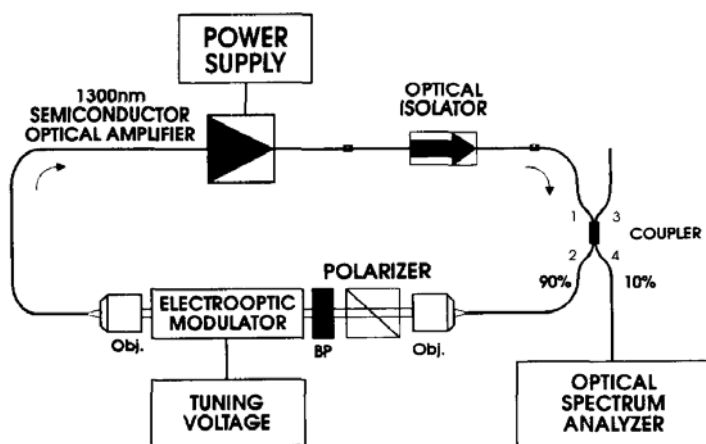


Fig. 2.2 Configuration of the tunable semiconductor fiber ring laser using electrooptic birefringent filter [4].

Zhou, et al. [5] also demonstrated wavelength tunable semiconductor laser oscillation at 1300 nm regime. The laser was capable of tuning over the 28 nm width of the gain medium. The combination of the linear polarizer, polarization controllers, highly birefringent components such as PM fibers, and the polarization dependent gain medium such as SOA provided the wavelength selective mechanism as shown in Fig. 2.3. Different wavelengths have different losses due to the polarization dependent loss through the linear polarizer. A wavelength with its electrical field vector lined up with the linear polarizer experienced the least loss. Hence, the combination of a polarization controller and linear polarizer provided a wavelength selection mechanism to generate a tunable laser output.

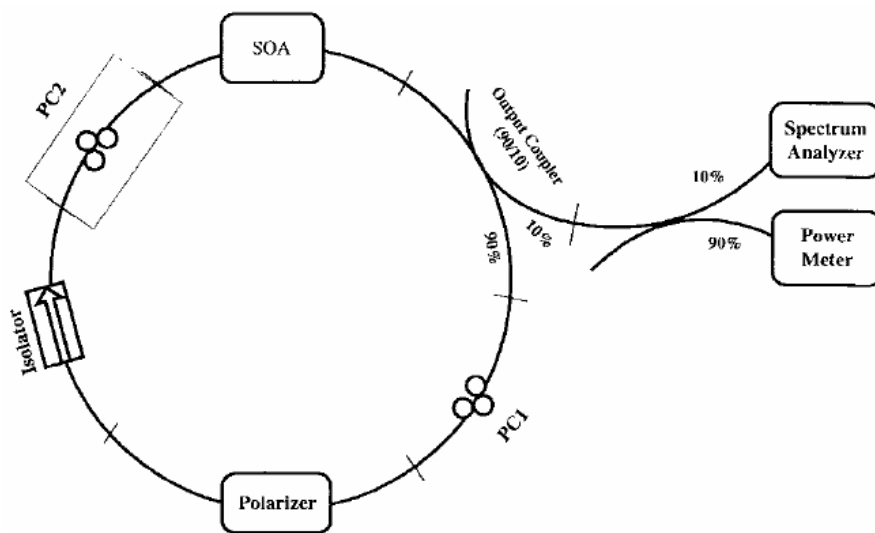


Fig. 2.3 Schematic diagram of the tunable semiconductor fiber ring laser [5].

A composite cavity semiconductor FRL was proposed by Hu et al. [6] as shown in Fig. 2.4. A passive sub-ring cavity with the same length as the main ring cavity was added to maximize the longitudinal-mode frequency separation as a vernier configuration. Increasing the frequency separation improved the stability of the laser system. Tuning over a range of 20 nm from 1291 to 1311 nm was achieved by applying voltage (0-30 V dc) to the piezoelectric transducer (PZT) placed in the sub-ring cavity.

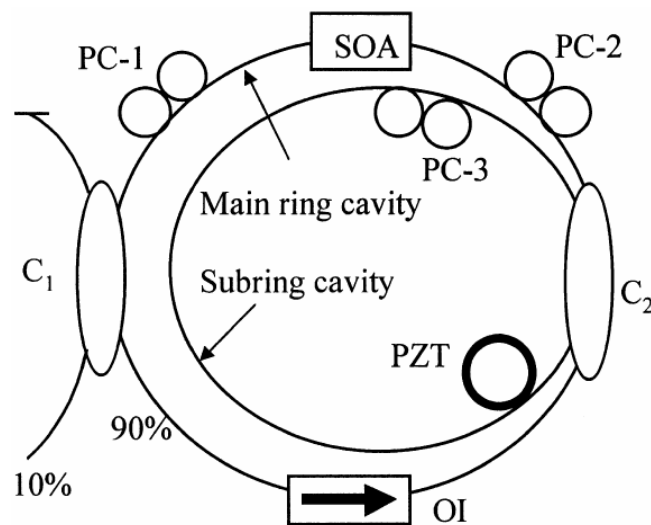


Fig. 2.4 Schematic diagram of the composite cavity semiconductor fiber ring laser [6].

2.2 Background review of multiwavelength FRL technologies

Multiwavelength fiber ring lasers have also been an area of extensive research for the last few decades. As the transmission capacity of the optical communication systems approaches tens of Tb/s through WDM concept, multiwavelength source technology becomes more important, considering that the complexity and the cost of the source will increase as the number of channels increase. In multiwavelength Erbium Doped Fiber (EDF) lasers, large homogeneous linewidth of EDF at room temperature has been the major barrier for achieving simultaneous oscillation of multiple wavelengths. According to the conventional laser theory, each channel output of the laser containing a gain medium with homogeneous line broadening becomes unstable due to gain competition effect inevitable with two or more frequency components satisfying the laser oscillation condition [7]. In order to effectively implement the stringent DWDM channel spacing requirement, the cross saturation effect present in a homogeneous gain media should be suppressed. The homogeneous linewidth of the gain medium determines the wavelength range of cross saturation effect. The homogeneous linewidth of EDF gain media is in the order of 10's of nm at room temperature. However, by cooling the EDF to cryogenic temperature (77° K), the linewidth could be reduced to 0.5-1 nm [8-10]. At this temperature, the gain medium becomes inhomogeneous which permits the multiwavelength generation. Nevertheless, the use of a cooler such as liquid nitrogen is inconvenient and may degrade the system durability, leading to the complexity of the source configuration.

In 1992, Park et al. [11] reported the first multiwavelength fiber laser generating 6 wavelengths, wherein the channels were separated by 4.8 nm. The linear fiber laser

cavity was fabricated by splicing a 10 m EDF to a WDM multiplexer. Both fiber ends of the linear cavity were connected to the two fiber loop mirrors. Six lasing lines were observed in the optical spectrum, however a temporal modulation on a millisecond time scale was also seen which was believed to be due to spatial hole burning and could be avoided in an unidirectional ring laser. Six lasing lines with a total output power of 1 mW were generated in such a ring cavity. The average power of each channel ranges from 50 to 150 μ W. The downside of this complicated design is the high insertion loss of 6 dB for each WDM channel and power fluctuation (\sim 3 dB) for each lasing line under multiwavelength operation.

In [12] a length of Polarization Maintaining (PM) fiber was added into a linear Nd-doped fiber laser to realize a comb filter as shown in Fig. 2.5. The comb filter was formed due to birefringence property of the PM fiber and simplified the structure of the laser cavity. Four lasing lines with a wavelength separation of 1 nm were generated in the laser cavity with a PM fiber length of 1.2 m at room temperature. The wavelength spacing was reduced to 0.7 nm with 2 m of PM fiber, which increased the number of lasing lines to eight within the same bandwidth. In this scheme only a few poorly defined wavelengths are produced.

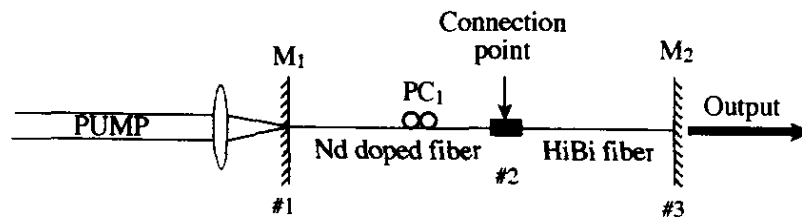


Fig. 2.5 Schematic configuration of fiber laser emitting comb-like spectrum [12].

Poustie et al. [13] realized multiwavelength generation using a multimode fiber as a comb filter in the single mode fiber cavity as depicted in Fig 2.6. The wavelength spacing was tuned by using different lengths of multimode fiber. Four lasing lines were observed with 50 m of erbium doped fiber at 1600 nm, whereas six lasing lines were seen with 3 m of neodymium doped fiber at 1065 nm. The limitation of this scheme is that the maximum number of lasing lines are limited to only six and are also not well defined.

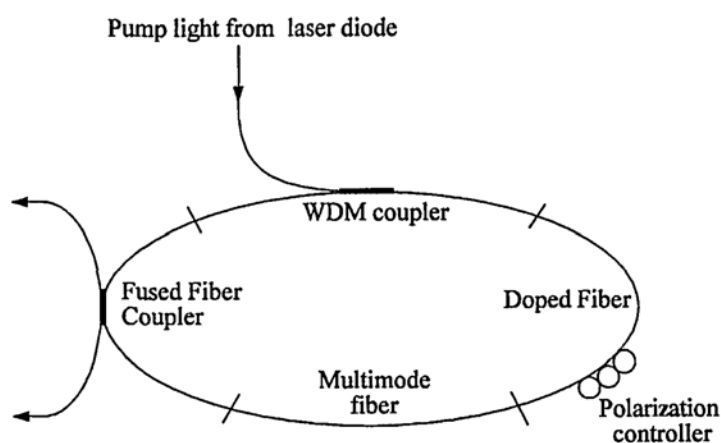


Fig. 2.6 Schematic of fiber laser cavity [13].

Chow et al. [14] proposed using two different types of in-fiber comb filter. The first proposed filter was a transmissive wide band Bragg grating Fabry P rot resonator, and the other a reflective sampled Bragg grating. The filters were incorporated into a ring cavity with a single inhomogeneously broadened EDF gain medium at 77° K and produced lasing combs around 1535 nm. Simultaneous operation of 11 wavelengths

separated by 0.65 nm (83 GHz) was achieved using a wideband in-fiber transmissive comb filter. However, only five lasing wavelengths separated by 1.8 nm (230 GHz) were generated using the sampled Bragg grating reflective comb filter.

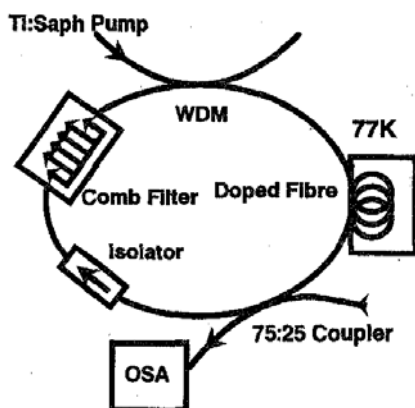


Fig. 2.7 Multiwavelength ring laser configuration [14].

Yamashita et al. [10] proposed multiple oscillations in a linear cavity including EDF along with a Fabry-Perot etalon at 77° K. At room temperature only three lasing wavelengths were observed with 0.8 nm wavelength spacing, which corresponds to the maximum transmission of the etalon. These oscillations were very unstable and strong mode competition was observed. However, cooling EDF to cryogenic temperature of 77° K increased the number of lasing wavelengths to 17, owing to strong suppression of the cross saturation at such a low temperature.

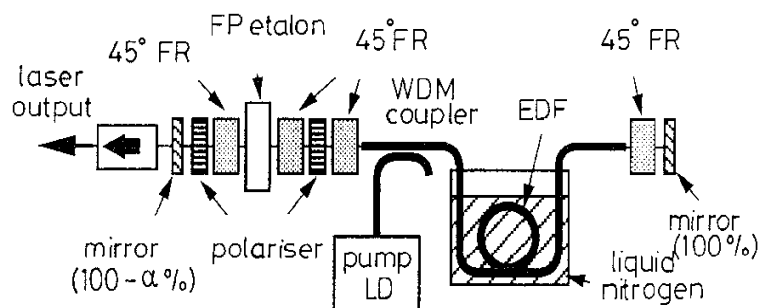


Fig. 2.8 Multiwavelength erbium doped fiber laser cooled by liquid nitrogen [10].

The aforementioned multi-wavelength generation configurations are related to the EDF laser operation at 77°K and hence are not very practical. In 1996, Cowle et al. [15] proposed a hybrid gain media for the fiber laser operating at room temperature. The hybrid gain media consisted of respectively Brillouin and EDF gain. The Brillouin gain was triggered by an optical pump source with a narrow linewidth. Stimulated Brillouin scattering effect generated Brillouin signals in the optical spectra. The frequency difference between the Brillouin signals was established due to acoustic velocity in the fiber. In a fiber laser scheme with such a hybrid gain media, simultaneous operation of multiple wavelengths with a channel spacing of 0.0824 nm (10.3 GHz) was realized by continuously seeding the Brillouin signals. The main purpose of EDF gain was to compensate the loss in the laser cavity and to increase the laser output power.

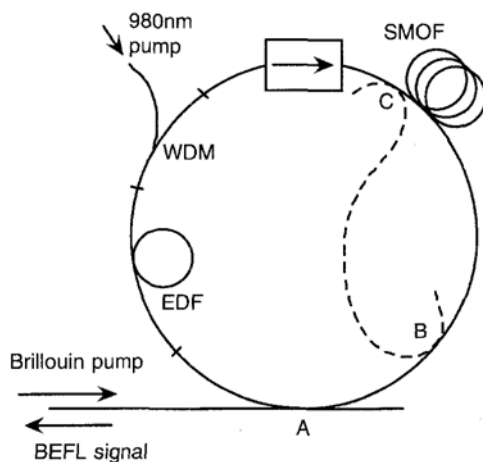


Fig. 2.9 Schematic of Erbium/Brillouin multiwavelength fiber ring laser [15].

Bellemare et al. [10] introduced a frequency shifter in the EDF ring laser cavity, as depicted in Fig. 2.10. The generated Amplified Spontaneous Emission (ASE) from the EDF circulated in the ring cavity. The periodic bandpass filter sliced the ASE spectrum during each round trip of the cavity and it ensured wavelength spacing of 0.8 nm (100 GHz). The acousto-optic frequency shifter placed in the laser cavity shifted the ASE spectrum during each round trip to avoid a steady state operation of a single frequency oscillation. The frequency shifter approach does not require liquid nitrogen cooling, which is considered to be a major advantage in the realization of this multiwavelength generation scheme. The EDF fiber laser with frequency shifted feedback allowed 14 wavelengths to oscillate simultaneously. The signal to noise ratio (SNR) and total power of the fiber laser were respectively 20 dB and 7.8 dBm.

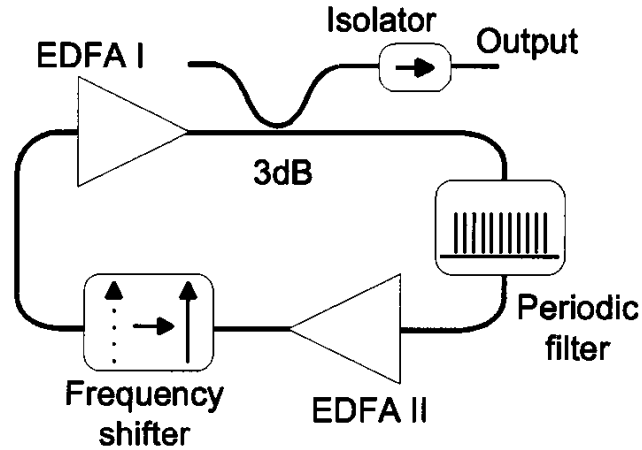


Fig. 2.10 Multiwavelength erbium doped fiber ring laser with an intra cavity frequency shifter [16].

Recently, Wang et al. [11] proposed a hybrid gain media consisting of an SOA and EDFA to generate multiwavelengths as shown in Fig. 2.11. Twenty four wavelengths were generated with a channel spacing of 0.5 nm at room temperature. This scheme partially solved the problem of mode competition caused by EDFA by incorporating an SOA in the cavity which provides inhomogeneous gain.

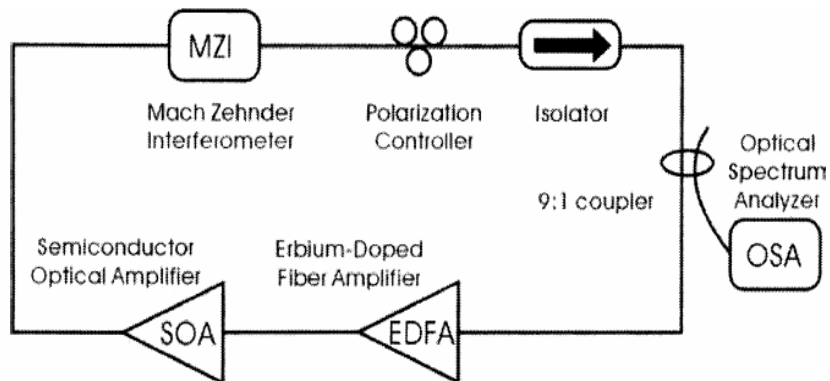


Fig. 2.11 Schematic of multiwavelength fiber ring laser with hybrid gain media [17].

2.3 Chapter Summary

In this chapter, the background review of different types of single frequency and multiwavelength semiconductor fiber ring lasers was presented. The merits and demerits of different configurations were also discussed.

References

- [1] J. X. Cai, D. G. Foursa, C. R. Davidson, Y. Cai, G. Domagala, H. Li, L. Liu, W. W. Patterson, A. N. Pilipetskii, M. Nissov, and N. S. Bergano, "A DWDM demonstration of 3.73 Tb/s over 11 000 km using 373 RZ-DPSK channels at 10 Gb/s", *OFC 2003*, Atlanta, Georgia, PDP22, Mar. (2003).
- [2] D. Anthon, J. D. Berger, and A. Ashmead, "Tunable external cavity semiconductor lasers for network application," *ECOC 2002, 28th European Conference on Optical Communication*, Sep. (2002).
- [3] M. J. Chawki, I. Valiente, R. Auffret, and V. Tholey, R. J. Manning and D. A. O. Davies, "All fibre, 1.5 μm widely tunable single frequency and narrow linewidth semiconductor ring laser with fibre Fabry Perot filter," *Electron. Lett.*, **29**, 2034–2035 (1993).
- [4] H. Porte, T. Frison, P. Mollier, and J. P. Goedgebuer, "Electrooptic tuning of a fiber ring semiconductor laser," *IEEE Photon. Technol. Lett.*, **7**, 700–702 (1995).
- [5] D. Zhou, P. R. Prucnal, and I. Glesk, "A widely tunable narrow linewidth semiconductor fiber ring laser," *IEEE Photon. Technol. Lett.*, **10**, 781–783 (1998).
- [6] Z. Hu, L. Zheng, Y. Zhang, and Q. Tang, "Composite cavity semiconductor fiber ring laser," *Optics Lett.*, **25**, 469-471 (2000).
- [7] A. E. Siegman, *Lasers*, University Science Books, Mill Valley, CA, (1986)
- [8] M. J. F. Digonnet, "Rare-Earth-Doped Fiber Lasers and Amplifiers" Second Edition, Marcel Dekker Inc., New York (2001).
- [9] J. L. Zyskind et al., "Determination of homogeneous linewidth by spectral gain hole burning in an Erbium-Doped Fiber Amplifier with GeO₂:SiO₂ core," *IEEE Photon.*

- Technol. Lett.*, **2**, 869-871 (1990).
- [10] S. Yamashita and K. Hotate, "Multiwavelength erbium-doped fibre laser using intracavity etalon and cooled by liquid nitrogen," *Elect. Lett.*, vol. **32**, 1298-1299 (1996).
- [11] N. Park, J. W. Dowson, and K. L. Vahala, "Multiple wavelength operation of an erbium-doped fiber laser", *IEEE Photon. Technol. Lett.*, **4**, 540-542 (1992).
- [12] U. Ghera, N. Friedman, and M. Tur, "A fiber laser with a comb-like spectrum," *IEEE Photon. Technol. Lett.*, **5**, 1159-1161 (1993).
- [13] A. J. Postie and N. Finlayson, "Multiwavelength fiber laser using a spatial mode beating filter," *Opt Lett.*, **19**, 716-718 (1994).
- [14] J. Chow, G. Town, B. Eggleton, M. Ibsen, K. Sugden and Ian Bennion, "Multiwavelength generation in an erbium doped fiber laser using in-fiber comb filters," *IEEE Photon. Technol. Lett.*, **8**, 60-62, (1996).
- [15] G. J. Cowle and D. Yu. Stepanov, "Multiple wavelength generation with Brillouin/erbium fiber lasers", *IEEE Photon. Technol. Lett.*, **8**, 1465-1467 (1996).
- [16] A. Bellemere, M. Karasek, M. Rochette, S. LaRochelle and M. Tetu, "Room temperature multifrequency erbium doped fiber lasers anchored on ITU frequency grid", *J. Lightw. Technol.*, **18**, 825-831 (2000).
- [17] D. N. Wang, F. W. Tong, Xiahui Fang, W. Jin, P. K. A. Wai, and J. M. Gong, "Multiwavelength erbium-doped fiber ring laser source with a hybrid gain medium," *Optics Comm*, **228**, 295-301 (2003).

Chapter 3

Semiconductor fiber ring lasers

3.1 Linear Optical Amplifiers

Gain clamped semiconductor optical amplifiers (GC-SOAs) offer many advantages compared to the conventional semiconductor optical amplifiers (SOAs). The response of GC-SOAs is more linear and they suffer less from crosstalk related problems. Conventionally gain clamping has been achieved by fabricating two distributed Bragg reflector (DBR) mirrors on both sides of the amplifier so that the amplifier forms a cavity for the frequencies selected by the DBRs [1-2]. However, the fabrication of DBRs makes the amplifier structure more complex and also the amplifier response less ideal. The advantage both the SOA and GC-SOA have over the fiber optical amplifiers is their integrability and direct modulation, which in the case of SOA comes at the cost of low performance.

In this chapter we introduce a new type of gain clamped semiconductor optical amplifier called a linear Optical Amplifier (LOA). Employing this amplifier a tunable single frequency laser with a wide tunable range was developed. Later a stable multiwavelength fiber ring laser was also constructed.

A different approach to gain clamping was introduced recently by the Finisar

Corporation [3] in their amplifier, called the LOA. In their amplifier structure, the laser is perpendicular, rather than parallel, to the signal and vertical in the actual amplifier structure as shown in Fig. 3.1. The LOA is a metal-organic chemical vapor deposition (MOCVD) grown InP-based semiconductor device that integrates an active waveguide and a vertical-cavity surface-emitting laser (VCSEL) on the same chip. The VCSEL has been elongated to coincide with the active waveguide along its entire length. This way, the active region of the device is shared between VCSEL and the amplifier. The VCSEL lases orthogonally to the signal direction, acting as an optical feedback to prevent the carrier depletion during the changes of input signal power level. This lasing action clamps the gain along the entire length of the waveguide, avoiding the inter-symbol interference and crosstalk that impede WDM operation in traditional SOAs.

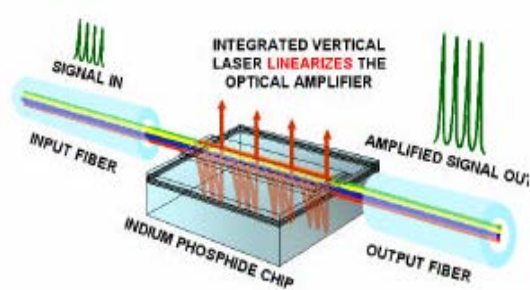


Fig. 3.1 Schematic of the linear optical amplifier [2]

The LOA has two antireflection (AR) coated facets with reflectivity $\sim 10^{-5}$. The typical gain of the LOA is around 14 dB at an injection current of 180 mA, with the polarization dependence less than 1 dB. The noise figure (NF) of the amplifier is 7.8 dB.

Figure 3.2 depicts the amplified spontaneous emission (ASE) spectra of the LOA at different injection currents. The ASE spectra are obtained by using an optical spectrum analyzer (OSA) with a spectral resolution of 0.1 nm. The device is thermo-electrically cooled and maintained at 20° C. The ASE profile has a gain peak at around 1545 nm for a biasing current of 180 mA. The ASE spectral flatness in C-band (1532-1562) nm is around 1.4 dB.

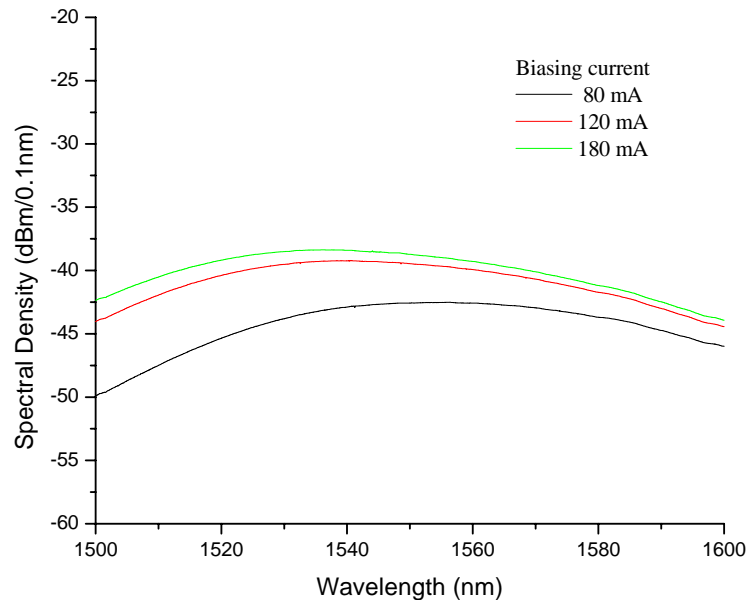


Fig. 3.2 ASE spectra of LOA for different biasing currents

Figure 3.3 depicts the output gain at different injection currents applied to the LOA at a fixed input signal power of -25 dBm. The test wavelength is 1550 nm. The LOA gain increases with an increase in the injection current. By increasing the injection

current from 60 to 240 mA, the LOA module gain increases from 4.13 to 14 dB respectively.

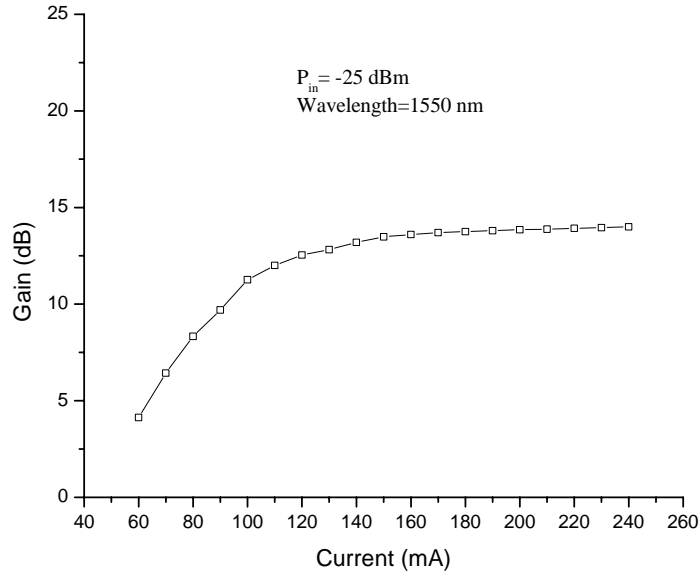


Fig. 3.3 Dependence of module gain on injection current; signal-light wavelength was 1550 nm.

Figure 3.4 depicts the gain saturation characteristics of the LOA at different biasing currents. The input signal wavelength was at 1550 nm. By reducing the current from 180 mA to 80 mA, the gain was reduced by 6 dB (from 13.9 to 7.9 dB). When the injection current was reduced, both the unsaturated gain and the saturated output power were decreased. The 3-dB saturation output power was 11 dBm when the biasing current was 220 mA. The small signal gain of the LOA in C-band is shown in Fig. 3.5. The maximum small signal gain was 14 dB at 1546 nm for an input power of -25 dBm at an injection current of 220 mA.

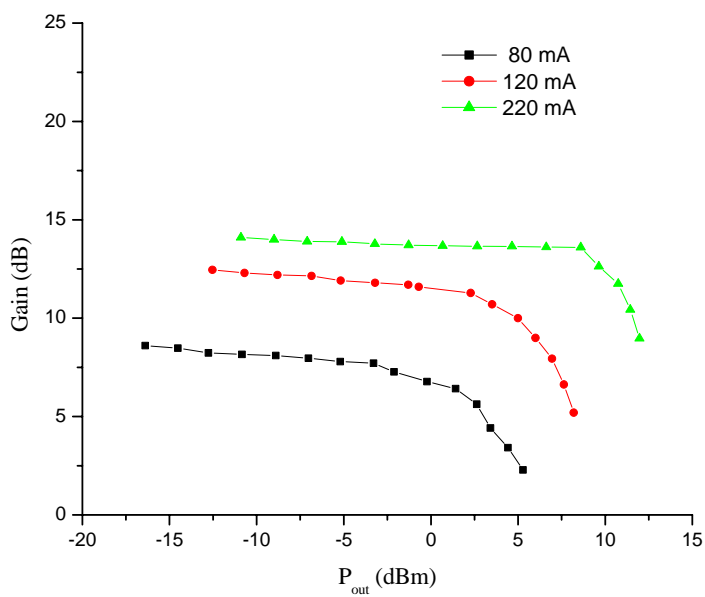


Fig. 3.4 Gain-saturation characteristics at different LOA currents for CW signal; signal-light wavelength was 1550 nm.

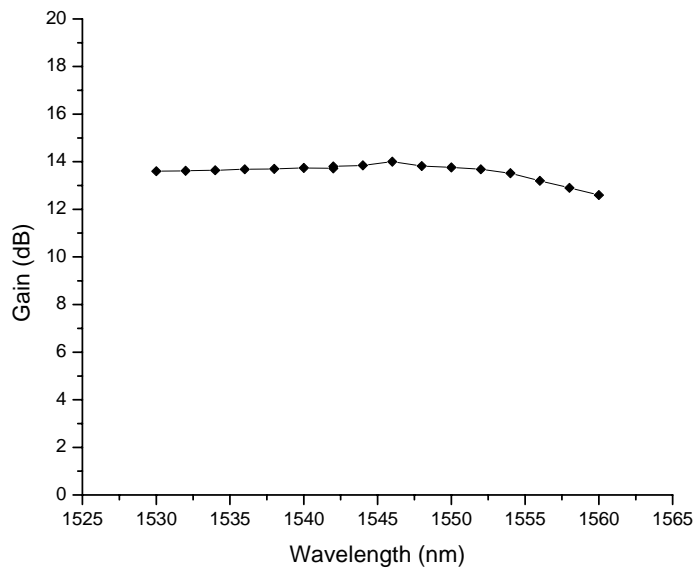


Fig. 3.5 Gain characteristics of LOA at injection current of 220 mA. The input signal is at -25 dBm.

3.2 Widely tunable single frequency semiconductor fiber ring laser

In this section we report our experimental findings regarding the widely tunable single frequency semiconductor fiber ring laser. The configuration of a traveling wave tunable semiconductor fiber ring laser constructed with an LOA is shown in Fig 3.6. The ring consists of an LOA, polarization controller (PC), 20% fused fiber coupler, two polarization independent isolators, and a fiber Fabry P erot tunable filter (FFP-TF). The polarization controller is used to control the state of polarization in the laser cavity and to maximize the signal to noise ratio (SNR). Two isolators are used in the cavity in order to avoid reflections from the input and output ends of FFP-TF to the LOA and as well as to ensure the unidirectional operation of the ring cavity. A broad free spectral range (FSR), FFP-TF was employed to tune the feedback lasing wavelength.

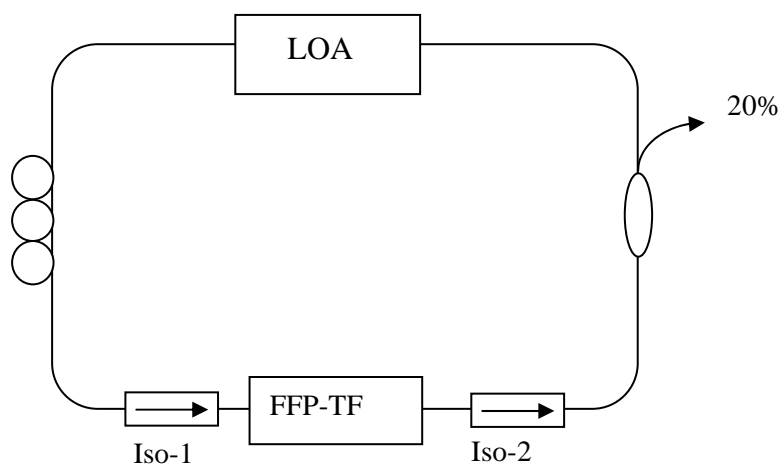


Fig. 3.6 Schematics of tunable semiconductor fiber ring laser (SFRL);
Note: LOA: Linear Optical Amplifier, PC: Polarization Controller, Iso: Isolator, FFP-TF: Fiber Fabry P erot tunable filter

3.2.1 Experimental Results

A narrowband, wide tunable range FFP-TF from the Micron optics Co, was employed to tune the lasing wavelength. By varying the voltage applied to the filter, the laser was tuned over 90 nm. The operable temperature range of FFP-TF is from -20 to +80 C and its tuning Voltage/FSR is from (0-16) Volts. The optical 3-bandwidth of this filter is 30 pm (3.75 GHz) and its FSR is around 102 nm, hence the Finesse of the FFP-TF is 3400. The insertion loss at the peak of its pass-band is about 2.2 dB. Figure 3.7 shows the output spectra of the FRL obtained from the 20% taper, which is measured with an optical spectrum analyzer (OSA) with a resolution of 0.1 nm. The LOA was pumped with a biasing current of 140 mA. By tuning the pass-band of the FFP-TF, the laser wavelength was tuned from 1507 nm to 1600 nm, exhibiting a broad tuning range of 93 nm. From the output spectra (Fig. 3.7), it is evident that over the range from 1525 nm to 1595 nm, the extinction ratio is over 45 dB and the average output power is greater than -2 dBm. However, outside this range, both the output power and the extinction ratio was reduced due to the smaller gain provided by the LOA. The total output power of this laser is 1.3 dBm. The extinction ratio and the output power can be further improved by increasing the biasing current applied to the LOA. It is worth noting that the ASE level in the output spectra increases when the lasing wavelength is tuned away from the wavelength range where the LOA provides higher flat optical gain.

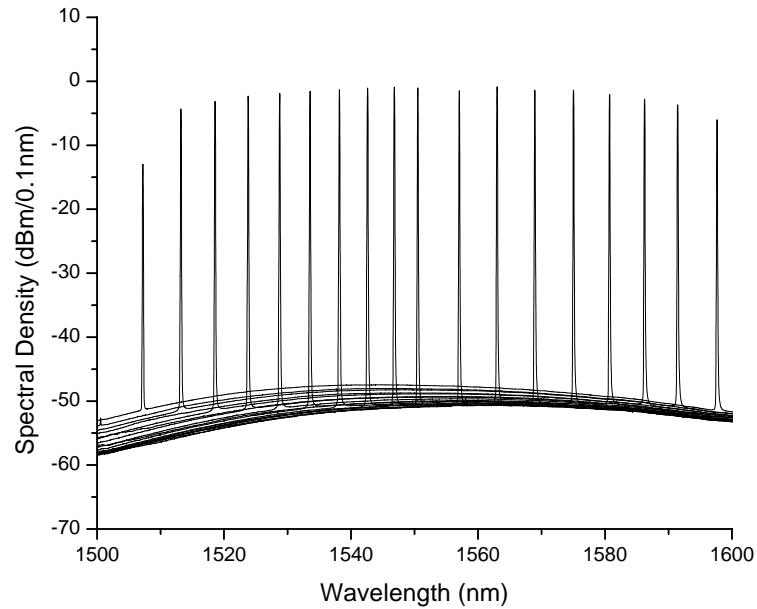


Fig. 3.7 Laser spectra measured with an OSA with 0.1 nm resolution.

A typical lasing spectrum was measured by an OSA using 0.01 nm resolution and is shown in Fig. 3.8. The asymmetric shape of the laser is mainly caused by the response of optical spectrum analyzer. The laser at 1541.80 nm has a 3 dB bandwidth of around 0.022 nm, limited by the resolution of OSA. Figure 3.9 shows the output power versus the lasing wavelengths at the output of the laser. The average output power of each lasing line is very flat over the entire range.

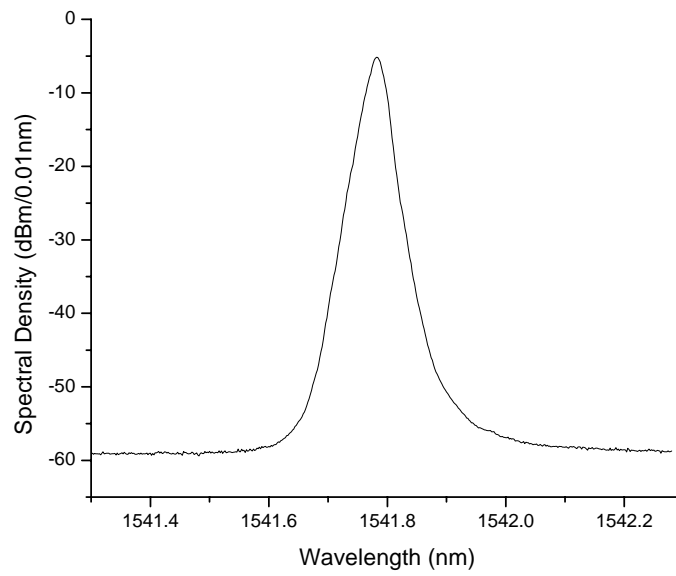


Fig. 3.8 Output spectrum of the tunable laser tuned at 1541.80 nm with an OSA resolution of 0.01 nm.

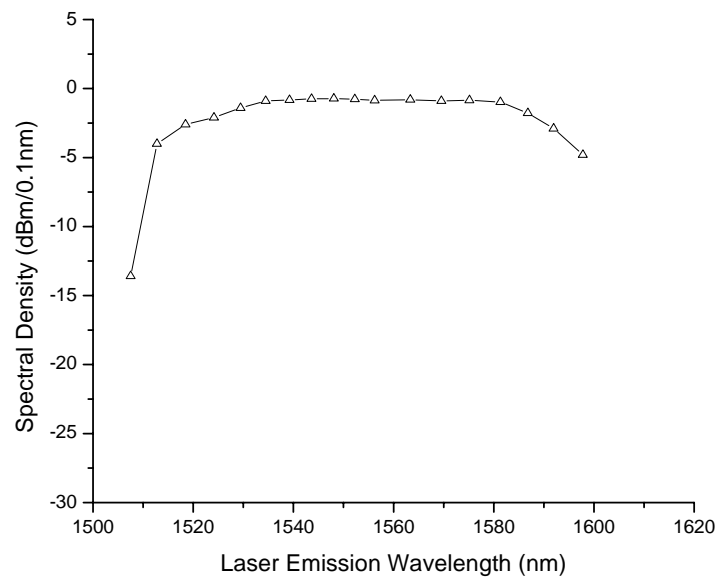


Fig. 3.9 Output powers versus lasing wavelengths measured at the output of the laser.

An important parameter that determines the performance of the laser is the output power stability. Figure 3.10 shows the measured total power fluctuation of the fiber laser when its output was maintained at one lasing wavelength for a period of 1 hour and 40 minutes. The wavelength being tested was at 1545.8 nm. The power fluctuation was less than 0.05 dB, confirming the stability of the laser source. It is worth noting that the experiment was conducted under a laboratory environment and no precautions were taken to isolate the setup from thermal and vibrational perturbations. Therefore, even better stability would be expected if the short-cavity fiber ring laser was properly packaged.

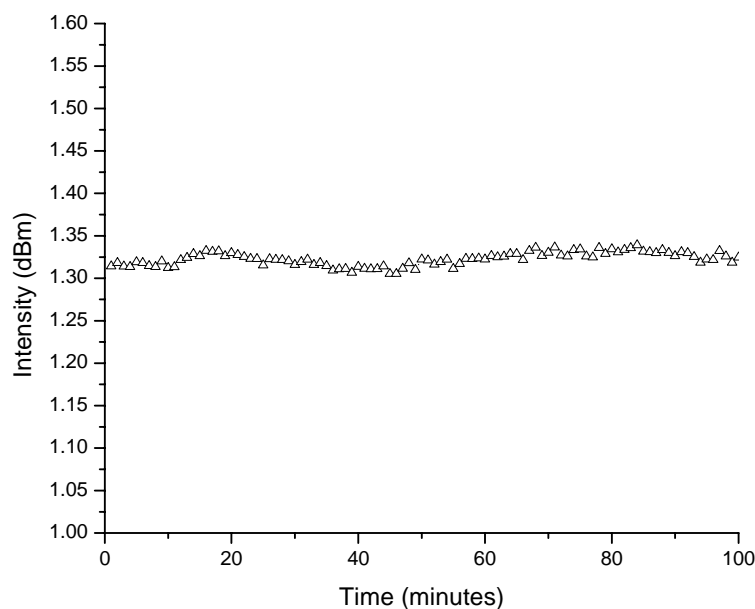


Fig. 3.10 Power variations of the fiber ring laser over a period of 100 minutes.

In the next section we explain the stability conditions for multiwavelength generation.

3.3 Stability conditions for multiwavelength generation

Gain competition in a laser cavity is a very complex phenomenon. In general different laser modes have different gains, losses and saturation parameters, and they compete for the available gain in the laser cavity. For the sake of simplicity we consider gain competition between two potentially oscillating modes. Here we consider only the self-saturation and cross-saturation effects on the respective gains of these two modes. We ignore any back-scattering or cross-scattering effects that may couple from one mode into the other. It is to be noted that the self-saturation and the cross-saturation effects between the two potentially lasing modes in the laser cavity depend on the spatial overlap of the two modes, and also on their spectral overlap and on whether the atomic transition involved is homogeneous or inhomogeneous [4].

The classical gain model of the laser can be defined as:

$$G(\nu) = \frac{G_0(\nu)}{1 + \frac{I_0}{I_{sat}}} \quad (3.1)$$

where $G_0(\nu)$ is the small signal gain, I_0 and I_{sat} are respectively the output and saturation intensity.

The equation (3.1) does not consider the cross saturation effect and hence should be modified to explain the two-mode gain competition effect in the laser cavity and is discussed below.

Consider two incoherently related signals I_1 and I_2 at different frequencies ν_1 and ν_2 . The gain saturation for the mode-1 can be written as:

$$G_1 = \frac{G_0(\nu_1)}{1 + \kappa_{11}I_1 + \kappa_{12}I_2} \approx G_0(\nu_1)[1 - \kappa_{11}I_1 - \kappa_{12}I_2] \quad (3.2)$$

Similarly, the gain saturation for the mode-2 can be written as:

$$G_2 = \frac{G_0(\nu_2)}{1 + \kappa_{22}I_2 + \kappa_{21}I_1} \approx G_0(\nu_2)[1 - \kappa_{22}I_2 - \kappa_{21}I_1] \quad (3.3)$$

where, coefficients κ_{11} and κ_{22} represent self saturation gains of the mode-1 and mode -2 by their own intensities, whereas the coefficients κ_{12} and κ_{21} represent the gain of mode-1 by the intensity of mode-2 and vice versa. The simplified approximation in the second term of (3.2) and (3.3) will only hold provided that the gain coefficient is not too strongly saturated by either signal.

In order to explain the mode competition between two potentially oscillating modes in a simple fashion, we can use the intensity growth equations for the two modes in a generalized form as:

$$\frac{dI_1}{dt} = G_1I_1 - \alpha_1I_1 \approx I_1[G_0(\nu_1).(1 - \kappa_{11}I_1 - \kappa_{12}I_2) - \alpha_1] \quad (3.4)$$

$$\frac{dI_2}{dt} = G_2I_2 - \alpha_2I_2 \approx I_2[G_0(\nu_2).(1 - \kappa_{22}I_2 - \kappa_{21}I_1) - \alpha_2] \quad (3.5)$$

where, G_1 and G_2 are the unsaturated growth rates of mode-1 and mode-2 respectively. α_1 and α_2 are the decay rates or losses of mode-1 and mode-2 in the laser cavity.

Suppose that the two signals with different optical frequencies are near the center of the strongly homogeneous gain profile and whose spatial patterns are also identical in the gain medium. Under this condition the four coefficients have roughly equal values.

Hence,

$$\kappa_{11} \approx \kappa_{22} \approx \kappa_{12} \approx \kappa_{21} \quad (3.6)$$

Now suppose that the gain medium is inhomogeneous broadening so that the two signals lie at different spectral packets. In this scenario the cross-saturation coefficients are very weak. Hence,

$$\kappa_{12} \cdot \kappa_{21} \ll \kappa_{11} \cdot \kappa_{22} \quad (3.7)$$

Since the Erbium doped fiber amplifiers (EDFA) inherently provide homogeneous gain, multiwavelength laser sources employing EDFA as a gain medium suffer from severe mode competition at room temperature. On the contrary the semiconductor based amplifiers provide inhomogeneous gain, hence multiwavelength laser sources employing semiconductor based gain medium suffers from minimal mode competition.

In the next section we describe the experimental results regarding the multiwavelength generation using a semiconductor based linear optical amplifier (LOA).

3.4 Multiwavelength semiconductor fiber ring laser using LOA

In the proposed scheme a linear optical amplifier (LOA) was utilized to provide inhomogeneous gain in the cavity to generate multiple wavelengths at room temperature. Figure 3.11 shows the configuration of multiwavelength FRL based on LOA as a gain medium. The laser source consists of an LOA, polarization controller (PC), polarization independent isolator, thin film etalon filter, and a 20 % fused coupler. The thin film etalon filter has a FSR of 0.8 nm (100 GHz) as shown in Fig 3.12 and exhibits absolute wavelength accuracy of +/- 1.25 GHz over a temperature range from 0 °C to 70 °C. The operation wavelength of the etalon filter is from 1520 nm to 1620 nm and its insertion loss is around 1.4 dB. The bandwidth of its wavelength peaks is around 0.1 nm and its extinction ratio is around 10 dB. The comb filters have spectral responses that are intensity modulated periodically in wavelength. The LOA is designed to operate in the C-band and has a maximum bandwidth gain flatness of 1.4 dB. The optical isolator in the cavity ensured a unidirectional operation of the ring cavity and avoided any unwanted reflections. The polarization controller adjusted the state of polarization in the laser cavity for achieving high SNR. The total length of the cavity was approximately 13 m and the total insertion loss of the cavity was estimated to be less than 3.2 dB. The laser output was taken from the 20% fused fiber coupler, which fed 80% of the light back into the cavity. The laser output was recorded respectively with an optical spectrum analyzer (OSA) with a spectral resolution of 0.1 nm and a power meter.

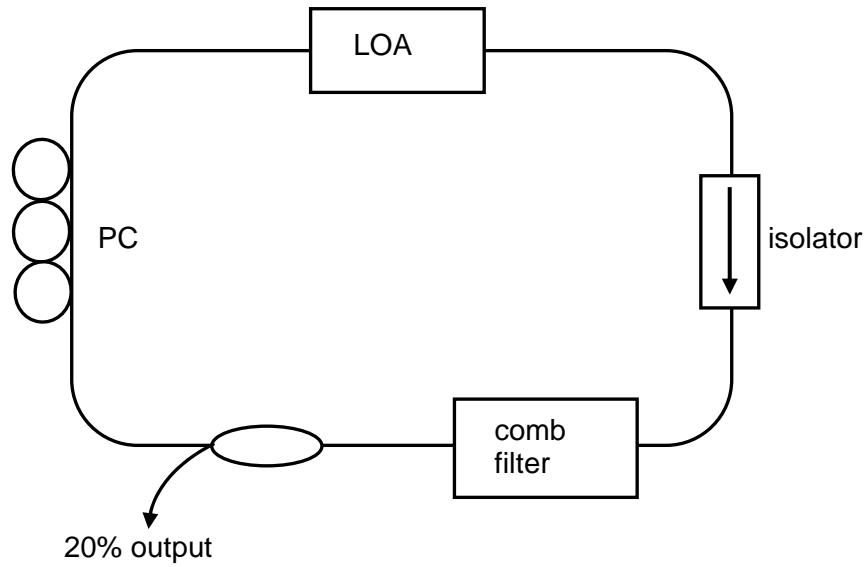


Fig. 3.11 Configuration of multiwavelength semiconductor fiber ring laser.
Note: PC: polarization controller; LOA: Linear optical amplifier

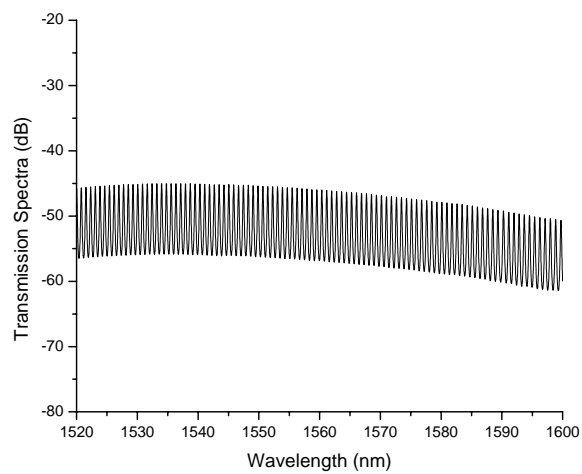


Fig. 3.12 Typical transmission spectrum of 100 GHz comb filter.

3.4.1 Experimental Results and Discussions

Figure 3.13 shows the spectrum of a multiwavelength semiconductor FRL that was measured with an OSA. The total power of the laser was 1.53 dBm. Over 38 wavelength simultaneous lasing oscillations were observed with a minimum signal to spontaneous noise ratio of ~ 20 dB. The wavelengths had the same frequency separation as that of thin film etalon filter, i.e 100 GHz. Around 20 lasing wavelengths exhibited optical signal to spontaneous noise ratio of greater than 45 dB as shown in Fig. 3.14. The output power of each lasing line is quite uniform and has an average value of around -12 dBm. The gain flatness in this range was maintained well without using a gain-equalizing filter, which contributes to the potential cost-effectiveness of the laser source. In multiwavelength lasers incorporating an inhomogeneous gain medium as LOA, the whole gain spectrum can be considered to be divided into discrete sections. The bandwidth of each such section is equal to the homogeneous linewidth of that medium. This makes the self saturation effect more pronounced than cross saturation effect. Hence, mode competition reduces appreciably in lasers incorporated with an inhomogeneous gain medium in contrast to lasers with homogeneous gain medium. Figure 3.15 shows the spectrum of a single channel measured with an OSA of 0.01 nm spectral resolution. The 3-dB linewidth is around 0.024 nm, limited by the resolution of OSA. The asymmetric shape of the laser is mainly caused by the response of OSA.

Although the LOA used in the cavity is designed for C-band but we operated it under saturated condition by applying optical feedback. Therefore, the carrier density of the LOA decreased due to strong optical feedback (80%) and shifted the gain profile

towards the longer wavelength side (red shift) of the spectrum [12].

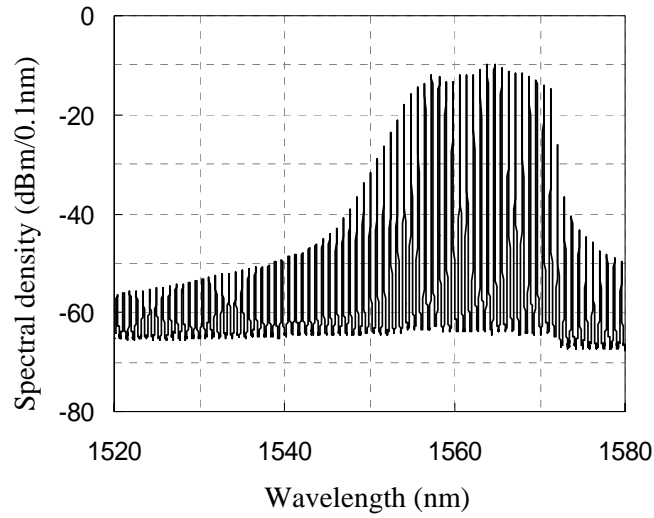


Fig. 3.13 MSFRL spectrum measured with an OSA with 0.1 nm resolution. .

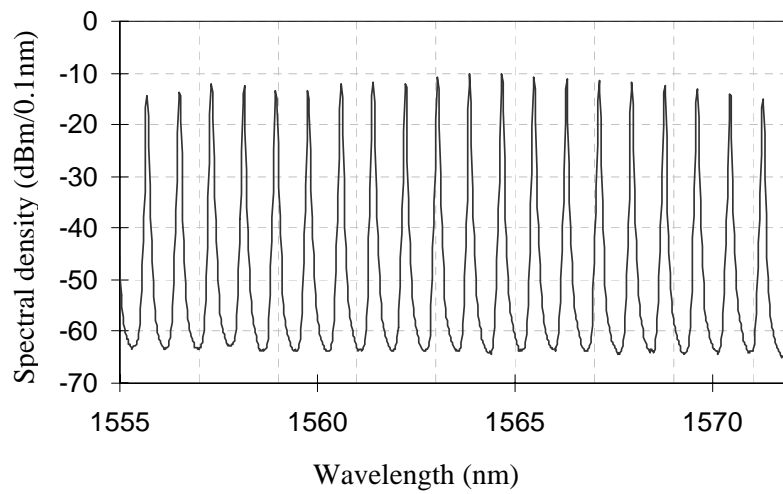


Fig. 3.14 Expanded view of laser spectrum of Fig 3.9 showing 20-simultaneous wavelength oscillations.

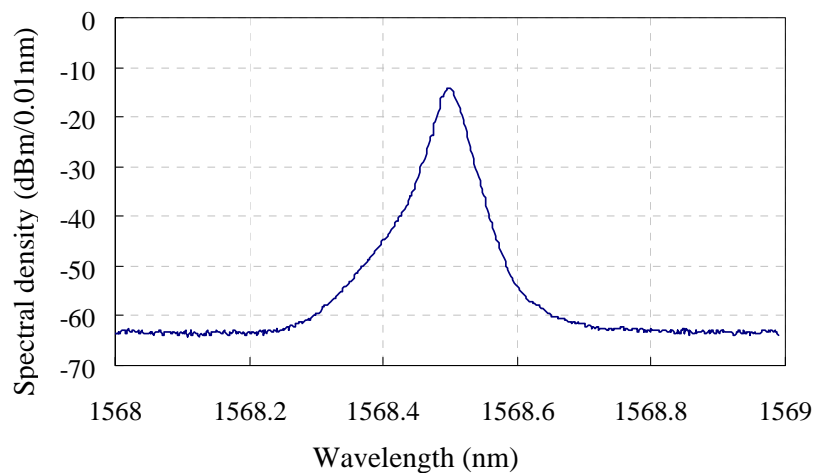


Fig. 3.15 Output spectrum of a single channel of MSFRL measured with an OSA of 0.01 nm resolution.

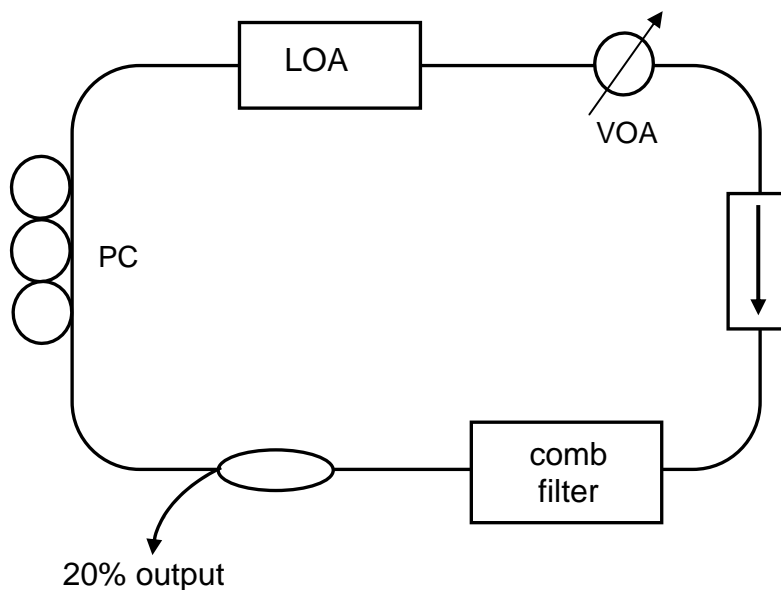


Fig. 3.16 Configuration of tunable multiwavelength semiconductor fiber ring laser.
 Note: PC; polarization controller; LOA; Linear optical amplifier; VOA; Variable optical attenuator.

The lasing spectra of the LOA-based ring laser can be tuned by varying the loss in the laser cavity. A variable optical attenuator with a dynamic range of 40 dB in the 1550 nm region was inserted inside the laser cavity as shown in Fig. 3.16. The multiple lasing wavelengths were tuned simultaneously as the attenuation level was adjusted. As the attenuation level was increased, the multiwavelength comb was blue shifted (to shorter wavelength region). The Figures 3.17(a-c) show the output spectra of the multiwavelength laser when the attenuation levels were set to 3, 5, and 7 dB respectively. Other parameters such as the biasing current applied to the LOA, and the output coupling ratio were kept constant during the tuning process. The experimental results have demonstrated a maximum tuning range of 22 nm (1548 ~1570 nm), which corresponds to the shift of the longest lasing wavelength as the attenuation level was increased from 0 to 7 dB. The maximum shift of shortest lasing wavelength is around 22 nm (1526~1548 nm).

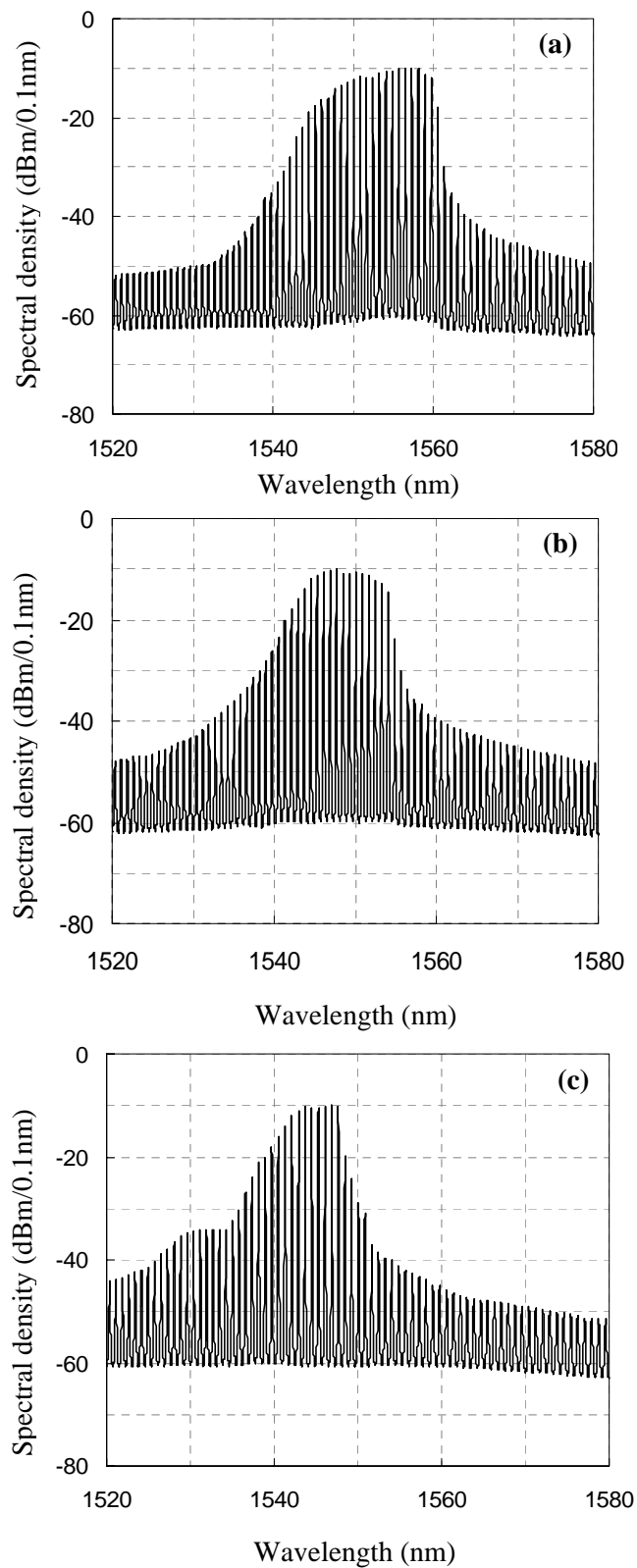


Fig. 3.17 MSFRL spectra tuning with variable optical attenuator. The attenuation levels are (a) 3 dB, (b) 5 dB, and (c) 7 dB.

In order to measure the stability of the laser source, a single laser channel was filtered out and its output power was observed for 3 hours using an optical power meter. The measurements were recorded after an hour of the initial startup of the setup to allow for the LOA current driver circuitry to be stabilized. The optical SNR of the lasing output was very large (> 50 dB). The measured total power of this channel was around -15.8 dBm. The data was collected after an interval of 1 minute. The power fluctuation measured with a power meter was less than 0.2 dB as shown in Fig. 3.18(a). The inset (i) of Fig. 3.18 (a) shows the spectrum of a single wavelength channel obtained by using a thin film tunable filter with a 3-dB bandwidth of 0.14 nm and designed for working in C-band, while the inset (ii) shows the micro-second time scale power fluctuation. The LOA in the cavity was then replaced with an SOA in order to compare the performance of the ring laser using two different gain media. The stability test was conducted for 2 hours and it was found that the power fluctuation was over 2 dB at different instances of time as shown in Fig. 3.18(b). The inset (i) shows the spectrum of a single wavelength channel obtained by using a tunable grating filter with a 3 dB bandwidth of 0.22 nm and designed for working in L-band, while the inset (ii) shows the micro-second time scale power fluctuation. This comparison has revealed that an LOA based multiwavelength ring laser is very stable when compared to SOA based laser source.

The manufacturer (Finisar) of LOAs has recently stopped its production. Therefore, in order to develop semiconductor devices with a similar performance, we developed a gain clamped SOA using external optical feedback and then employed it for stable multiwavelength generation. The proceeding section 3.5 explains the realization of a gain clamped SOA.

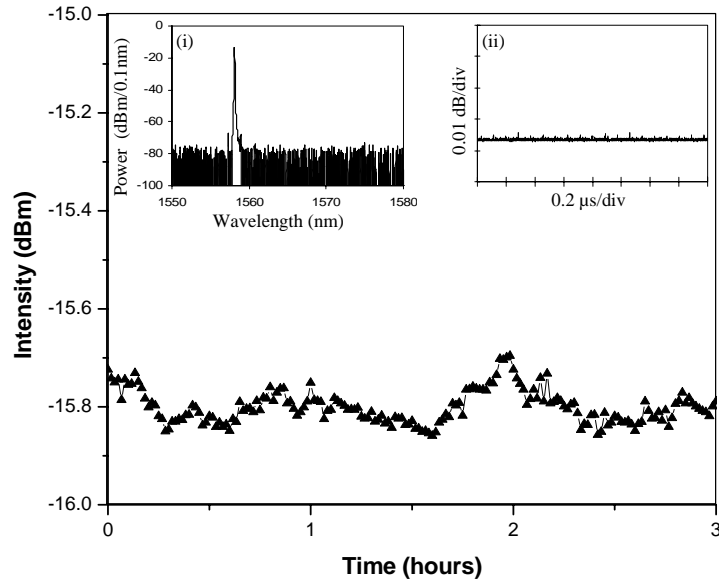


Fig. 3.18 (a)

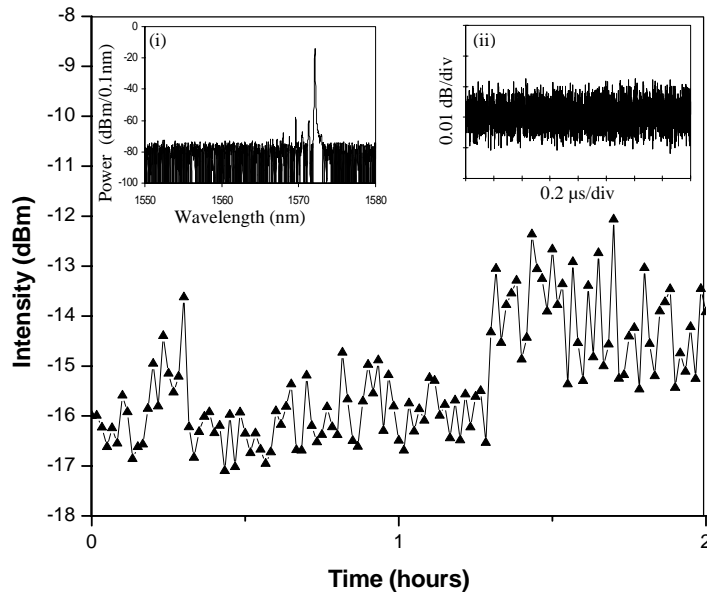


Fig. 3.18 (b)

Fig. 3.18 (a) Variation of intensity with time for a single wavelength channel for a LOA based ring laser. Inset (i) shows the spectrum of a single filtered channel from the output of the LOA-based ring laser. Inset (ii) shows the micro-second time scale power fluctuation. (b) Variation of intensity with time for a single wavelength channel for a SOA based ring laser. Inset (i) shows the spectrum of a single filtered channel from the output of the SOA-based ring laser. Inset (ii) shows the micro-second time scale power fluctuation.

3.5 Gain clamped SOAs

External light injection into SOA has been extensively studied. Manning and Davies [13] theoretically demonstrated that external light injection into SOA could increase the stimulated recombination rates and reduce their gain recovery times. Yoshino and Inoue [14] experimentally demonstrated that external light injection into an SOA could increase its saturation output power and that it could shorten its gain response time and improve the waveforms of the amplified signal outputs modulated at 7.5 Gb/s [15]. Applications of this technique include reducing the crosstalk in a wavelength division multiplexing (WDM) system [16,17] or a multichannel quadratic-amplitude-modulation (QAM) system [18], improving the cascability of SOA gates [19,20], and reducing the response time in all-optical nonlinear devices [21-23].

In [24,25] the light injection at or near transparency wavelength of the SOA has been used to achieve fast response without reducing the gain of the SOA. In the following section we delineate the experimental verification of gain clamping by employing different techniques.

3.5.1 Gain clamping techniques

The output gain of SOA can be controlled by two methods, namely (i) gain control by current injection, and (ii) gain control by optical feedback.

3.5.1.1 Gain Control using Current Injection

The SOA module used in the following experiments was manufactured by Samsung Corporation (Korea) and was designed for operation in C-band (1520-1565 nm). When the SOA was biased at 185 mA, it exhibited a small signal gain of about 18 dB with a polarization sensitivity of less than 1 dB. The 3-dB saturation output power was around ~3 dBm at a wavelength of 1550 nm.

Figure 3.19 shows the amplified spontaneous emission (ASE) spectra of the SOA at different biasing currents. The ASE spectrum is obtained by using an OSA with a spectral resolution of 0.1 nm. The ASE profile has a gain peak at around 1540.6 nm for a biasing current of 185 mA. The 3-dB gain flatness at this biasing current is 30 nm.

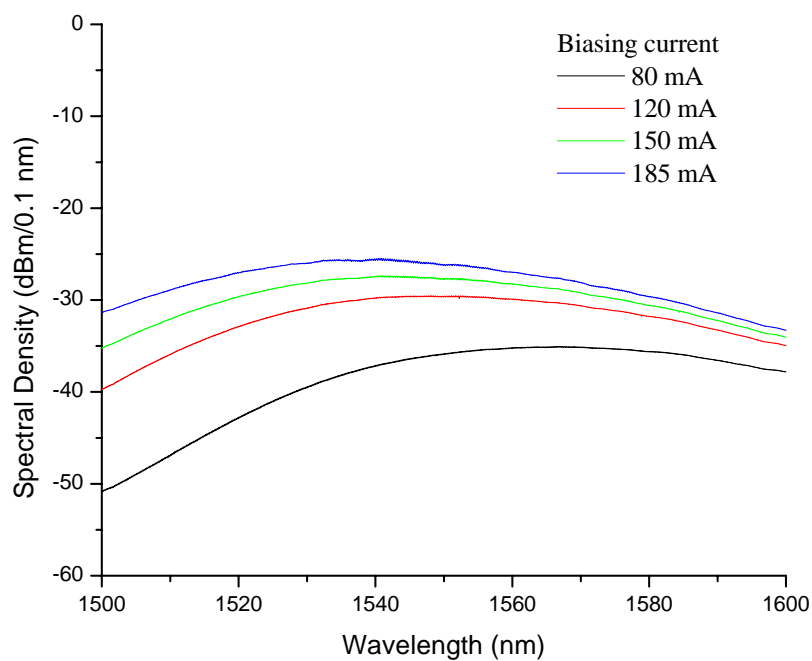


Fig. 3.19 ASE spectrum of the SOA for different biasing currents

Figure 3.20 plots the dependence of SOA gain on injection current. The SOA gain increases with an increase in injection current. By reducing the injection current from 185 to 60 mA, the module gain was reduced by 16.65 dB (from 18.5 to 1.85 dB) for a signal light wavelength of 1550 nm.

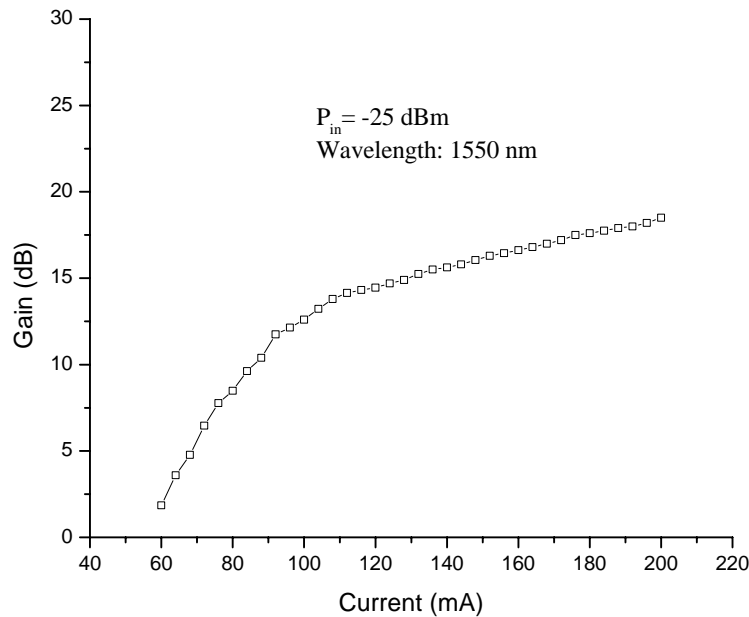


Fig. 3.20 Dependence of module gain on injection current; signal-light wavelength was 1550 nm.

Figure 3.22 plots the gain saturation characteristics of SOA at different injection currents. The experimental setup used to perform this analysis is depicted in Fig. 3.21. A wavelength tunable laser at a wavelength of 1550 nm was used as a light source. A variable optical attenuator (VOA) was used at the input side of the SOA to adjust the input signal power fed to the SOA module. By reducing the current from 185 mA to 80 mA, the gain was reduced by 9.25 dB (from 17.8 dB to 8.55 dB). When the injection current was reduced, both the unsaturated gain and the saturation output power were reduced.



Fig. 3.21 Experimental setup for gain saturation characteristics

Note: TLS – Tunable Laser Source, SOA – Semiconductor Optical Amplifier; VOA – Variable Optical Attenuator; OSA – Optical Spectrum Analyzer

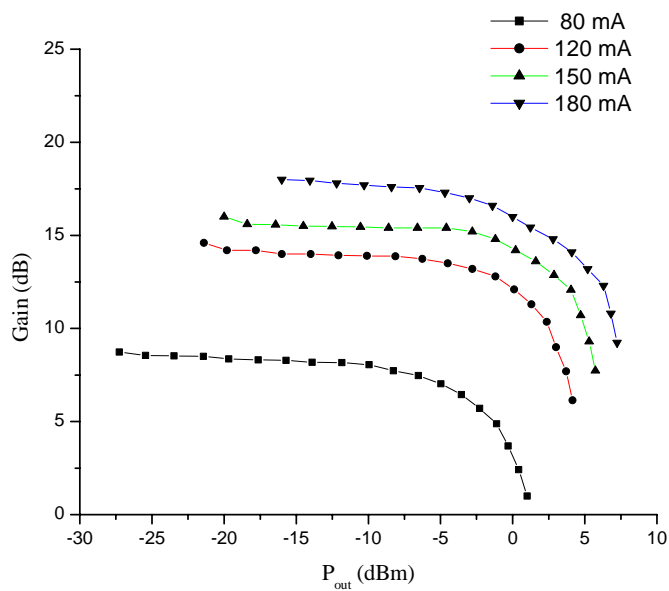


Fig. 3.22 Gain-saturation characteristics at different SOA currents for CW signal; signal-light wavelength was 1550 nm.

3.5.1.2 Gain control by optical feedback

In this section, the gain-control characteristics of an SOA by external feedback injection are discussed. When a CW light, other than the signal light is fed back to the SOA as a control light, it will change the gain seen by the input signal, since the depth of the gain saturation in the SOA is changed. This is also known as cross gain modulation (XGM). Increasing the feedback signal power decreases the input signal gain, while the saturation output power remains constant or increases. This is because the feedback control signal shortens the carrier lifetime due to an enhanced stimulated emission process [14-16]. The benefit of this scheme is that by decreasing the signal gain while increasing the saturation output power raises the upper limit for the allowable signal input level. This is quite different than that of gain-control method using injection current. It gives the SOA the practical capability of controlling the output level, which achieves both a high target output level and a wide input dynamic range with high input levels [26,27].

3.5.1.2.1 Using CWDM couplers

Figure 3.23 shows the experimental setup for the demonstration of gain clamped SOA realized using a single oscillating laser in feedback. In order to measure the gain characteristics of this scheme, the input continuous wave (CW) signal was injected at 1550 nm. The SOA biasing current was fixed at 185 mA. The feedback laser was generated by inserting a Fabry P erot tunable filter (FFP-TF) in the ring cavity as depicted in the experimental setup. The coarse wavelength division multiplexing (CWDM)

couplers were used at the input and output respectively. The two CWDM couplers have a pass-band centered at 1550 nm and their 3-dB bandwidth is around 17.5 nm as shown in Fig. 3.24. The reflection spectrum of the CWDM coupler is also depicted in Fig. 3.24. The out of band reflection from the ends of the FFP-TF is high and hence two isolators were used at the input and output end of the FFP-TF. The two isolators reduced the reflection from FFP-TF to the SOA as well as they ensured unidirectional operation of feedback. The operable temperature range of this FFP-TF is from -20 to +80 C. The tuning Voltage/FSR is from (0-16) Volts. The Finesse of the fiber FFP-TF is around 3400 and the insertion loss of its pass-band is around 2.2 dB. The optical intensity of feedback laser was controlled by inserting a variable optical attenuator (VOA) in the cavity. In the proposed scheme, first the feedback laser was generated in the co-propagation direction to the input CW light beam and later its characteristics were studied by introducing feedback laser in counter-propagation direction. The direction of feedback laser is established by the two isolators in the cavity.

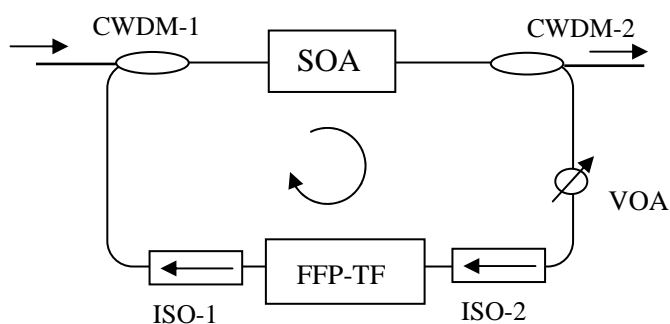


Fig. 3.23 Experimental setup of the gain-clamped SOA with co-propagation feedback. Note: SOA – Semiconductor Optical Amplifier; CWDM – Course Wavelength Division Multiplexer; VOA – Variable Optical Attenuator; FFP-TF – Fiber Fabry PÉrot-tunable filter; ISO – Isolator

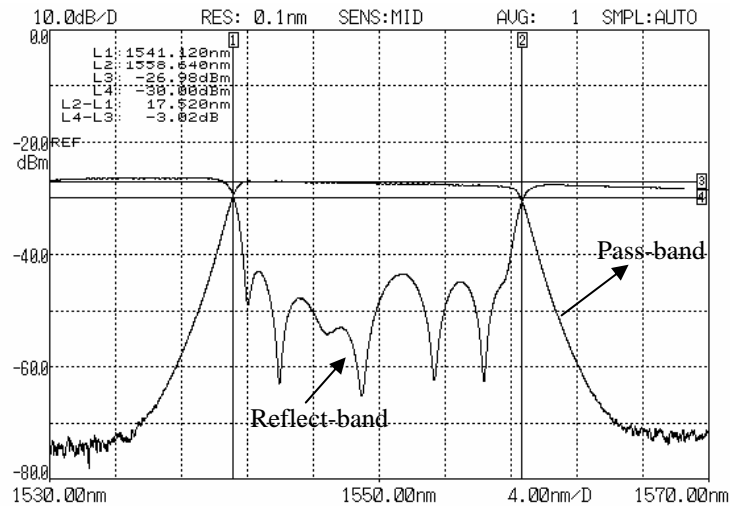


Fig. 3.24 Transmission and Reflection spectra of CWDM

Figure 3.25 plots the gain of the gain clamped SOA (GC-SOA) for a CW signal set at 1550 nm for different wavelengths of feedback oscillating laser. When the intensity of the feedback laser is increased the linear gain seen by input CW signal is decreased. This is because of shortening of the carrier lifetime due to an enhanced stimulated emission process as discussed before. The optical intensity of the feedback laser was maximum when the VOA was set at 0 dB. It is also evident from Fig. 3.25 that the linear gain for the input CW signal is lower when the feedback laser is within the gain bandwidth of the SOA compared to the case when the feedback is applied outside the gain bandwidth. The linear gain is around 15 dB when the feedback wavelength is 1597 nm, which is outside the gain bandwidth of the SOA whereas it decreases to around 12.5 dB, when the feedback wavelength is 1537 nm which lies within gain bandwidth of the SOA. The gain clamping effect could be sustained for the input signal power up to -8.5 dBm and -11 dBm for the feedback laser at 1537 nm and 1597 nm respectively. The gain

flatness was within 1 dB. The gain flatness was maintained without using any gain-equalizing filter, which contributes to the potential cost-effectiveness of this scheme.

When the feedback laser lies within the gain bandwidth of SOA, it depletes the gain seen by the incoming input signal more in contrast to the feedback laser outside the gain bandwidth. The 3-dB saturation output power of the normal SOA (without gain clamping) was ~ 3 dBm which increases to ~ 6 dBm for the GC-SOA.

In the continuation of the present analysis of gain control by external feedback, the feedback intensity in the cavity was reduced by 5 dB using VOA. In this case, the feedback laser would not deplete the gain seen by the incoming CW beam as much as before (when the VOA was 0 dB) and hence the gain seen by the incoming beam was higher than before. Figure 3.26 plots gain of the GC SOA for a CW signal set at 1550 nm for different wavelength of feedback oscillating laser. The gain is around 13.9 dB when the feedback wavelength is 1537 nm, which is within the gain bandwidth of the SOA, whereas the gain increases to around 15.8 dB when the feedback wavelength is 1597 nm. The 3-dB saturation output power is around ~ 5 dBm in both cases.

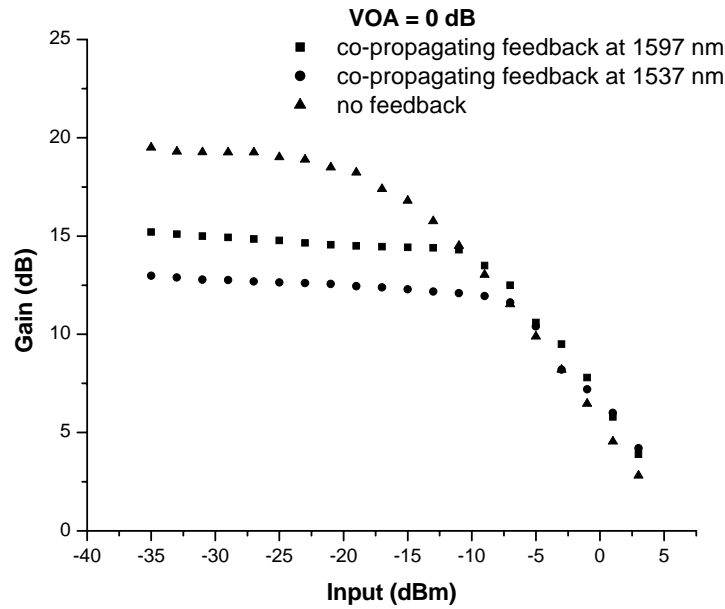


Fig. 3.25 Gain-characteristics with different wavelength feedback oscillating laser in co-propagating direction; SOA was biased at 185 mA. Signal light wavelength was 1550 nm. VOA= 0 dB

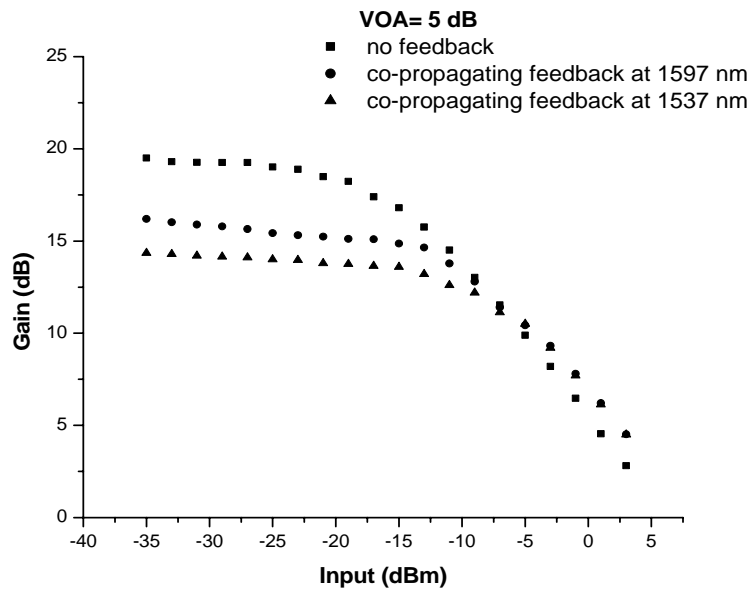


Fig. 3.26 Gain-characteristics with different wavelength feedback oscillating laser in co-propagating direction; SOA was biased at 185 mA. Signal light wavelength was 1550 nm. VOA= 5 dB

Next we evaluated the effect of counter-propagation feedback on the gain of the input CW signal at 1550 nm. Figure 3.27 illustrates the experimental setup for the GC-SOA using counter-propagation feedback scheme. The experimental setup for this scheme is similar to the one for co-propagation scheme except that the direction of the two isolators is reversed here.

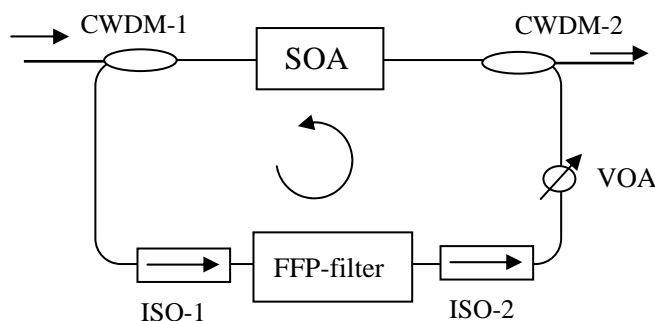


Fig. 3.27 Experimental setup of gain-clamped SOA with counter-propagating feedback
Note: SOA – Semiconductor Optical Amplifier; CWDM – Course Wavelength Division Multiplexer; VOA – Variable Optical Attenuator; FFP-TF – Fiber Fabry PÉrot-tunable filter; ISO – Isolator

Figure 3.28 plots the gain of the GC-SOA for a CW signal set at 1550 nm. The gain was measured for different wavelengths of feedback oscillating laser. When the VOA was set to 0 dB, the intensity of the feedback laser was maximum and hence the gain experienced by the input CW signal is minimal. The linear gain is around 15.1 dB

when the feedback light wavelength is 1597 nm, which is outside the gain bandwidth of the SOA, whereas it reduces to around 12.54 dB when the feedback wavelength is 1537 nm, which is within the gain bandwidth of the SOA. The 3-dB saturation output power in both cases is around ~ 5 dBm. The gain clamping effect can be sustained for the input signal power level up to -8.4 dBm and -11 dBm for the feedback laser light at 1537 nm and 1597 nm respectively. For the linear regime, the gain flatness is within 1 dB.

Next, the feedback intensity in the cavity was reduced by 5 dB using a VOA. In this case, the feedback laser would not deplete the gain seen by the incoming CW beam as much as before and hence the gain seen by the incoming beam is higher than before. Figure 3.29 depicts the gain of the GC-SOA for a CW signal set at 1550 nm for different wavelengths of feedback oscillating laser. The gain is around 13.8 dB when the feedback light wavelength is 1537 nm which is within the gain bandwidth of the SOA. However, the gain is around 15.6 dB when the feedback light wavelength is 1597 nm. The gain flatness is within 2 dB for the two cases.

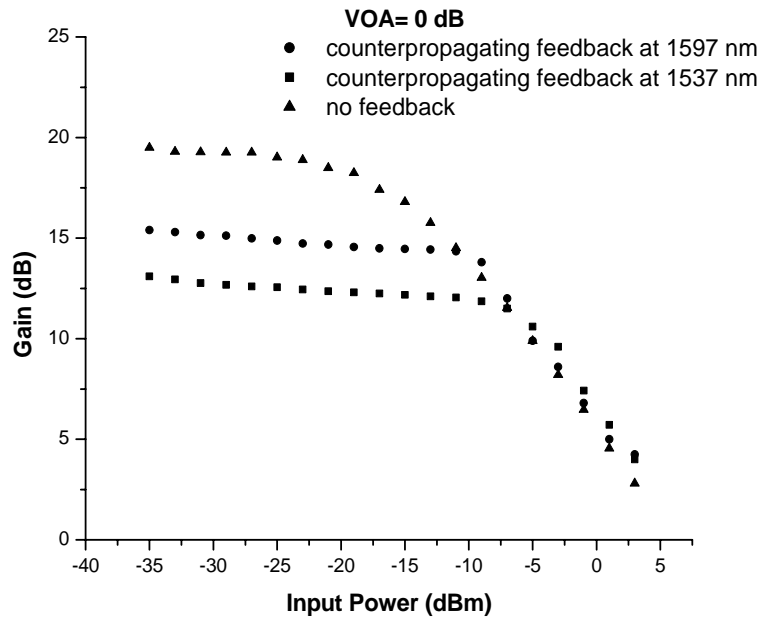


Fig. 3.28 Gain-characteristics with different wavelength feedback oscillating laser in counter-propagating direction; SOA was biased at 185 mA. Signal light wavelength was 1550 nm. VOA= 0 dB.

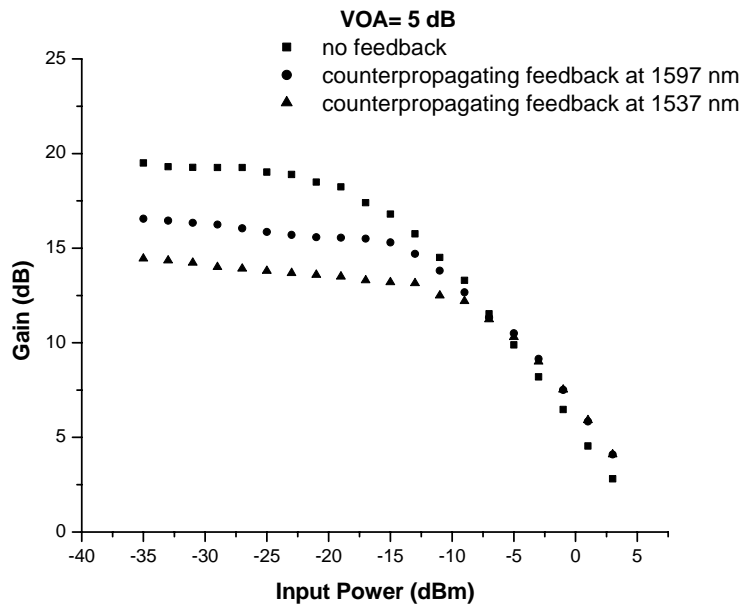


Fig. 3.29 Gain-characteristics with different wavelength feedback oscillating laser in counter-propagating direction; SOA was biased at 185 mA. Signal light wavelength was 1550 nm. VOA= 5 dB.

After the detailed investigation of co and counter-propagation schemes, it can be concluded that the direction of feedback does not affect the gain characteristics of the input CW light beam. In the next section we utilize two circulators to simplify the configuration of the GC-SOA. In this configuration, the circulators perform two functions. Firstly, they couple the light into the GC-SOA as well as provide the output path. Secondly, they establish the direction of the feedback oscillating laser.

3.5.1.2.2 Using circulators

Figure 3.30 shows the experimental setup for the demonstration of gain clamping of an SOA using single oscillating laser in feedback. In order to measure the gain of this scheme, the input signal was injected at 1550 nm. The feedback laser was generated by inserting a FFP-TF in the ring cavity. The two circulators in the ring defined the direction of feedback laser oscillation. In the proposed scheme, the feedback laser was in counter-propagation direction to the input CW light beam.

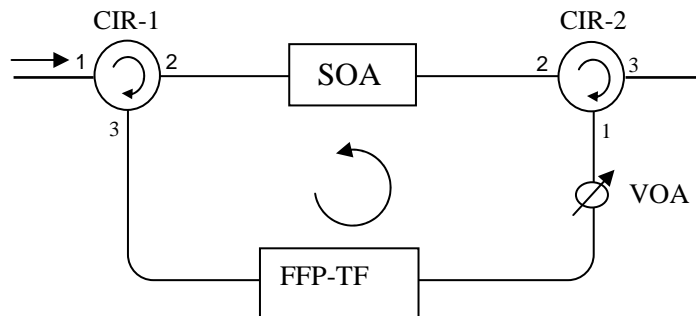


Fig. 3.30 Experimental setup of the gain-clamped SOA.

Note: SOA – Semiconductor Optical Amplifier; CIR – Circulator;

VOA – Variable Optical Attenuator; FFP-TF – Fiber Fabry Pérot-tunable filter.

A variable optical attenuator (VOA) was also inserted in the cavity to control the intensity of the feedback oscillating laser. The FFP-TF has a large free spectral range (FSR) and is employed to tune the feedback lasing wavelength. The optical bandwidth of the FFP-TF is about 30 pm and the FSR is about 100 nm. The insertion loss of the FFP-TF at the peak of its pass-band is about 2.2 dB. The out of band reflection from both ends of the FFP-TF is high. The circulators at both ends of the FFP-TF are used to reduce the reflection from FFP-TF to the SOA. They also ensure unidirectional operation of the feedback. The operable temperature range of this FFP-TF is from -20~80 C. The tuning Voltage/FSR is about 16 V. The experiment was performed at different feedback lasing wavelengths. We provided the feedback at two different wavelengths (i) within the gain bandwidth of SOA (1520 – 1560 nm) (ii) outside the gain bandwidth of SOA. The wavelengths chosen for feedback laser were 1537 nm and 1597 nm respectively.

Figure 3.31 illustrates the gain of the GC SOA for a CW signal set at 1550 nm for different wavelengths of feedback oscillating laser. When the intensity of the feedback laser was increased the linear gain seen by input CW signal was reduced. When VOA was set at 0 dB, the intensity of the feedback laser was maximum. The linear gain is around 15.0 dB when the feedback wavelength is 1597 nm, which is outside the gain bandwidth of the SOA, whereas it reduces to around 12.45 dB when the feedback laser wavelength is 1537 nm, which is within the gain bandwidth of the SOA. The 3 dB saturation output power in both cases is around ~ 6 dBm. The gain clamping effect can be sustained for the input signal power up to -8.0 dBm and -11 dBm for the feedback lasers at 1537 nm and 1597 nm respectively. The gain is clamped within ~ 0.5 dB for both cases.

Now the feedback intensity in the cavity is reduced by 5 dB using a VOA. In this case the feedback laser would not deplete the gain seen by the incoming CW beam as much as before and hence the gain seen by the incoming beam is higher. Figure 3.32 plots the gain of the GCSSOA for a CW signal set at 1550 nm for feedback oscillating lasers of different wavelengths. The gain is around 15.2 dB when the feedback laser wavelength is 1537 nm which is within the gain bandwidth of the SOA. The gain is around 16.2 dB when the feedback laser wavelength is 1597 nm. In this case the linear gain is clamped within ~ 1 dB.

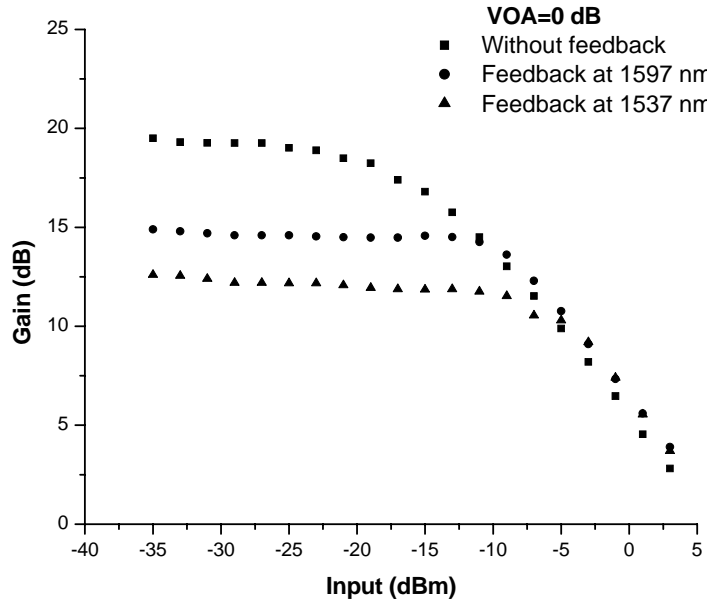


Fig. 3.31 Gain-characteristics with different wavelength feedback oscillating laser in counter-propagating direction; SOA was biased at 185 mA. Signal light wavelength was 1550 nm. VOA= 0 dB.

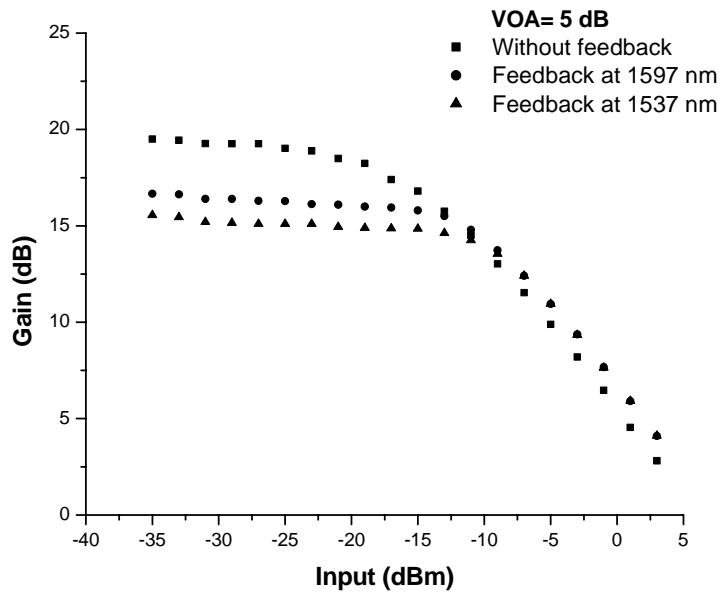


Fig. 3.32 Gain-characteristics with different wavelength feedback oscillating laser in counter-propagating direction; SOA was biased at 185 mA. Signal light wavelength was 1550 nm. VOA= 5 dB.

3.5.2 Switching transients in a multiwavelength scenario

In order to determine the mode competition experienced by different wavelength channels in a multiwavelength environment, the switching transient response of the GC-SOA should be studied. The aim is to understand how the gain of the surviving wavelength channel varies when the other wavelength channels are added or dropped abruptly. When the wavelength channels are added or dropped, the power of the surviving channel decreases or increases due to the phenomenon of cross saturation in the amplifier as discussed in section 3.3. To maintain quality of service for surviving wavelength channels, it is necessary to limit the power excursions they experience. Next we will describe the use of a gain clamped SOA, realized by introducing optical feedback as discussed in section 3.4.1, to minimize the power excursions experienced by the surviving channels.

3.5.2.1 Experiments and Discussions

The experimental setup used for performing the gain excursion measurements is schematically depicted in Fig. 3.33. Two tunable lasers simulated the power of 8 wavelength channels. The tunable laser (TL-1) was externally modulated (on/off) at 20.9 KHz to mimic the on-off channels in a multiwavelength scenario. Another tunable laser (TL-2) acted as a surviving channel. The wavelength of TL-1 and the TL-2 were 1550 nm and 1554 nm respectively. The two light sources were combined using a 3-dB coupler and then launched into the gain clamped SOA configuration. The two lasers were set so that when both the lasers are on, the total input power to the gain clamped

SOA is -15 dBm, as would result from eight wavelength channels with an input power of -24 dBm each. The input power from TL-1 is around -15.58 dBm to simulate 7 wavelength channels. The power of surviving channel (TL-2) is fixed at -24 dBm. The gain for the surviving channel is maintained at 15 dB. After the gain clamped SOA, a band-pass filter was used to select the un-modulated channel. The optical power of this channel was detected and the transient response was measured by an oscilloscope. Figure 3.34 shows the output transients experienced by the surviving channel upon the add/drop channels in three cases: (a) without optical feedback (b) with optical feedback at 1597 nm, and (c) with optical feedback at 1537 nm. The maximum transient ratio is defined as $K_m = (P_{max} - P_{min})/P_a$, where P_{max} , P_{min} , and P_a are respectively, maximum, minimum, and average output power of the surviving channel. The maximum steady state transient ratio of the surviving channel is 0.3529 for the case when there is no feedback gain clamping mechanism. In contrast, the steady state transient ratios are 0.25 and 0.095, when the applied feedback is at 1597 nm and 1537 nm respectively. Clearly, the feedback laser at 1537 nm provides the tightest transient control. When no feedback is applied, the surviving channel experiences a very strong cross gain modulation effect which reduces when the feedback is used. The feedback signal at 1537 nm provides the tightest transient control since it is within the gain bandwidth of SOA and hence shares the gain with the surviving channel more effectively than the signal at 1597 nm which is outside the gain bandwidth of the SOA.

In order to see the effect of direction of feedback on the gain transients we reversed the direction of the two isolators as shown in Fig. 3.35. From Fig. 3.36 it can be seen that the steady state transient ratios are 0.235 and 0.1, when the applied feedback is

at 1597 nm and 1537 nm respectively. Clearly, the feedback laser at 1537 nm provides the tightest transient control. Hence, it can be concluded that the direction of feedback does not affect the ratio of steady state transients appreciably.

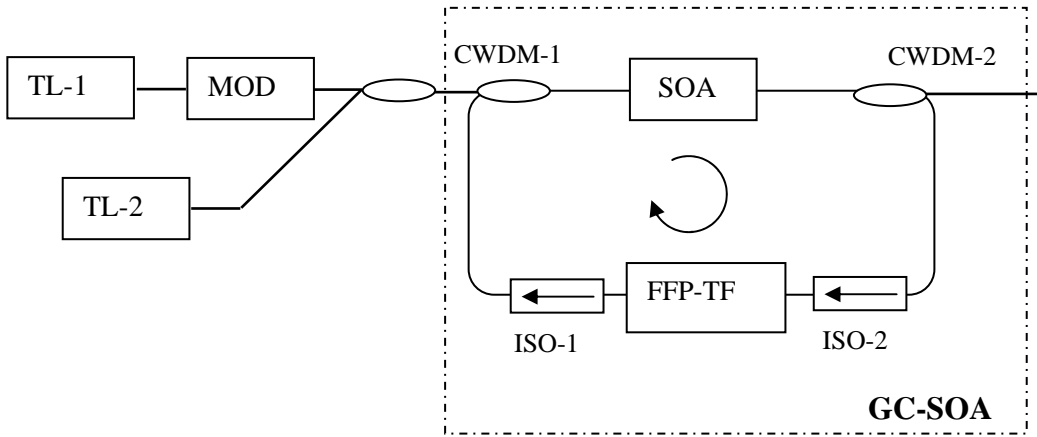


Fig. 3.33 Experimental setup to study the transient control of surviving channel (1554 nm) in the presence of add/drop signal at 1550 nm (feedback is applied in co-propagating direction).

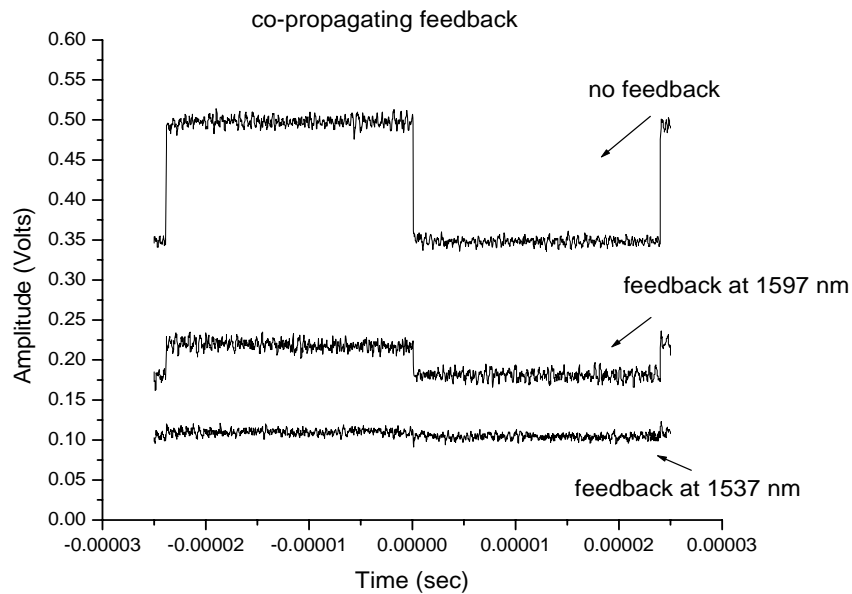


Fig. 3.34 Output transients of surviving channel (1554 nm) in the presence of add/drop signal at 1550 nm (feedback is applied in co-propagating direction).

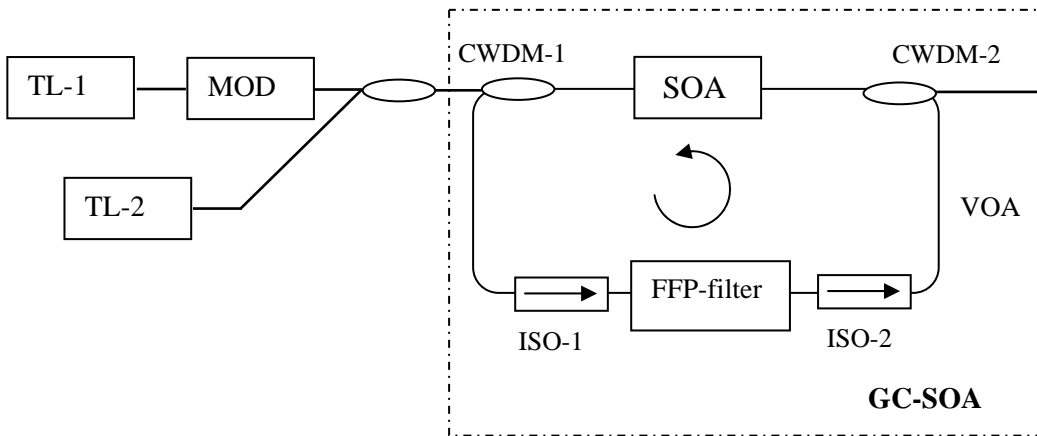


Fig. 3.35 Experimental setup to study the transient control of surviving channel (1554 nm) in the presence of add/drop signal at 1550 nm (feedback is applied in counter-propagating direction).

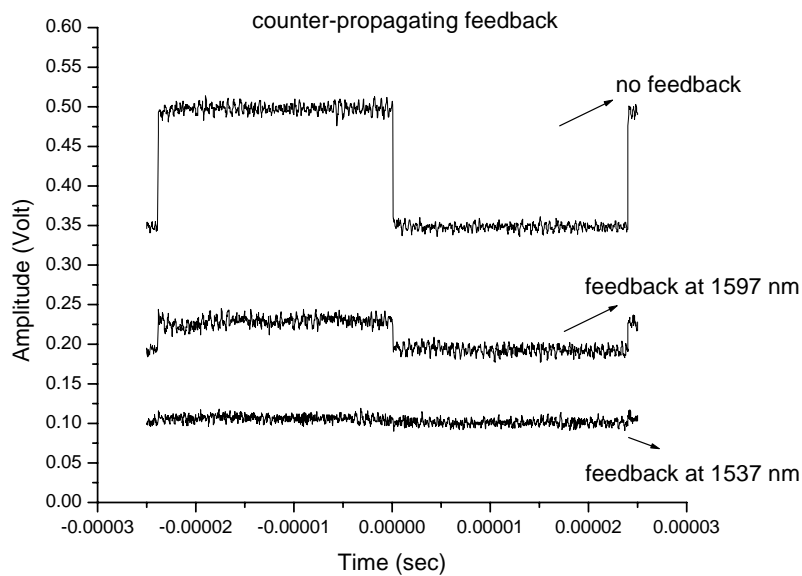


Fig. 3.36 Output transients of surviving channel (1554 nm) in the presence of add/drop signal at 1550 nm (feedback is applied in counter-propagating direction).

In the continuation of the present analysis we replaced the two CWDMs and the two isolators in the cavity of GC-SOA with two circulators to simplify the configuration of the GC-SOA. The experimental configuration used to study the gain transient performance of this GC-SOA is shown in Fig. 3.37. The circulators in this setup can only provide the feedback in the counter-propagating direction. However, it is worth mentioning that the direction of feedback does not affect the performance of this scheme, as was observed in the previous experiments described in section 3.5.1.2. In Fig. 3.38, the steady state transient ratios are 0.21 and 0.048, when the applied feedback is at 1597 nm and 1537 nm respectively. Clearly, the feedback laser at 1537 nm provides the tightest transient control. The GC-SOA is not only useful for dynamic WDM systems but can also be used as a gain medium in a laser source configuration where different wavelengths should be amplified by the laser cavity gain medium and the gain or loss of one wavelength should not affect the other wavelengths. In the next section we delineate that how this GC-SOA scheme can be effectively utilized to realize a stable multiwavelength laser source.

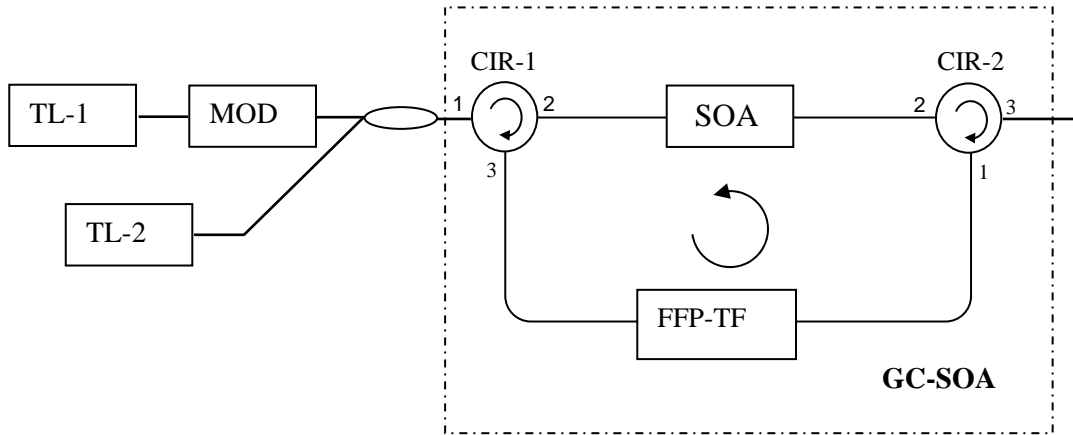


Fig. 3.37 Experimental setup to study the transient control of surviving channel (1554 nm) in the presence of add/drop signal at 1550 nm (feedback is applied in counter-propagating direction).

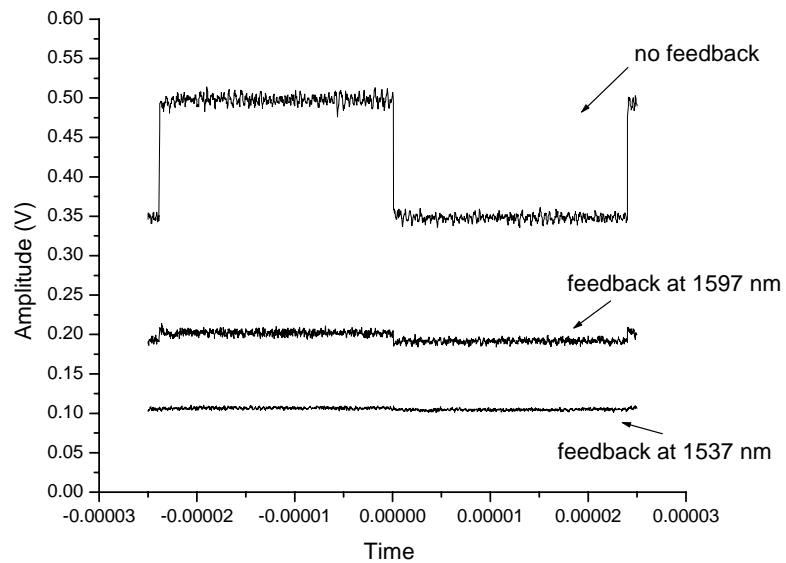


Fig. 3.38 Output transients of surviving channel (1554 nm) in the presence of add/drop signal at 1550 nm (feedback is applied in counter-propagating direction).

3.6 Multiwavelength generation using a gain clamped SOA

In section 3.5 it was experimentally demonstrated that the performance of a GC-SOA improves in terms of gain transients excursions by applying optical feedback. This attribute of the GC-SOA is essential for realizing a stable multiwavelength laser source. Here we are implementing a multiwavelength laser source using the aforementioned GC-SOA as a gain medium. The multiwavelength semiconductor FRL is illustrated schematically in Fig. 3.39. The laser source consists of two rings. The first ring provides the optical feedback to realize a gain clamped SOA, whereas the second ring serves as the main ring of the laser source. The feedback laser was tuned to 1537 nm, since this wavelength provides the tightest transient control and would help to reduce the gain competition in a multiwavelength environment. The direction of feedback laser in the GC-SOA was established by the two circulators and was in counter-propagating direction to the main cavity direction. The two circulators in the GC-SOA determine the direction of feedback laser as well as avoid any unwanted reflections from the FFP-TF to the SOA. The main ring consists of a polarization controller (PC), thin film etalon filter, variable optical attenuator (VOA), and a 20 % fused coupler. The thin film etalon filter has a FSR of 0.8 nm (100 GHz) as shown in Fig 3.12 and exhibits absolute wavelength accuracy of ± 1.25 GHz over a temperature range from 0 °C to 70 °C. The operation wavelength of the etalon filter is from 1525 nm to 1620 nm and its insertion loss is around 1.4 dB. The bandwidth of its wavelength peaks is around 0.1 nm. The extinction ratio of the etalon filter is around 10 dB. The SOA is designed to operate in the C-band and was biased at 185 mA. The polarization controller adjusts the state of polarization in the laser cavity to achieve high SNR. The total insertion loss of the cavity was estimated to be less than 4

dB. The laser output was taken from the 20% fused fiber coupler, which fed 80% of the light back into the cavity. The laser output was recorded with an optical spectrum analyzer with a spectral resolution of 0.1 nm.

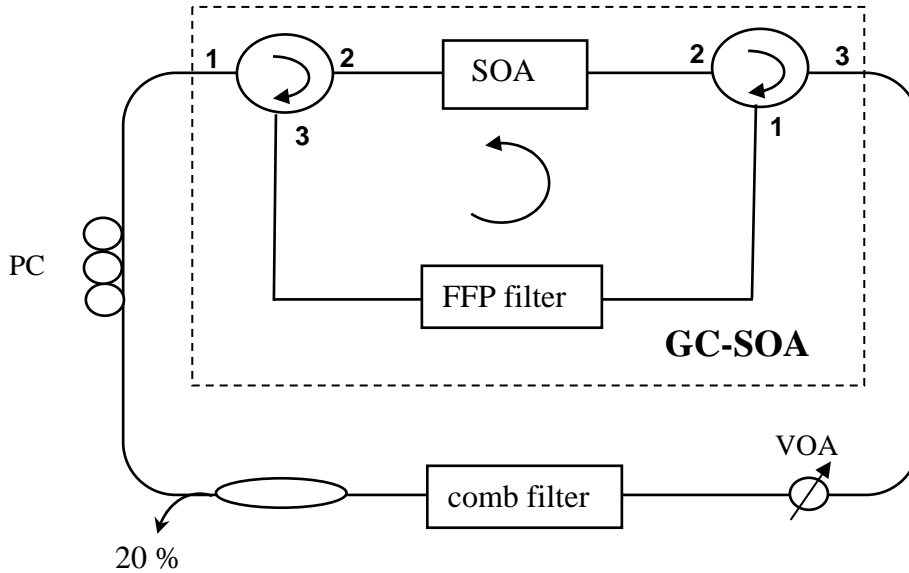


Fig. 3.39 Configuration of multiwavelength semiconductor fiber ring laser using gain clamped SOA. Note: PC: polarization controller; SOA: Semiconductor optical amplifier, VOA; Variable optical attenuator

Figure 3.40 shows the multiwavelength semiconductor fiber ring laser (SFRL) spectrum that was measured with an optical spectrum analyzer. The lasing lines have the same frequency separation as that of thin film etalon filter, i.e 100 GHz. In order to measure the stability of the laser source, a single laser channel was filtered out and its output power was observed for 1 hour and 40 minutes using an optical power meter. The

measurements were recorded after an hour of initial startup of the setup to allow for the LOA current driver circuitry to be stabilized. The optical SNR of the lasing output was very large. The data was taken after an interval of 1 minute. The power fluctuation measured with a power meter was within 0.2 dB as shown in Fig. 3.41. This measurement proved that the performance of a laser source employing a gain clamped SOA is comparable to that of a laser source employing an LOA as a gain medium in terms of stability.

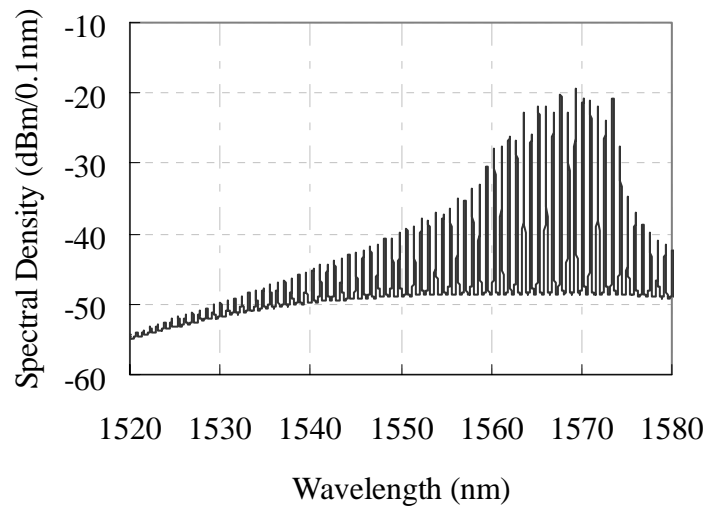


Fig. 3.40: MSFRL spectrum measured with an OSA with 0.1 nm resolution. .

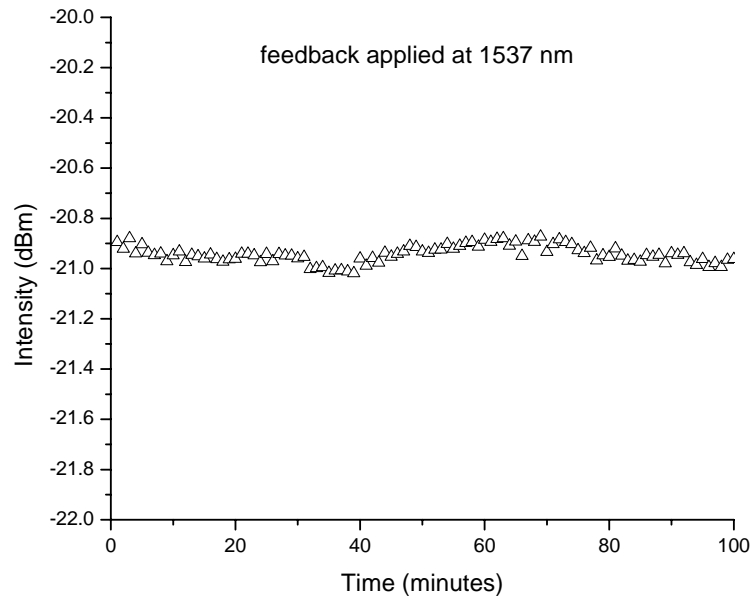


Fig. 3.41 (a) Variation of intensity with time for a single wavelength channel for a SOA based ring laser.

3.7 Chapter Summary

This chapter has introduced a new type of gain clamped semiconductor optical amplifier (LOA). Different properties of LOA were described and verified by experiments. LOA exhibits a flat gain over a wide spectral range. This property was used to construct a single frequency SFRL with a wide tunable range. A broad tuning range of over 90 nm was achieved by employing a narrow linewidth tunable Fabry P erot filter in the cavity.

Next the conditions for stable multiwavelength operation of a laser were described using intensity growth equations. The analysis revealed that the stable multiwavelength generation depends on the strong self-saturation effect rather than the cross-saturation effect. A multiwavelength SFRL using an LOA as a gain medium was constructed and compared to an SOA based laser. The results of the stability test on a single channel revealed that a laser source employing LOA as a gain medium is more stable than an SOA based laser.

Finally, a gain clamped SOA was constructed and was subsequently used as a gain medium for the multiwavelength laser source. A single channel stability test was conducted and the results were comparable in performance to that of an LOA based laser source.

References

- [1] D. Wolfson, S. L. Danielsen, C. Joergensen, B. Mikkelsen, and K.E. Stubkjaer, “Detailed theoretical investigation of the input power dynamic range for gain-clamped semiconductor optical amplifier gates at 10 Gb/s,” *IEEE Photon. Technol. Lett.*, **10**, 1241–1243 (1998).
- [2] G. Giuliani and D. D’Alessandro, “Noise analysis of conventional and gain-clamped semiconductor optical amplifiers,” *J. Lightwave Technol.*, **18**, 1256–1263 (2000).
- [3] D. Francis, S. P. DiJaili, and J. D. Walker, “A single-chip linear optical amplifier,” presented at the Optical Fiber Communication Conf. Exhibit (OFC2001), Anaheim, CA, **PDP** (2001).
- [4] A. E. Siegman, *Lasers*, University Science Books, Mill Valley, CA, 1986
- [5] M. J. F. Digonnet, “Rare-Earth-Doped Fiber Lasers and Amplifiers” Second Edition, Marcel Dekker Inc., New York (2001).
- [6] J. L. Zyskind et al., “Determination of homogeneous linewidth by spectral gain holeburning in an Erbium-Doped Fiber Amplifier with GeO₂:SiO₂ core,” *IEEE Photon. Technol. Lett.*, **2**, 869-871 (1990).
- [7] M. J. Connelly, “Wideband semiconductor optical amplifier steady-state numerical model,” *IEEE J. Quantum Electron*, **37**, 439-447 (2001).
- [8] R. J. Manning and D. A. O. Davies, “Three-wavelength device for all optical signal processing,” *Opt. Lett.*, **19**, 889–891 (1994).
- [9] M. Yoshino and K. Inoue, “Improvement of saturation output power in a semiconductor laser amplifier through pumping light injection,” *IEEE Photon.*

- Technol. Lett.*, **8**, 58–59 (1996).
- [10] K. Inoue and M. Yoshino, “Gain dynamics of a saturated semiconductor laser amplifier with 1.47 μm LD pumping,” *IEEE Photon. Technol. Lett.*, **8**, 506–508 (1996).
- [11] K. P. Ho, S. K. Liaw, and C. Lin, “Reduction of semiconductor laser amplifier induced distortion and cross talk for WDM systems using light injection,” *Electron. Lett.*, **32**, 2210–2211 (1996).
- [12] Y. Sun, A. K. Srivastava, S. Banerjee, J. W. Sulhoff, R. Pan, K. Kantor, R. M. Jopson, and A. R. Charplyvy, “Error-free transmission of 32×2.5 Gb/s DWDM channels over 125 km using cascaded in-line semiconductor optical amplifiers,” *Electron. Lett.*, **35**, 1863–1865 (1999).
- [13] C. Tai, S. L. Tzeng, H. C. Chang, and W. I. Way, “Reduction of nonlinear distortion in MQW semiconductor optical amplifier using light injection and its application in multichannel M-QAM signal transmission systems,” *IEEE Photon. Technol. Lett.*, **10**, 609–611 (1998).
- [14] J. Yu, A. Buxens, A. Clausen, and P. Jeppesen, “ 16×10 Gb/s WDM bidirectional gating in a semiconductor optical amplifier for optical crossconnects exploiting network connection symmetry,” *IEEE Photon. Technol. Lett.*, **12**, 702–704 (2000).
- [15] J. Yu and P. Jeppesen, “Improvement of cascaded semiconductor optical amplifier gates by using holding light injection,” *J. Lightw. Technol.*, **19**, 614–623 (2001).
- [16] M. Usami, M. Tsurusawa, and Y. Matsushima, “Mechanism for reducing

- recovery time of optical nonlinearity in semiconductor laser amplifier,” *Appl. Phys. Lett.*, **72**, 2657–2659 (1998).
- [17] Y. H. Kao, T. J. Xia, and M. N. Islam, “Limitations on ultrafast optical switching in a semiconductor laser amplifier operating at transparency current,” *J. Appl. Phys.*, **86**, 4740–4747 (1999).
- [18] S. Bischoff, M. L. Nielsen, and J. Moerk, “Improving the all-optical response of SOAs at modulated holding signal,” *J. Lightw. Technol.*, **22**, 1303–1308 (2004).
- [19] M. A. Dupertuis, J. L. Pleumeekers, T. P. Hessler, P. E. Selbmann, B. Deveaud, B. Dagens, and J. Y. Emery, “Extremely fast high-gain and low-current SOA by optical speed-up at transparency,” *IEEE Photon. Technol. Lett.*, **12**, 1453–1455 (2000).
- [20] J. L. Pleumeekers, M. Kuer, K. Dreyer, C. Burrus, A. G. Dentai, S. Shunk, J. Leuthold, and C. H. Joyner, “Acceleration of gain recovery in semiconductor optical amplifiers by optical injection near transparency wavelength,” *IEEE Photon. Technol. Lett.*, **14**, 12–14 (2002).
- [21] K. Morito, “Output-level control of semiconductor optical amplifier by external light injection,” *J. Lightw. Technol.*, **23**, 4332–4341 (2005).
- [22] K. Morito and Y. Kotaki, “New output level control method for semiconductor optical amplifiers by external light injection,” presented at the *Optical Amplifiers and their Applications Conf.*, Stresa, Italy, OTuE10-1 (2001).

Chapter 4

Overview of optical signal processing techniques

The use of light for transmission over optical fiber links is now a commonplace in many telecommunication networks, with signal processing being performed electronically after optoelectronic conversion. Given the success with transmission, it was natural to investigate the possibility of undertaking processing tasks entirely in the optical domain without converting from optics to electronics and back again. The advantages offered by optics are its speed and reduced complexity relative to the electronic method in which processing at higher speeds becomes difficult. In order to be practical and competitive, all-optical switching devices must be able to fulfill criteria similar to those of electronics, i.e., small footprint, allow the integration of different functionalities, and have the potential for cheap mass-production.

All-optical signal processing techniques can be divided into two main categories, i.e., (i) semiconductor based and (ii) fiber based. We first begin with an overview of Semiconductor Optical Amplifier (SOA) nonlinearities and will then look into the optical fiber nonlinearities.

4.1 SOA nonlinearities

Nonlinearities in SOAs are principally caused by the carrier density dynamics induced by the amplifier input signals. The three main types of nonlinearities are: Cross gain modulation (XGM), cross phase modulation (XPM), and four wave mixing (FWM).

4.1.1 Cross-gain modulation (XGM)

Cross-gain modulation (XGM) employs interactions between two optical signals via carrier populations as shown in Fig 4.1 [1]. The gain in an SOA saturates as the optical power level increases. Therefore, it is possible to modulate the amplifier gain with an input data signal and in turn encode this gain modulation on a new CW wavelength passing through the amplifier, nevertheless with an inversion of data. A signal beam carrying information at λ_s depletes the carriers and thereby modulates the gain of the SOA. This carrier depletion also causes a change in the refractive index.

The probe beam at wavelength λ_c encounters the modulated gain and refractive index and thus the probe amplitude and phase are perturbed by the input signal. As shown in Fig 4.1, the input signal and the CW signal can be launched either in co- or counter propagation direction into the SOA. In the latter case the output filter, necessary for the co-propagation scheme, can be avoided. One of the drawbacks of this scheme is the deterioration in the SNR due to spontaneous emission background level. Typical noise figures are 7–8 dB for SOAs, and the noise figure for switching process is usually larger than the intrinsic noise figure.

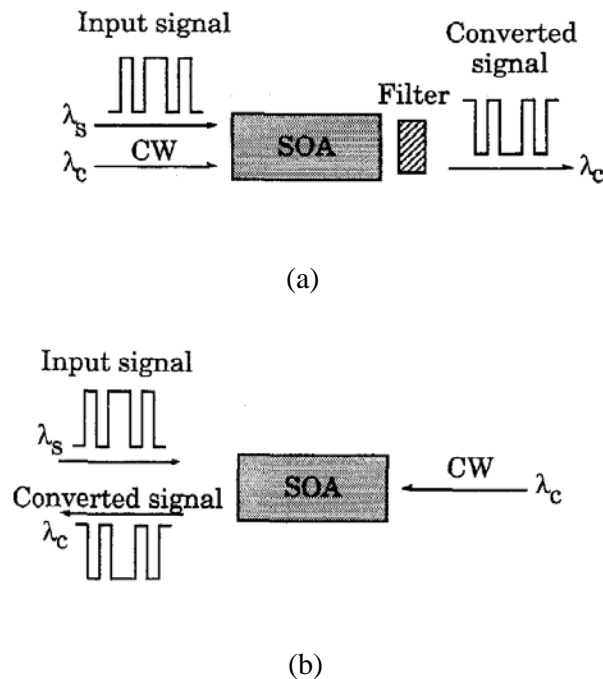


Fig. 4.1 (a) Co-propagating and (b) counter-propagating switch configurations using XGM in an SOA [1].

4.1.2 Cross-phase modulation

The cross-phase modulation (XPM) scheme relies on the dependency of the refractive index on the carrier density in the active region of the SOA. The incoming data signal depletes the carrier density and modulates the refractive index and hence results in the phase modulation of the CW signal also coupled into the SOA. Since XPM causes phase changes, the SOA must be placed in some form of interferometric configuration to convert phase changes in the signals to intensity changes using constructive or destructive interference. Typically, there are three different types of interferometers. In a Mach-Zehnder interferometer (MZI) as shown in Fig. 4.2 (a), SOAs are incorporated in both the arms and electrical currents are injected in both amplifiers. An input optical signal passes through one of the arms and modulates the phase of that arm. The interferometric nature of the device converts this phase modulation to the amplitude modulation of the probe signal at a new wavelength. Figure 4.2 (b) shows the transfer function of the interferometer [1]. The second type, Michelson interferometer (MI) [2] is similar to the MZI but requires only one beam splitter as shown in Fig 4.2 (c). In the sagnac interferometer the input beam is split into two beams that traverse the same distance but in opposite direction before recombination. Compared to XGM, the use of XPM in an interferometer configuration greatly improves the quality of the converted signal in terms of chirp and

extinction ratio. In order to achieve high operation stability and compactness, the MZI should be monolithically integrated with the SOAs.

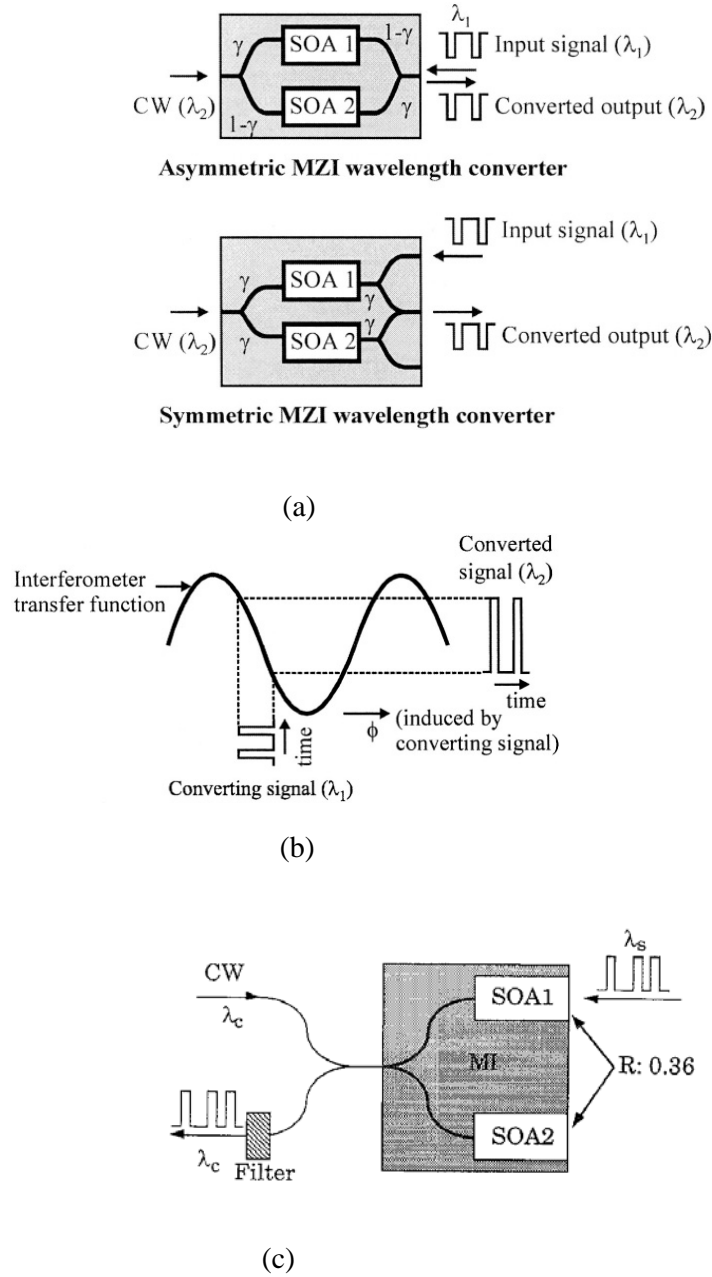


Fig. 4.2 (a) MZI switches based on XPM in SOAs. The coupler splitting ratios are different and equal in the asymmetric and symmetric configurations respectively [1]. (b) MZI switching transfer function [1] (c) MI based switch [2].

4.1.3 Four-wave mixing (FWM)

Four-wave mixing (FWM) is a coherent nonlinear process that can occur between two optical fields. In SOAs, the conjugate wave is generated by scattering from the dynamic gain and refractive index grating that is induced by the beating of the two input beams in the semiconductor gain medium. The outcome of FWM is the generation of a signal at a new frequency whose intensity is proportional to the product of the interacting wave intensities. The phase and frequency of the generated wave is the linear combination of those of the interacting waves. For triggering efficient FWM, the polarization states of pump and probe must be identical and the detuning between them should be small.

4.2 Fiber Nonlinearities

Nonlinear processes which involve the modulation of a medium parameter such as the refractive index are referred to as parametric processes. They can be classified as the second and third-order processes depending on whether $\chi^{(2)}$ or $\chi^{(3)}$ is responsible for the process. There are two categories of fundamental optical nonlinear effects in fibers. They are refractive-index effects and stimulated scattering effects. Refractive index effects are associated with modulation of the refractive index due to changes in the light intensity. Stimulated scattering effects arise from parametric interactions

between light and acoustic or optical phonons (due to lattice or molecular vibrations) in the fiber.

The refractive index n of silica is not a constant but increases with power (or light intensity) according to the relationship:

$$n(\omega, P) = n_0(\omega) + n_2 I = n_0(\omega) + n_2 \frac{P}{A_{eff}} \quad (4.1)$$

where $n_0(\omega)$ is the linear refractive index of silica, n_2 is the intensity-dependent refractive index coefficient, and $I = P/A_{eff}$ is the effective intensity in the medium. The typical value of n_2 is $2.6 \times 10^{-20} \text{ m}^2/\text{W}$ [3]. This number takes into account the averaging of the polarization states of the light as it travels in the fiber. The intensity dependence of the refractive index gives rise to three major effects:

- (i) Self Phase Modulation (SPM)
- (ii) Cross Phase Modulation (XPM), and
- (iii) Four Wave Mixing (FWM)

The aforementioned effects can significantly degrade the performance of a WDM lightwave system. XPM and FWM are more severe in multi-channel systems, while SPM can occur in both single channel and multi-channel environments. However, nonlinear effects can also be beneficial since they find interesting applications in optical pulse compression, in logic gates for all-optical signal processing and network

functions and stimulated scattering effects can be used for signal amplification and sensing applications.

4.2.1 Self Phase Modulation (SPM)

Self-phase modulation (SPM) occurs due to light-matter interaction. A light pulse while traveling down the fiber will induce a varying refractive index of the medium due to optical Kerr effect. This variation of the refractive index will produce a phase shift in the pulse, leading to a change in pulse's spectrum.

The phase shift ϕ_{NL} due to optical power P , for the light pulse propagating in a fiber is given by [3].

$$\phi_{NL} = \gamma PL_{eff} \quad (4.2)$$

where γ is the nonlinear coefficient, P is the optical power and L_{eff} is the effective fiber length. The quantities in (4.2) are defined as:

$$\gamma = \frac{2\pi n_2}{\lambda A_{eff}} \quad (4.3)$$

$$L_{eff} = [1 - \exp(-\alpha L)] / \alpha \quad (4.4)$$

where A_{eff} is the effective core area of the fiber and α is the fiber attenuation coefficient.

Although nonlinear coefficient for SMF-28 is small, nonetheless the powers that have been made possible by the use of the optical amplifiers (EDFAs) could induce nonlinear phase shifts large enough to play a significant role in the state-of-the-art lightwave systems [3,4].

4.2.2 Cross Phase Modulation (XPM)

Cross-phase modulation (XPM) is the phenomenon in which intensity fluctuations in one channel propagating in the fiber modulate the phase of all the other channels or alternatively all the WDM channels in the fiber modulate the phase of any one channel [3,5]. In a multi-channel system, the excess bandwidth ΔB generated by this XPM effect is given by:

$$\Delta B = \frac{d\phi_{NL}}{dt} = \gamma L_{eff} \frac{dP_1}{dt} + 2\gamma L_{eff} \frac{dP_2}{dt} \quad (4.5)$$

Note that the XPM induced chirp is twice as much as that of the SPM induced chirp. This factor of 2 arises from counting of terms in the expansion of the nonlinear polarization inside the fiber [3,5]. Although, it appears that XPM can impose severe limitation than SPM for multi-channel systems since its effect is twice as large for each interfering channel. However, fiber dispersion plays a significant role in the system impact of XPM [3]. Due to dispersion, pulses at different wavelengths travel with different speeds inside the fiber because of group velocity mismatch. In normal

dispersion regime ($D < 0$), a longer wavelength travels faster while the opposite occurs in the anomalous dispersion regime ($D > 0$). This feature leads to a walk-off effect that tends to reduce XPM effect.

4.2.3 Four Wave Mixing (FWM)

Generally, the third-order parametric processes involve nonlinear interaction among four optical waves and include four-wave mixing (FWM) often also called four-photon mixing, third-harmonic generation, and parametric amplification. FWM [6-10] occurs when photons from one or more waves are annihilated to create new photons at different frequencies for energy conservation during the parametric process. There are two types of FWM. The first case occurs when three waves transfer their energies to a single wave at the frequency $\omega_4 = \omega_1 + \omega_2 + \omega_3$. However, in general, it is difficult to have high efficiency in optical fibers owing to the difficulties in satisfying the phase-matching condition for such processes. The second case occurs when two waves at frequencies ω_1 and ω_2 are annihilated to generate simultaneously two symmetric sidebands at frequencies ω_3 (downshifted) and ω_4 (upshifted) in frequency such that

$$\omega_3 + \omega_4 = \omega_1 + \omega_2 \quad (4.6)$$

$$\omega_3 = 2\omega_1 - \omega_2 \quad (4.7)$$

$$\omega_4 = 2\omega_2 - \omega_1 \quad (4.8)$$

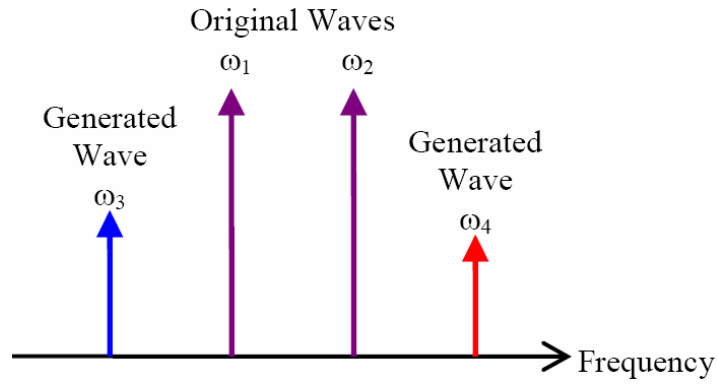


Fig. 4.3 Two channel pump Four wave mixing

If the frequencies of the two pump waves are equal, $\omega_1 = \omega_2$, it is relatively easy to satisfy the phase-matching condition. This specific case is called degenerated FWM or three-wave mixing because only three distinct frequencies are involved in this nonlinear process. It is most relevant for optical fibers and is in direct analogy with SRS in that the low-frequency band is referred to as the Stokes and the high-frequency band is referred to as the anti-Stokes, such that

$$\omega_4 = 2\omega_1 - \omega_3 \quad (4.9)$$

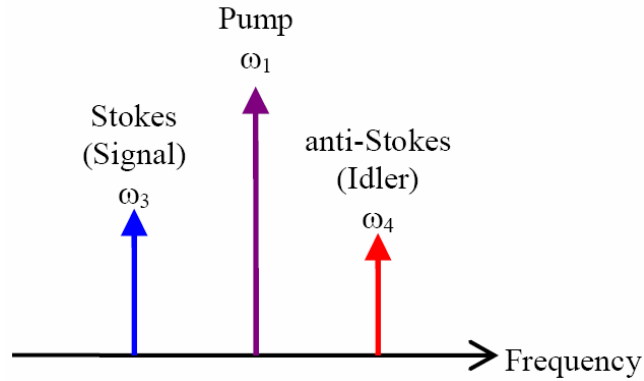


Fig. 4.4 Single channel pump Four wave mixing (Degenerated FWM)

If only the pump wave at frequency ω_1 is incident and phase-matching requirement is satisfied, the Stokes and anti-Stokes waves at frequencies ω_3 and ω_4 , respectively can be generated. On the other hand, if a weak signal at frequency ω_3 is coupled together into a fiber with the pump, the signal is amplified while a new wave at frequency ω_4 is generated at the same time. When the signal is amplified through such process of FWM, the Stokes and the anti-Stokes are often called the signal and the idler, respectively and the gain caused by such amplification is called the parametric gain.

4.2.4 Stimulated Scattering Effects

The nonlinear effects delineated above are governed by the power dependence of refractive index, and are elastic in the sense that no energy is exchanged between the electromagnetic field and the dielectric medium. A second class of nonlinear effects results from stimulated inelastic scattering in which the optical field transfers part of its energy to the nonlinear medium. Two important nonlinear effects fall in this category [3]: (i) stimulated Raman scattering (SRS), and (ii) stimulated Brillouin scattering (SBS). The main difference between the two is that optical phonons participate in SRS, while acoustic phonons participate in SBS. In a simple quantum mechanical picture applicable to both SRS and SBS, a photon of the incident field is annihilated to create a photon at a downshifted frequency. The newly generated photon propagates along with the original signal in the same direction in SRS, while it propagates in the backward direction in SBS. The Brillouin threshold is found to occur at a critical pump power P_o^{cr} obtained by using the relation.

$$g_B P_o^{cr} L_{eff} / A_{eff} \approx 21k \quad (4.10)$$

where P_o^{cr} is the critical pump power, L_{eff} is the effective length as given by Equation (4.3), A_{eff} is the area and g_B is the Brillouin-gain coefficient. The numerical factor of 21 is only approximate as it depends on the exact value of the Brillouin gain linewidth. The factor k varies between 1 and 2 depending on whether

pump and Stokes waves retain their polarization along the fiber. The primary difference between parametric processes such as FWM and the stimulated scattering processes such as stimulated Raman scattering (SRS) and stimulated Brillouin scattering (SBS) is related to the condition of phase-matching [11]. It is automatically satisfied in the case of SRS and SBS as a result of active participation of a nonlinear media. However, in the case of parametric processes, it requires specific choice of frequencies and refractive indices in order to satisfy the phase-matching conditions for efficient occurrence.

SRS can be used for signal amplification in a fiber by utilizing so called Raman amplification. Raman amplifiers are becoming more and more cost effective and are extensively researched in recent years because of its unique features. It is interesting to note that unlike EDFA, Raman amplification can virtually occur at any wavelength by properly choosing the pump wavelength and a large bandwidth can be achieved by combining several pump wavelengths.

In the following chapters we will present all optical signal processing devices realized during this study using fiber and semiconductor based technologies.

References

- [1] M. J. Connelly, *Semiconductor optical amplifiers*, Kluwer Academic Publishers, London, 2002.
- [2] T. Durhus, B. Mikkelsen, C. Joergensen, S. L. Danielsen, and E. Stubkjaer, "All-optical wavelength conversion by semiconductor optical amplifiers," *IEEE J. Lightwave Technol.*, **14**, 942-954 (1996).
- [3] G. P. Agrawal, *Nonlinear fiber optics*, Academic Press, New York, 2001.
- [4] I. P. Kaminow and T. L. Koch, *Optical Fiber telecommunication. III*, Academic Press, 1997.
- [5] D. Marcuse, A. R. Chraplyvy, and R. W. Tkach, "Dependence of cross-phase modulation on channel number in fiber WDM systems", *IEEE J. Lightwave Technol.*, **9**, 885-890 (1994).
- [6] R. H. Stolen, J. E. Bjorkholm, and A. Ashkin, "Phase-matched three-wave mixing in silica fiber optical waveguides," *Appl Phys Lett*, **24**, 308-310 (1974).
- [7] R. H. Stolen, "Phase-matched-stimulated four-photon mixing in silica-fiber waveguides," *IEEE Journal of Quantum Electronics*, **Q-11**, 100-103, (1975).
- [8] G. Cappellini and S. Trillo, "Third-order three-wave mixing in single-mode fibers: exact solutions and spatial instability effects," *J. Opt. Soc. of America B*, **8**, 824-838 (1991).

- [9] K. Inoue, "Four-wave mixing in an optical fiber in the zero-dispersion wavelength range," *IEEE J. Lightw. Technol.*, **10**, 1553-1561 (1992).
- [10] J. E. Sharping, M. Fiorentino, A. Coker, P. Kumar, and R. S. Windeler, "Four-wave mixing in microstructure fiber", *Opt. Lett.*, **26**, 1048-1050, (2001).
- [11] D. Marcuse, A. R Chraplyvy, and R. W. Tkach, "Effect of fiber nonlinearities on long distance transmission", *IEEE J. Lightwave Technol.*, **9**, 585-590 (1991).

Chapter 5

Highly nonlinear bismuth oxide fiber based devices

5.1 Introduction

The third order optical nonlinearity of SiO₂-based single mode fibers has been widely applied to all-optical signal processing such as optical wavelength converters, optical logic gates, optical switches, and optical phase conjugators, which will play key roles in future wideband wavelength-division-multiplexed (WDM) networks and ultra-high-speed optical time-division-multiplexed (OTDM) systems. However, the nonlinear coefficient γ of SiO₂-based single mode fibers is very low. For example, γ of the conventional dispersion shifted fiber (DSF) is 2.2 W⁻¹ km⁻¹. Therefore, in order to achieve good nonlinear device performance when the pump power is limited to below 1 W, we need a very long fiber length, typically, over 1 km, which limits practical applications of SiO₂-based single mode fibers [1]. The long fiber length causes some serious problems which are considered to be the major limiting factors for

response time and switching bandwidth. The problems include the pulse walk-off between control and signal pulses caused by group-velocity mismatch, the control pulse broadening caused by group velocity dispersion (GVD), and the polarization sensitivity caused by external environmental perturbations such as temperature drift and stresses. Therefore, fibers with high nonlinearities are essential in nonlinear fiber devices to shorten the device length required for acquiring sufficient nonlinear phase shifts. In addition, the effective mode area should be smaller for a given optical power to shorten the device length. High nonlinearity (HNL) glasses can satisfy these requirements since they have both high nonlinear-index coefficients and high linear refractive indices. A high linear refractive index of the core allows smaller core radius, while maintaining single-mode operation at the desired wavelength, and thus, the effective mode area decreases.

In this chapter, a new type of highly nonlinear fiber based on bismuth oxide glass will be introduced. The characteristics of bismuth based highly nonlinear fiber (Bi-HNLF) will be outlined and its applications in all optical signal processing devices will be delineated. The design of a fast all-optical on-off switch, tunable pulsewidth generator, and an all-optical AND gate, using a short length of Bi-HNLF, which utilizes four wave mixing effect will be described.

5.2 Bismuth Oxide Based Highly Nonlinear Fibers

Bi-HNLFs are recently developed by Asahi Glass Corp. Ltd of Japan and offers many advantages over the conventional HNLF. The main advantage of Bi-HNLF over conventional silica based HNLF is its high nonlinear coefficient which is due to high nonlinear refractive index of its core and small core effective area, therefore leading to the realization of very short-length and compact all-optical signal processing devices [2-3]. These devices are competitive with schemes based on semiconductor devices. The fabrication technology of optical fibers based on bismuth oxide (Bi_2O_3) material has advanced significantly in recent years, and has resulted in the production of a variety of high quality Bi_2O_3 -based optical fibers: for example, highly nonlinear Bi_2O_3 based step-index fiber (Bi-HNLF) [4], rare-earth doped Bi_2O_3 fiber [5], and Bi_2O_3 based holey fiber [6]. In particular, Bi-HNLFs, which possess ultra-high Kerr nonlinearity ~ 100 times larger than conventional silica-based highly-nonlinear fiber and can be readily fusion-spliced to conventional silica fibers, have attracted much attention for their practical applications to the implementation of a variety of nonlinear optical signal processing devices within fiber-optic communication systems.

Owing to the extremely-high nonlinear coefficient n_2 of the Bi_2O_3 glass, such a high nonlinearity of $\gamma \sim 1360 \text{ W}^{-1}\text{km}^{-1}$ can be readily achieved by use of a conventional step-index fiber structure [4] without employing any special fiber structure design.

This means that only a meter or less length would be long enough to generate a nonlinear optical phase shift sufficient for obtaining various nonlinear signal processing functions. The compactness and stability issues of fiber-based devices relative to semiconductor-based devices could thus be substantially improved by using a short length of such ultra-high nonlinearity fiber. In addition to the huge enhancement of Kerr nonlinearity, the Bi-HNLF has a unique advantage of a relatively high stimulated Brillouin scattering (SBS) threshold compared to the silica based highly nonlinear fiber, and this means that any additional SBS suppression scheme is not required for the implementation of a range of optical devices based on four-wave mixing or parametric amplification. The estimated SBS thresholds for the Bi-HNLF and the HNL-DSF reported in [7] are 2.65 and 0.22 W respectively. This high SBS threshold can be attributed to the short fiber length and the relatively low Brillouin gain co-efficient compared to the ultrahigh Kerr nonlinearity.

The cross section of Bi-HNLF, obtained using scanning electron microscope (SEM) is depicted in Fig. 5.1 [8]. The core diameter is 1.72 μm and fiber diameter is 125.4 μm . Therefore the mode field diameter (MFD) and the effective core area A_{eff} are estimated to be 2.1 μm and 3.3 μm^2 respectively. If direct fusion-splicing of the Bi-HNLF to SMF is done, the splicing loss must be very large because of large MFD mismatch (Bi-NLF:2.1 μm , SMF:10.5 μm). Therefore, ultra high NA SiO_2 fiber

(UHNA4, Nufern), whose MFD is 4.0 μm was used as intermediary fiber. These fibers were fusion-spliced by arc discharge using a conventional fusion splicing machine as shown in Fig. 5.2. As a result, the splicing loss of SMF to UHNA4 and UHNA4 to Bi-NLF were reduced on each side to <3.0 dB. The near field pattern (NFP) of Bi-HNLF measured at 1310 nm is depicted in Fig. 5.3. When Bi-HNLF is fusion spliced to high NA SiO_2 fiber (HI980, Corning), whose MFD is 6.0 μm , some light traveling through the cladding was observed in NFP due to large MFD mismatching and the measured splicing loss was 9.6 dB [9]. However, the cladding mode was reduced by employing UHNA4 as an intermediary fiber because of the improved MFD matching. Bi-HNLF has a large normal GVD which is mainly due to the material dispersion of the high refractive index glass. However, its effect is not so serious because of the short fiber length.

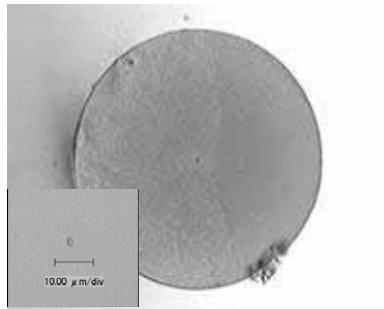


Fig 5.1 Microscopic view of Bi-HNLF [8]



Fig 5.2 Splicing point of Bi-HNLF to the intermediary fiber [8]

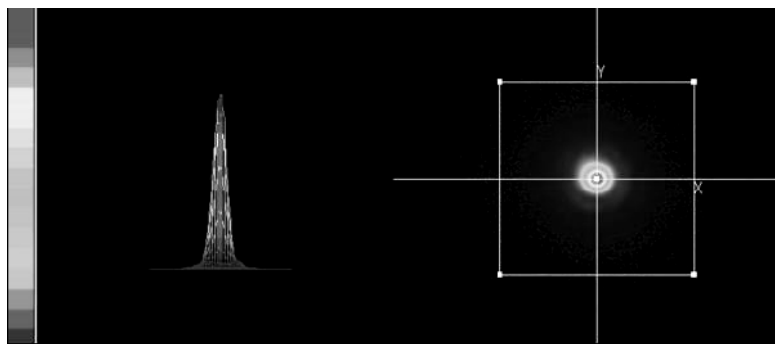


Fig 5.3 Near Field Pattern of Bi-HNLF measured at 1310 nm [8]

In the following sections, we will describe the design of an all optical on-off switch, tunable pulsewidth generator, and an all optical AND gate using 1.9-m of Bi-HNLF. Four-wave mixing process in this fiber was utilized to realize these devices.

5.3 All optical on-off switch

Optical networks utilizing fast packet switching are expected to provide the required capacities and flexibility in the next generation high-speed optical networks. All-optical switches will be one of the key components in these high capacity optical networks such as optical time division-multiplexed and wavelength division-multiplexed systems. Switching speed, switching energy, and repetition rate are the important issues for practical applications. Hitherto, a variety of switching schemes have been reported and demonstrated [10–20,23].

Nonlinear optical fiber loop mirror (NOLM) pioneered by Doren and Wood [10], is basically a Sagnac interferometer that makes use of cross-phase modulation (XPM) for optical switching has attracted much attention and is one of the candidates for ultrafast demultiplexing [11-12]. NOLM based devices can switch pulses that are several femto-second long since they utilize small non-resonant nonlinearity in the fiber. However, these devices require long interaction lengths, which makes the overall system very bulky and also its operation suffers from the signal polarization dependence. In order to overcome the requirement of long fiber in an NOLM, Eiselt et al. [13] and Sokoloff et al. [14] independently reported the semiconductor laser amplifier in a loop mirror (SLALOM) and the terahertz optical asymmetric demultiplexer (TOAD). Both of these devices are the derivatives of the original

NOLM [10], and they incorporate a semiconductor optical amplifier placed asymmetrically in a loop mirror.

Another promising technique is the use of highly efficient optical nonlinearity, which is resonantly excited in semiconductor devices. Nakamura et al. [17] demonstrated ultrafast all-optical switching based on frequency shift accompanied by the semiconductor band filling effect. The switch demonstrates ultrafast speed (1.5 Tb/s demultiplexing and 200 fs switching) and can operate at a high repetition rate of 10 GHz.

The switches based on SOAs in interferometric configurations have been accomplished. A switching scheme based on self-induced gain modulation (SGM) in the cascaded SOA configuration by counter propagating the data and control signals has been demonstrated [18]. In these switches, an optical gain leads to gain saturation due to carrier depletion in SOAs, and controls refractive index changes in the gain medium of SOAs. The data can be switched by controlling the optical control pulse. The switch is integrative since it includes only two SOAs and a wave-guide. It is capable of all-optical switching at 2.5 Gb/s.

Chan et al. [19] demonstrated an all-optical switch working at 10 Gb/s using multiwavelength mutual injection locking of a Fabry P erot laser diode. The switch-on and switch-off time is within a bit period so that only one bit is required to

serve as a guard period between packets for packet demultiplexing. The drawback of this switch is its sensitivity to the polarization of the input signals.

Ultrafast switching based on FWM in polarization maintaining fiber loop has been reported [20]. This scheme has low efficiency and relatively narrow parametric bandwidth. These shortcomings can be countered by using spectral spreading technique and Raman amplification [21,22]. Xu et.al. [23] demonstrated all-optical switching based on Raman-assisted FWM using 12 km of dispersion shifted fiber. The downside of this scheme is the severe walk-off effect between the two pump pulses due to long fiber length being used.

In this project we have proposed and demonstrated an all-optical on-off switch based on FWM in only 1.9-m long bismuth-based highly nonlinear fiber (Bi-HNLF) (courtesy of Asahi Glass Co. Ltd). The control and data signals together are launched into the Bi-HNLF which serves as the all-optical on-off switch. When the control signal is high, i.e. the ON state, the data signal will be switched onto the idlers generated by the FWM effect. When the control signal is low, i.e. the OFF state, no idlers will be generated. The data signal will therefore not be switched. As a result, the data signals will be switched onto the new wavelength depending on the states of the control signals.

5.3.1 Experiments and Discussions

Figure 5.4 shows the FWM conversion efficiency of 1.9 m long Bi-HNLF which is defined as the ratio of the output wavelength converted signal power to the input signal power as a function of signal wavelength detuning relative to the fixed pump wavelength. In this experiment the pump wavelength is kept fixed at 1550 nm. A maximum conversion efficiency of -16.8 dB is achieved with a 3-dB bandwidth of ~ 10 nm. The conversion-bandwidth limit of ~ 10 nm can be attributed to the walk-off effect caused by the GVD, which still remained in spite of the short fiber length. Due to the extremely high material dispersion of the Bismuth glass, the GVD control for the Bi-HNLF is not achieved in a straightforward manner unless a special waveguide structure such as photonic crystal fiber structure is employed [6].

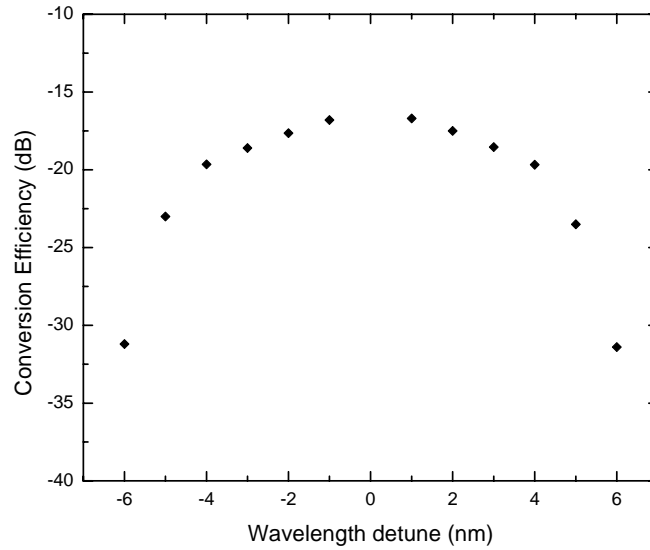


Fig 5.4 Measured conversion efficiency versus signal wavelength detuning relative to fixed pump wavelength of 1550 nm.

All optical switching was achieved by using FWM in 1.9-m long Bi-HNLF. The data signal, and the control signal were injected into the Bi-HNLF through a DWDM coupler. The duration of the ON state in the control signal was equal to the length of the packet to be switched (de-multiplexed) from the data signal. The detuning and power of the control beam with respect to data signal were chosen so as to achieve maximum conversion efficiency. All optical switching is achieved because whenever the control and data signal are present, FWM takes place and the idlers carry the switched data signal. The Bi-HNLF thus works as an all optical on-off switch, i.e.,

the Bi-HNLF transmits the data signal when the control signal is ON and blocks the data when the control is OFF.

Figure. 5.5 shows the schematic of the experimental setup to demonstrate the proposed all-optical on-off switching using Bi-HNLF. The data signal at 1553.33 nm is encoded by $2^{31}-1$ non-return-to-zero pseudorandom bit patterns at 10 Gb/s. The data signal is generated by externally modulating a tunable laser (TL-1) with an electro-optic Lithium Niobate (LiNbO_3) modulator driven by a 10 Gb/s pulse pattern generator. The control signal at 1554.13 nm was generated by external modulation of another tunable laser (TL-2). The wavelength separation between the control and data signals is chosen to be 0.8 nm so that the idlers wavelength will be placed 0.8 nm apart. The data and the control signals were amplified separately to an average power of about 300 mW by using erbium doped fiber amplifiers (EDFAs) which have maximum saturation output power of 500 mW. Polarization controllers (PCs) were used to ensure coincidence of the states-of-polarization of the control and data signals. The data and control signals were combined in an 8-channel DWDM multiplexer and then launched into 1.9 m of Bi-HNLF.

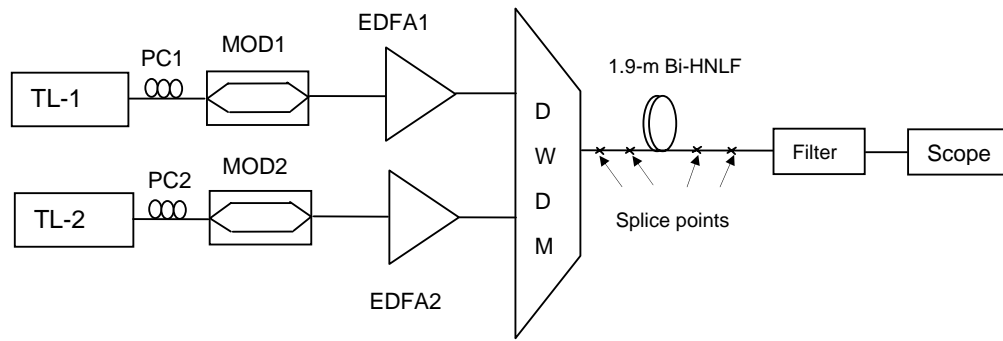


Fig. 5.5 Experimental setup of the all-optical Bi-HNLF based on-off switch.

TL: Tunable laser; PC: Polarization controller; MOD: Modulator; EDFA: Erbium doped fiber amplifier; DWDM: Dense wavelength division multiplexer.

Bi-HNLF has a mode field diameter (MFD) of $\sim 1.97 \mu\text{m}$, hence in order to reduce splicing losses, the two ends of the Bi-HNLF are first connected to two segments of ultra high numerical aperture (NA) silica fiber (UHNA4, Nufern) which has a MFD of $\sim 4 \mu\text{m}$. The two high NA fibers are then connected to conventional silica fiber (SMF28) which has a MFD of $\sim 10 \mu\text{m}$. The total loss at the input side of the Bi-HNLF, which includes the splice loss between the SMF28 and UHNA4, the splice loss between the UHNA4 and the Bi-HNLF, and the propagation losses in the SMF28 and the UHNA4, is 1.1 dB. The total loss at the output side of the Bi-HNLF is 2.6 dB. The propagation loss of the Bi-HNLF is 2.0 dB/m at 1550 nm. The total loss of the Bi-HNLF is therefore 7.5 dB. The refractive index of the core and cladding are 2.22 and 2.13 respectively. Thus the numerical aperture of this fiber is 0.64. The GVD

and the nonlinearity coefficients of the Bi-HNLF at 1550 nm are -280 ps/nm/km and 1000 W⁻¹km⁻¹ respectively. Since the length of the Bi-HNLF is 1.9 m, the total accumulative GVD is only -0.532 ps/nm. It is interesting to mention that the nonlinearity coefficient of this fiber is ~ 100 times larger than that of the conventional silica-based highly nonlinear dispersion shifted fiber. Although the Bi-HNLF has a large normal GVD coefficient, which is mainly due to the material dispersion of the high refractive index glass, its effect however is not significant because of short fiber length used. Figure. 5.6 shows the spectra of FWM signals measured at the output of the Bi-HNLF. Multiple wavelengths generated by the FWM process are observed. The newly generated wavelengths are 0.8 nm apart and they all carry the switched data.

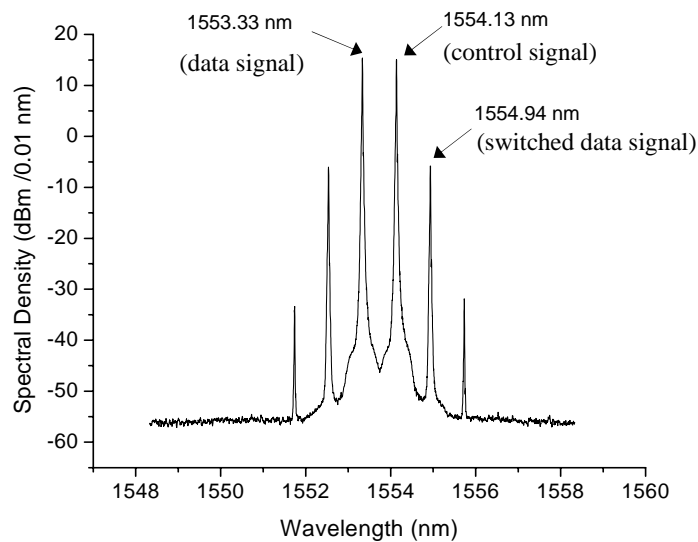


Fig. 5.6 Output spectra of FWM signals

We used a thin film filter with a bandwidth of 0.6 nm to filter out the switched signal. The output is observed using an optical spectrum analyzer with 0.01 nm resolution and a 50 GHz sampling oscilloscope. Figure 5.7(a) and 5.7(b) depict the timing diagrams of the data and control signals respectively. The control signal has an ON/OFF duration of 64 ns. The portion of data signal which coincides with the ON duration of the control signal will be switched and wavelength-converted by the FWM process whereas the portion of the data signal which coincides with the OFF period will be blocked. It is worth mentioning that the ON/OFF duration of the control beam can be easily controlled depending on the data stream to be switched. Figure 5.7(c) shows the timing diagram of the switched data signal at 1554.94 nm. Figure 5.8 depicts the magnified timing diagrams of Fig. 5.7. The switched data has a relatively low noise level and high extinction ratio. The proposed on-off switch therefore can potentially operate at speed beyond 10 Gbit/s. The Figures 5.9(a) and 5.9(b) show the eye diagrams of the input data signal and the switched data signal respectively. The thickness of the '1' rail is due to the beating between the in-band ASE of the two EDFAs which get transferred to the idlers.

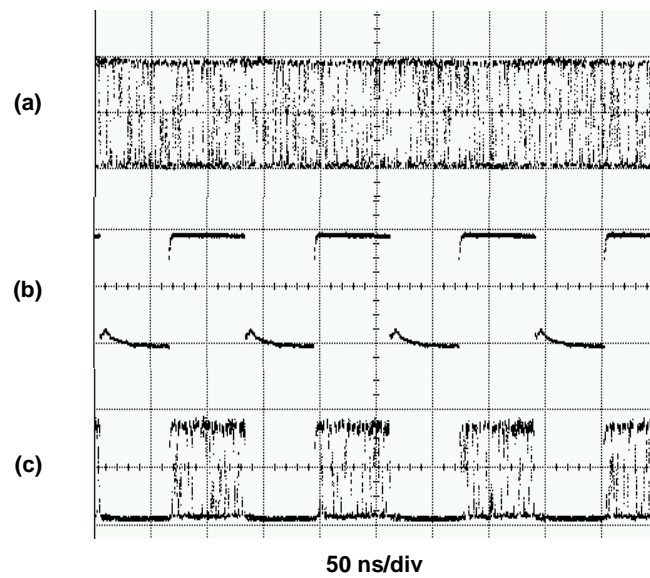


Fig. 5.7 Timing diagrams of (a) 10 Gb/s NRZ data signal at 1553.33 nm, (b) synchronized control signal with on-off duration of 64 ns at 1554.13 nm, and (c) switched 10 Gb/s data signal at 1554.94 nm.

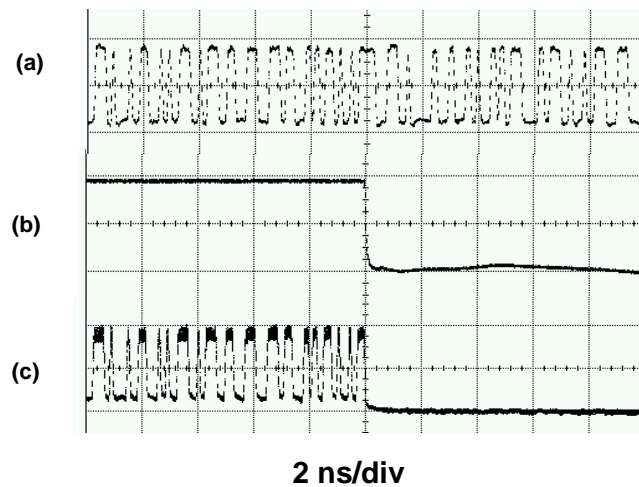


Fig. 5.8 Magnified timing diagrams (a) 10 Gb/s NRZ data signal at 1553.33 nm, (b) synchronized control signal with 64 ns on-off duration at 1554.13 nm, (c) switched 10 Gb/s data signal 1554.94 nm.

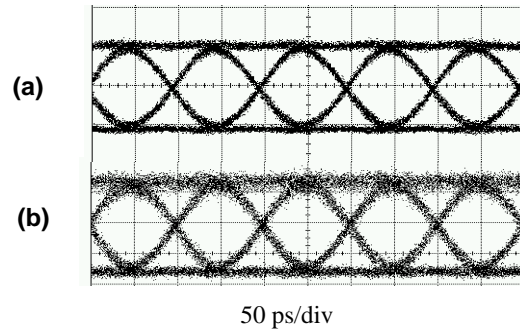


Fig. 5.9 Eye diagrams of the (a) input data signal and (b) switched data signal

5.4 Tunable pulsewidth generator

Optical sources capable of generating pulses with tunable pulsewidth are useful to applications such as high speed optical communication, optical sampling, and all-optical signal processing. In high speed transmission, return-to-zero (RZ) format is better than non-return-to-zero (NRZ) format because the former can be used in phase shift keying technique which can provide higher immunity against fiber impairments [24,25].

Takada et al., [26] reported actively mode-locked pulses generated from a 1.59 μm multi-quantum well (MQW) laser integrated with MQW electro-absorption modulator driven at the monolithic cavity frequency. The pulsewidth is controlled by changing the reverse bias applied to the electro-absorption modulator and by linear pulse compression using a 1.3 μm fiber.

Chernikov, et al., [27] demonstrated duration tunable pulse generation using an electro-absorption modulator and a tunable-dispersion chirped fiber Bragg grating at a repetition rate of 10 GHz. The pulsewidth is compressed by using an adiabatic pulse compressor comprising of 1 km of standard SMF and 1.6 km of dispersion decreasing fiber (DDF). The scheme requires electrical modulation which suffers from electrical bit rate.

Jiang et al., [28] reported tunable RZ pulse generation at 10 GHz based on spectral

line-by-line pulse shaping of a mode-locked laser. Spectral line-by-line pulse shaping is implemented by an ultra-short pulse shaping technique [29] using a fiber coupled Fourier-transform pulse shaper. Although, a wide tuning range is demonstrated nevertheless the grating-based pulse shaper has a large insertion loss of 15 dB.

Recently, a number of fiber based configurations have been utilized for tunable pulsewidth generation [30,31]. By employing different kinds of fibers as nonlinear media, tunable pulsewidth generation is achieved using FWM effect. Yu et al. [30] proposed using 1 km of highly nonlinear fiber [30] whereas Zhang et al. [31] reported using 20 m of photonic crystal fiber (PCF). The downside of these schemes is long length of the fiber being used and hence more compact tunable pulsewidth sources are desired.

In this work we demonstrate generation of optical pulses with tunable pulsewidth based on FWM effect in only 1.9 meter of Bi-HNLF (courtesy of Asahi Glass Co., Ltd). The operation principle of this scheme is that when two pulse trains at different wavelengths with fixed pulsewidth are launched into the Bi-HNLF, pulse trains at new wavelengths are generated through FWM effect in the nonlinear medium. The pulsewidth of the pulse in the newly generated pulse train depend on the extent of the temporal overlap between the two optical pump-train sources. By tuning the relative

delay between the two pump pulses trains, the pulsewidth of generated pulse train can be continuously tuned.

5.4.1 Theory

In this section, the properties of the tunable pulsewidth pulse generator are investigated based on a simple model and using the measured data obtained from the performed experiments.

5.4.1.1 Model

Since the effect of chromatic dispersion is relatively weak compared to the nonlinear effect in this piece of Bi-HNLF, the evolution of the optical field is governed by

$$i \frac{dq}{dz} + \gamma |q|^2 q = -i \frac{\alpha}{2} q \quad (5.1)$$

where $q(z)$ is the slowly varying amplitude of the pulse envelope, z is length of the fiber traversed, γ is the nonlinear coefficient, and α is the attenuation coefficient. Equation (5.1) only includes the nonlinear phase modulation and the attenuation effect.

We assume that there is no phase mismatch between the two pump pulses. The solution of Eq. (5.1) is given by

$$q(z) = q(0) \exp \left\{ -\frac{\alpha}{2} z + \frac{i}{\alpha} |q(0)|^2 [1 - \exp(-\alpha z)] \right\} \quad (5.2)$$

The experiment can be analysed by using two pump signals with different carrier frequencies as initial condition in Eq. (5.2). Different frequency components, such as pumps and idlers, are selected using an ideal filter. By applying an inverse Fourier transform on these components, the relative pulse shapes of these frequency components are measured. The fiber attenuation is chosen to be 2.0 dB/m with a nonlinear coefficient of $\gamma = 1000 \text{ W}^{-1}\text{km}^{-1}$. For simplicity, we consider the two input pulses to be identical with each pulse having a peak power of 0.4 W.

During our investigation, we found that the shape of the initial input pulse plays a key role in the evaluation of results. Since FWM is an intensity sensitive nonlinear process, the fitting of peak shape of these pulses become important. The RZ format output of the amplitude-modulated Mach-Zehnder modulator has a raised-cosine (RC) profile. However, when compared with the standard RC pulse, the experimentally observed pulse shapes at 5 GHz and 10 GHz have shorter rise times. Therefore, we defined a combined RZ pulse which is formed by rise/fall time of RC function with a flat pulse top. This RZ pulse was used to fit the measured pulse shape and was decided by choosing several parameters, such as pulsewidth, rise/fall time, power and extinction ratio. In order to obtain a combined RZ pulse having the best fitting of the waveform data, we calculated the least square errors between the measured waveform and combined RZ pulses. As accurate fitting at the pulse top is important in this case,

weighting was added at the upper parts of pulse rising edges. Table 5.1 lists two groups of parameters based on two sets of data obtained from the two different modulators. In each group, two values of total least square errors are listed, which represent the combined RZ generated pulse obtained using pulsewidths and rise times from oscilloscope and the combined RZ pulse with modified values of rise time, respectively. In both groups, combined RZ pulses using modified values of rise time produces smaller error than those using parameters obtained from oscilloscope. In other words, using modified parameters one can get a better fitting for the upper parts of input pulse.

		FWHM (ps)	Rise time (ps)	Total least squares error
Group One (modulator one)	Combined RZ	42.1	24.3	0.0429
	combined RZ (modified rise time)	44	26	0.0386
Group Two (modulator two)	Combined RZ	44	19.9	0.0838
	Combined RZ (modified rise time)	44	26	0.0348

Table 5.1: Experimental and modified parameters

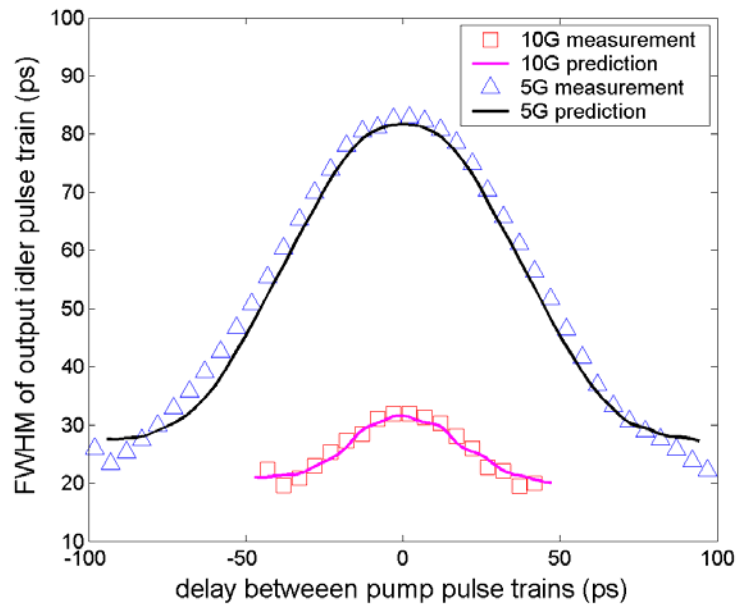


Fig. 5.10 Measured and predicted FWHM of generated pulses versus pump delay at 5 GHz and 10 GHz repetition rates respectively.

Figure 5.10 shows the pulsewidth versus the optical delay at 5 Gb/s (triangles) and 10 Gb/s (squares). It has been found that the output pulsewidth varies approximately linearly with the relative delay between the pump pulses. The maximum pulsewidth occurs when the two pump pulse trains are synchronized. The experimental results are in close agreement with the theoretical predictions.

5.4.1.1.1 Effect of initial pulse shape parameters on the evaluation results

Evaluation results are shown in Fig. 5.11 for the better understanding of the characteristics of tunable pulse generator. Combined RZ pulses with fixed FWHM of 45 ps at 10 GHz are used as an initial condition.

As shown in Fig 5.11 (a), for a fixed initial extinction ratio of 20 dB and input peak power of 0.4 W, steeper rise time can maximize the tuning range of the generated pulsewidth. It is interesting to note that the slope of the trace is also steeper for shorter rise time. In Fig 5.11 (b), we fixed the rise time and extinction ratio at 25 ps and 20 dB respectively, while changing the input peak power. Strong nonlinear effects are introduced due to high pulse intensity in the Bi-HNLF. Increase of input power will not cause dramatic change in the trace of idler pulsewidth versus pump delay, until it reaches a threshold, which is at around an input peak power of 28 dBm per pulse (nonlinear length < 1.9 m). Beyond this threshold, the spectrum of both idler and pump pulses will tend to broaden due to nonlinear phase modulation. In Fig 5.11 (c), due to low extinction ratio, the pedestals of pulses introduce extra FWM effect, and reduce the minimum width of generated pulse. In this figure, the rise time and peak power were kept fixed at 25 ps and 20 dBm, respectively. Initial chirp is also investigated, as shown in Fig.5.11 (d). Stronger initial chirp can cause extra shift in the central frequency of the idler and is also responsible for generation of small peaks within the idler pulse. However, from simulations we found that small initial chirp will not cause obvious frequency shift of the idler.

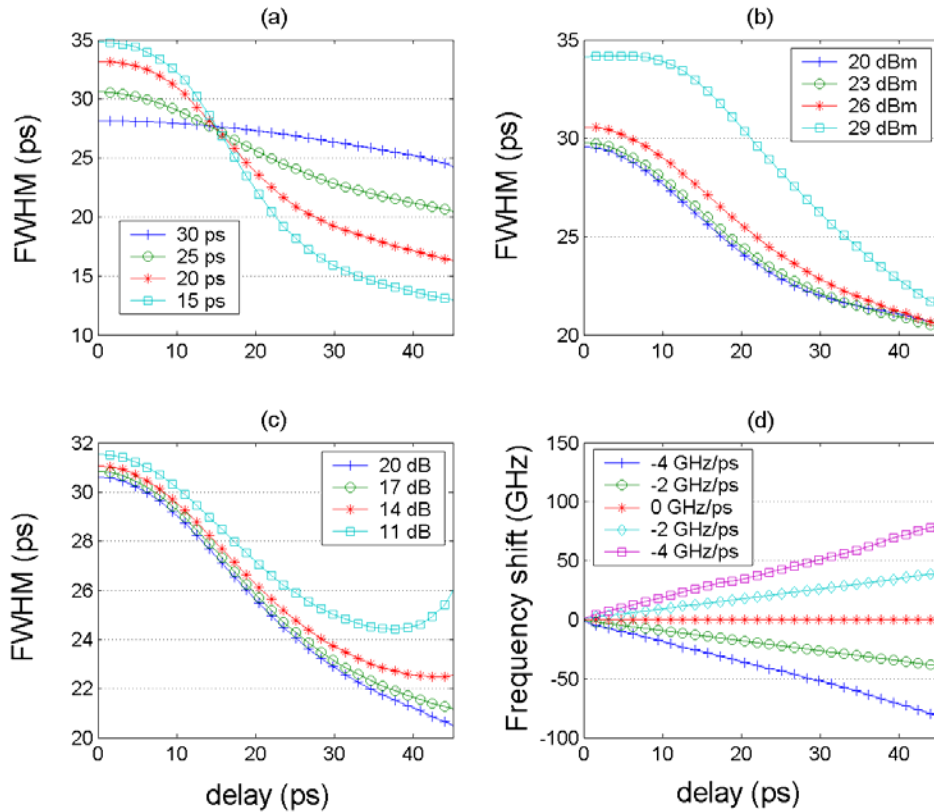


Fig. 5.11 Relationship between output idler pulsewidth and input pump delay for different (a) rise time (b) input power (c) input extinction ratio and (d) frequency shift for different initial chirp.

5.4.1.1.2 Tunable pulse generation at 40 GHz

Based on the above model, a series of studies are carried out to further understand the properties of this tunable pulse generator. The timing jitters of the tunable pulsewidth generator are first analyzed. The input pump pulses timing jitters, which mainly originate from the fluctuation of electrical triggers, are the major sources of output timing jitter. Figure 5.12, shows the theory results at 10 GHz. These results are obtained using inputs consisting of combined RZ pump pulses with fixed pulsewidth and different rising times. Short pulses of 12 ps are generated when the

pump pulses have steep rise times. For clarity, the trace of idler pulsewidth versus pump delay in Fig. 5.12 can be divided into three sections, corresponding to pump delay from 0~10 ps; 10~25 ps and 25~50 ps respectively. When the delay between the two pumps is small, timing jitter does not have a significant effect on the output pulsewidth and peak intensity. For a delay from 10 ~ 25 ps, 1 ps of pump delay jitter causes a 1.5 ps change in the FWHM of the output pulse. When the delay between two pulses is large, 1 ps pump delay jitter may cause a 0.5 dB intensity fluctuation of the output pulse. From the above analysis, we can conclude that when using combined RZ pulse train as the initial pump pulses of the tunable pulse generator, the stability of its output pulsewidth degrades if the pump timing jitter is large. In addition, for systems requiring relatively longer fiber, walk-off effect can also introduce such degradation.

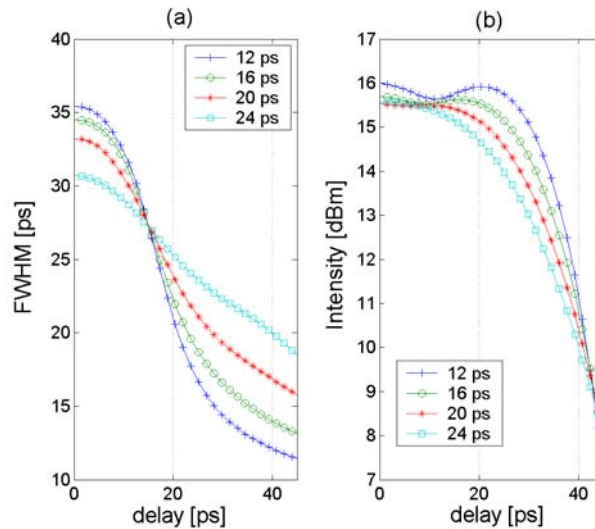


Fig. 5.12 (a) FWHM of generated pulses at 10 GHz versus pump delay for different rise time of input pulses and (b) intensity of the generated pulses versus pump delay.

Figures 5.13 and 5.14 show the theory results regarding tunable pulse generation at 40 GHz. The peak power of input pulse train is 0.4 W, the fiber length is 1.9 meters, the fiber attenuation is chosen to be 2.0 dB/m, and the nonlinear coefficient $\gamma = 1000 \text{ W}^{-1}\text{km}^{-1}$. When using a 40 GHz combined RZ pulse with a fixed pulsewidth of 12 ps as input, the trace of pulsewidth versus pump delay and idler peak power versus pump delay at different rise times show similar trend as that of 10 GHz case. The timing jitter of pump becomes an issue for the quality of output pulse. For input pump pulses having relatively short rise time, the idler shows large fluctuations in pulse intensity and pulsewidth. However, when the rise time of input pulse is 6 ps, the prediction result shows a linear relationship between the pulsewidth and the pump delay. This allows the idler pulsewidth to be continuously tuned from 8 ps to 4.5 ps. Figure 5.14 shows the theory results with different initial conditions, where non-chirped Gaussian pulse was used as RZ pump signal. From these results, we can conclude that the pulsewidth does vary significantly with the pump delay. The comparison also shows that at 40 GHz repetition rate, the shape of the RZ pulse plays an important role in deciding the tuning range of the pulse generator.

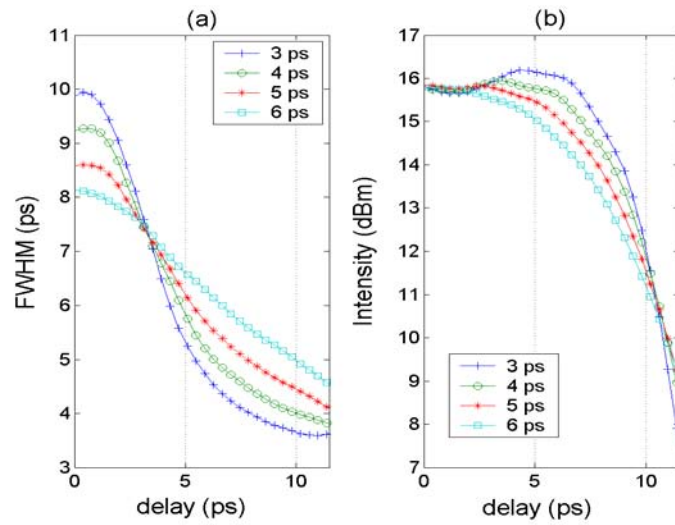


Fig. 5.13 (a) FWHM of generated pulses at 40 GHz versus pump delay and (b) intensity of generated pulses versus pump delay. (Note: 40 GHz combined RZ pulses with different rise time are used as an initial condition).

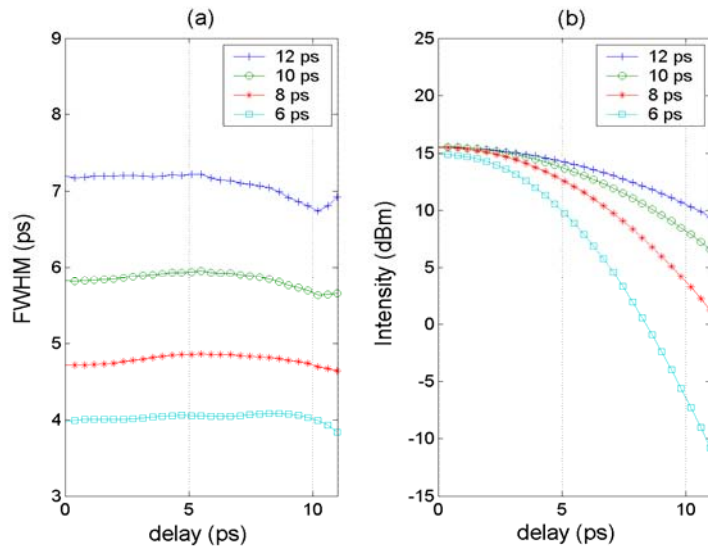


Fig. 5.14 (a) FWHM of generated pulses at 40 GHz versus pump delay and (b) intensity of generated pulses versus pump delay. (Note: 40 GHz non-chirped Gaussian pulses with different input pulsewidth are used as an initial condition)

5.4.2 Experiments

Figure 5.15 depicts the schematic of the experimental setup used for the generation of duration tunable optical pulses using bismuth-based highly nonlinear fiber. The two pump pulse trains are generated by external modulation of two tunable lasers (TL-1 & TL-2) using LiNbO_3 electro-optic modulators. The wavelengths of two lasers are set at 1553.33 nm (λ_1) and 1554.10 nm (λ_2) respectively. The two modulators are driven by two pulse pattern generators (PPGs) which are synchronized. The delay between the two pulses trains is controlled by an optical delay line (ODL) placed after one of the modulators (MOD-2) as shown in Fig. 5.15. A polarization controller placed after the other modulator (MOD-1) is used to optimize the conversion efficiency of the FWM process inside the Bi-HNLF by aligning the states-of-polarization of the two pulse trains. The two pulse trains are then combined using a 3-dB coupler and are amplified to a peak power of ~25 dBm by using an erbium doped fiber amplifier (EDFA) with a maximum saturation output power of 27 dBm. The combined signals are then launched into Bi-HNLF. The splicing losses at the input and output side of the fiber and other fiber parameters are provided in section 5.3.

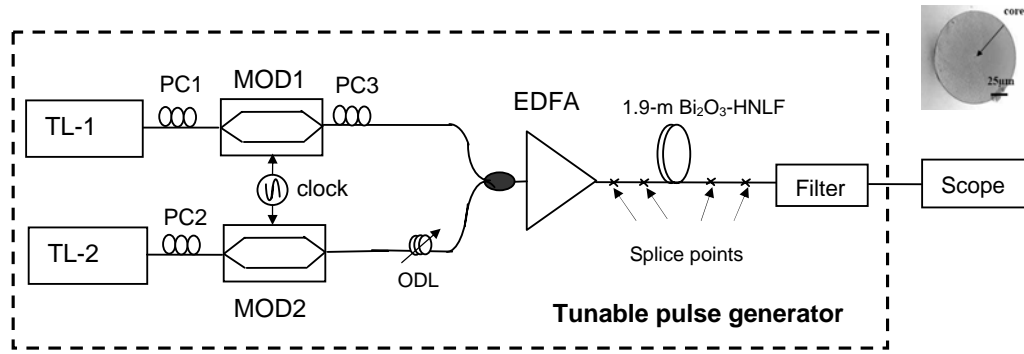


Fig. 5.15 Experimental setup of width tunable pulse generator. (Inset shows the microscopic view of Bi-HNLF). TL: Tunable laser, PC: Polarization controller, MOD: Modulator, EDFA: Erbium doped fiber amplifier, BPF: ODL: Optical delay line.

Figure. 5.16 shows the output spectra of FWM signals at 10 Gb/s measured before and after the Bi-HNLF. We observed that the two pump pulse trains generated new pulse trains at new wavelengths through the FWM process. The pulse train is generated at 1554.92 nm (λ_4). The optical peak power at this wavelength is around 0 dBm.

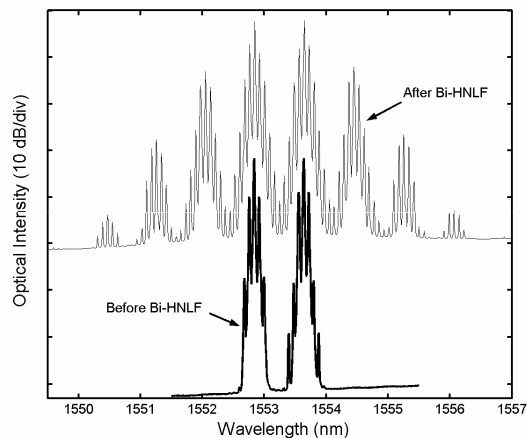


Fig. 5.16 Spectra obtained before and after Bi-HNLF.

Finally, a thin film filter with a 3-dB bandwidth of 0.6 nm is used to select the newly generated pulse train at λ_4 . The filtered output is sent to an optical spectrum analyzer with 0.01 nm resolution and a 50 GHz sampling oscilloscope with a 40 GHz photo-detector. The pulsewidth of the generated pulse at λ_4 depends on the extent of the temporal overlap between the pump pulses which can be varied with the optical delay line.

Figures 5.17 show the temporal pulse profiles of the generated pulses train at 10 GHz for FWHM of 38.4, 29.8, and 19 ps. Figure 5.18 show the temporal pulse profiles of the generated pulses train at 5 GHz for FWHM of 56, 30, and 18.5 ps respectively. It is to be noted that the narrowest pulsewidth has the minimum peak power since it is obtained when there is minimum overlap between the two pump pulses.

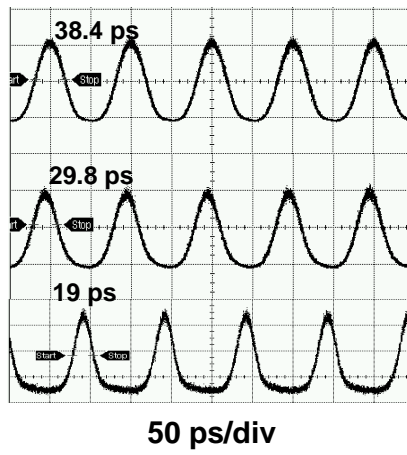


Fig. 5.17 Timing diagrams for tunable pulse generation at 10 Gbit/s clock rate.

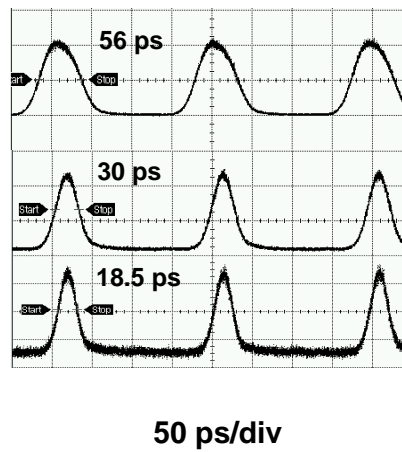


Fig. 5.18 Timing diagrams for tunable pulse generation at 5 Gbit/s clock rate.

5.5 All-optical AND gate

All-optical implementation of high-speed logic gates, which make up the central element in a wide variety of signal processing functionalities, are desired for future networks to avoid the cumbersome and power consuming electro-optic conversion.

An all-optical AND gate can perform on-the-fly bit-level functions such as address recognition, packet header modification and data integrity verification. It is also an integral part of all optical binary half adders, full adders and parity checkers [32-34].

Hitherto, several approaches have been reported to realize AND logic operation using fiber based, semiconductor optical amplifier based or waveguide based devices [32-41]. Hall et al. [32] demonstrated the AND logic utilizing a combination of cross-phase modulation (XPM) and cross-gain saturation (XGS) in the semiconductor laser amplifier (SLA) which is configured in an ultrafast nonlinear interferometer (UNI).

Kang et al. [36] showed that the XPM all-optical wavelength converter, which is composed of a Mach-Zehnder interferometer (MZI) and SOA waveguides, can be utilized to perform logic AND for high speed RZ signals.

In [37] an all-optical AND gate is reported using cross-polarization modulation in a SOA. This effect is observed when the polarization of the probe signal propagating

in an SOA is affected by the polarization and the power of the control beam introduced simultaneously into the amplifier.

FWM in an SOA has also been utilized to demonstrate AND logic [38]. However, the slow carrier recovery time of the SOA limits the performance of this scheme at higher speeds. Recently, InGaAsP-InP based microring resonators have attracted a lot of attention due to their compact size and have been utilized to realize AND operation using FWM [39].

Bogoni et al. [40] reported all-optical ultra-fast and reconfigurable logic gates based on nonlinear optical loop mirrors (NOLMs) exploiting self-phase modulation (SPM) and cross-phase modulation (XPM) in 1 km long dispersion shifted fiber (DSF). The reconfigurability feature was a result of a non-polarization maintaining (PM) implementation that allowed changing the NOLMs nonlinear characteristics by tuning the polarization controller in the loop. All optical AND, OR, XOR, and NOR, XNOR functions, respectively were realized using this scheme.

The fiber based logic devices have many advantages over their semiconductor based counterparts. Examples include, no additional noise, no electrical bias, high speed operation, and no heat dissipation. However, the requirement of long length of fiber to trigger nonlinear effects would be a limiting factor in terms of practical and compact logic devices.

In this project we propose a compact, high speed all-optical AND gate based on FWM in only 1.9-meter long Bi-HNLF. The principle of the AND logic is that in the presence of the pump signals (A and B) into the HNLF the FWM process will generate additional sidebands on each side of pump signals. Since these sidebands are only generated when both the pump signals are present (ON-state) and thus represent the AND function between the two input logic signals.

5.5.1 Experiments and Discussions

Figure 5.19 shows the schematic of the experimental setup to demonstrate the proposed all-optical AND gate based on FWM in 1.9-m long Bi₂O₃-HNLF. The input-A pump beam at 1553.33 nm is a 2³¹-1 bits NRZ pseudorandom signal at 10 Gbit/s. It is prepared by externally modulating a tunable laser (TL-1) with an electro-optic Lithium Niobate (LiNbO₃) modulator driven by a pulse pattern generator. The input-B pump signal at 1554.13 nm was generated after external modulation of tunable laser (TL-2). These two pump beams were separately amplified to an average power of about 300 mW by using EDFAs with a maximum saturation output power of 500mW. Polarization controllers (PCs) were included on both the data and control launching paths into the Bi₂O₃-HNLF to ensure coincidence of the state of polarization (SOP). The two inputs (A&B) were combined using a 100 GHz channel spacing

dense wavelength division multiplexer to reduce amplified spontaneous emission (ASE) noise from the two EDFAs. The combined signals were then launched into 1.9-m long Bi-HNLF. The splicing losses at the input and output side of the fiber and other fiber parameters are provided in section 5.3.

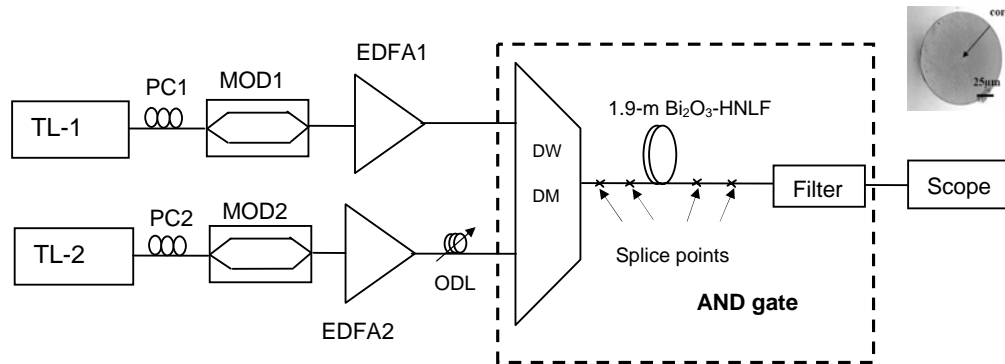


Fig. 5.19 Experimental setup of an all optical AND gate. (Inset shows the microscopic view of Bi-HNLF). TL: Tunable laser, PC: Polarization controller, MOD: Modulator, EDFA: Erbium doped fiber amplifier, DWDM: Dense Wavelength division multiplexer, ODL: Optical delay line

The output spectra of FWM signals measured after the $\text{Bi}_2\text{O}_3\text{-HNLF}$ is shown in Fig. 5.20. More than two new wavelengths are generated due to FWM process in the $\text{Bi}_2\text{O}_3\text{-HNLF}$. All these wavelengths carry the same AND signal simultaneously.

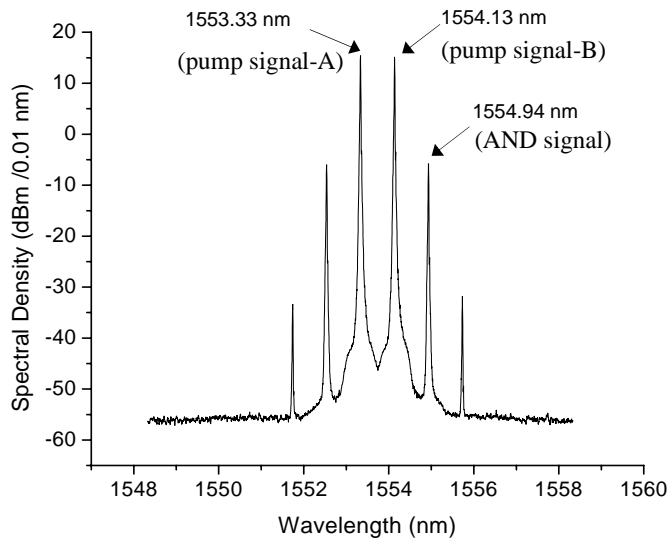


Fig. 5.20 Output spectra of FWM signals

Finally, we used a thin film filter with a bandwidth of 0.6 nm to filter out the AND signal at 1554.94 nm. The output is investigated using an optical spectrum analyzer of 0.01 nm resolution and a 50 GHz sampling oscilloscope. The Fig. 5.21(a) and 5.21(b) depict the time domain diagrams of the input-A and input-B pump beams respectively. Fig. 5.21(c) shows the timing diagram of the AND signal at 1554.94 nm. The AND signal has a relatively low noise level and high extinction ratio. The '0' rail of the AND signal is not perfectly flat due to small variation in the extinction ratios of the two modulators. Nevertheless, the proposed scheme has a potential of operating beyond 10 Gbit/s.

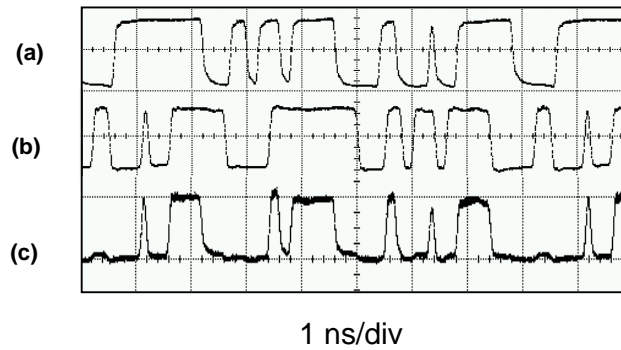


Fig. 5.21 Timing diagrams (a) 10 Gb/s NRZ pump signal-A, (b) 10 Gb/s NRZ data signal-B (c) AND signal

The eye diagram of the output AND signal is shown in Fig. 5.22. Clear eye opening of the AND signal is observed. The thickness of the '1' rail is due to the beating between the in-band ASE of the two EDFAs which get transferred to the idlers. Further performance improvement can be achieved by reducing the splicing loss and increasing the fiber nonlinearity.

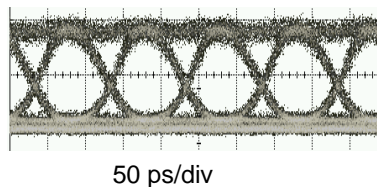


Fig. 5.22 Eye diagram of AND signal

5.6 Chapter Summary

In this chapter a new type of highly nonlinear fiber based on bismuth glass was introduced. Using a very short length of this special fiber all-optical signal processing devices were proposed and experimentally demonstrated. An all-optical on-off switch, tunable pulsewidth generator, and an all-optical AND gate were realized with the added advantage of compact size. Bi-HNLF technology will prove to be a powerful way to realize a range of practical signal processing devices. These devices will play an indispensable role in the future all-optical signal processing systems based on HNLFs.

References

- [1] G. P. Agrawal, *Nonlinear fiber optics*, Academic Press, New York, 2001.
- [2] J. H. Lee, T. Nagashima, T. Hasegawa, S. Ohara, N. Sugimoto, T. Tanemura, and K. Kikuchi, “Wavelength conversion of 40-Gbit/s NRZ signal using four-wave mixing in 40-cm-long bismuth oxide based highly-nonlinear optical fiber,” in *Proc. OFC*, Anaheim, CA, paper PDP23, (2005).
- [3] J. H. Lee, “All-fiber 80-Gbit/s wavelength converter using 1-m-long bismuth oxide-based nonlinear optical fiber with a nonlinearity of $1100 \text{ W}^{-1} \text{ km}^{-1}$,” *Opt. Express*, **13**, 3144–3149 (2005).
- [4] N. Sugimoto, T. Nagashima, T. Hasegawa, S. Ohara, K. Taira, and K. Kikuchi, “Bismuth-based optical fiber with nonlinear coefficient of $1360 \text{ W}^{-1} \cdot \text{km}^{-1}$,” in *Proc. OFC LA*, paper PDP26 (2004).
- [5] S. Ohara, N. Sugimoto, K. Ochiai, H. Hayashi, Y. Furusawa, T. Hirose, T. Nagashima, and M. Reyes, “Ultrawideband amplifiers based on Bi_2O_3 -EDFAs,” *Opt. Fiber Technol.* **10**, 283-295 (2004).
- [6] H. Ebendorff-Heidepriem, P. Petropoulos, S. Asimakis, V. Finazzi, R. C. Moore, K. Frampton, F. Koizumi, D.J. Richardson, and T. M. Monro, “Bismuth glass holey fibers with high nonlinearity,” *Opt. Express* **12**, 5082-5087 (2004).
- [7] J. H. Lee, T. Tanemura, T. Nagashima, T. Hasegawa, S. Ohara, N. Sugimoto,

- and K. Kikuchi, "Experimental comparison of Kerr nonlinearity figure-of-merit including stimulated Brillouin scattering threshold for state of-the-art nonlinear optical fibers," *Opt. Lett.*, **30**, 1698-1670 (2005).
- [8] T. Nagashima, T. Hasegawa, S. Ohara, and N. Sugimoto, "Bi₂O₃ based glass with high refractive index for nonlinear optical applications," *20th international congress on glass, Japan*, 14-006, (2004).
- [9] T. Nagashima, T. Hasegawa, S. Ohara, N. Sugimoto, K. Taira and K. Kikuchi, "Bi₂O₃-based highly nonlinear fiber with step index structure," *Photonics West, San Jose*, 5350-7 (2004).
- [10] N. J. Dorren and D. Wood, "Nonlinear optical loop mirror," *Opt. Lett.*, **13**, 56-58 (1988).
- [11] K. L. Blow, N. J. Dorren, and B. P. Nelson, "Demonstration of the nonlinear loop mirror as an ultrafast all-optical demultiplexer," *Electron. Lett.*, **26**, 962-964 (1990).
- [12] H. C. Lim, T. Sakamoto, and K. Kikuchi, "Polarization independent optical demultiplexing by conventional nonlinear optical loop mirror in a polarization diversity loop configuration," *IEEE Photon. Technol. Lett.*, **12**, 1704-1706 (2000).
- [13] M. Eiselt, W. Pieper, and H. G. Weber, "SLALOM as high speed

- multiplexer/demultiplexer,” *Elect. Lett.*, **28**, 1505-1507 (1992).
- [14] J. P. Sokoloff, P. R. Prucnal, I. Glesk, and M. Kane, “A terahertz optical asymemetric demultiplexer (TOAD),” *IEEE Photon. Technol. Lett.*, **5**, 787-789 (1993).
- [15] C. Schunert, J. Berger, S. Diez, H. J. Ehrke, R. Luwig, U. Feiste, C. Schmidt, H. G. Weber, G. Toptchiyski, S. Randel, and K. Petermann, “Comparison of all optical switches for demultiplexing applications in high speed OTDM systems,” *IEEE J. Lightw. Technol.*, **20**, 618-624 (2002).
- [16] M. T. Hill, A. Srivatsa, N. Calabretta, Y. Liu, H. de Waardt, G. D. Khoe, and H. J. S. Dorren, “ 1×2 optical packet switch using all optical header processing,” *Electron. Lett.*, **37**, 774-775 (2001).
- [17] S. Nakamura, Y. Ueno, amd Tajima, “Ultrafast all-optical switching based on frequency shift accompanied by the semiconductor band-filling effect, *IEEE LEOS* ,**1**, 160-161 (1998).
- [18] J. H. Kim, K. R. Oh, H. S. Kim, and K. Chao, “All-optical switching by counter propagating operation in cascaded semiconductor optical amplifiers,” *IEEE Photon. Technol. Lett.*, **12**, 513-515 (2000).
- [19] L. Y. Chan, P. K. A. Wai, L. F. K. Lui, B. Moses, W. H. Chung, H. Y. Tam, and M. S. Demokan, “ Demonstration of an all optical switch by use of a

- multiwavelength mutual injection-locked laser diode,” *Opt. Lett.*, **28**, 837-839 (2003).
- [20] T. Morioka, S. Kawanishi, K. Uchiyama, H. Takara and M. Saruwatari “Polarisation-independent 100 Gbit/s all-optical demultiplexer using four-wave mixing in a polarisation-maintaining fibre loop”, *Electron. Lett.*, **30**, 591-592 (1994).
- [21] P. O. Hedekvist and P. A. Andrekson, “Demonstration of fibre four-wave mixing optical demultiplexing with 19dB parametric amplification”, *Electron. Lett.*, **32**, 830-831 (1996).
- [22] K. Kikuchi and C. Lorattanasane, “Design of highly efficient four-wave mixing devices using optical fibers”, *IEEE Photon. Technol. Lett.*, **6**, 992-994 (1994).
- [23] L. Xu, P. K. A. Wai, L. F. K. Lui, and H. Y. Tam, “ All optical shutter based on Raman-Assisted Four-wave mixing in dispersion shifted fiber,” TuC7, *OFC*, (2004).
- [24] L. S. Yan, S. M. R. M. Nezam, A. B. Sahin, J. E. McGeehan, T. Luo, and A. E. Willner, “Performance optimization of RZ format in WDM systems using tunable pulse-width management at the transmitter,” *IEEE J. Lightw. Technol.*, **23**, 1063-1067 (2005).

- [25] D. Kovsk, E. A. Goolvchenko, and A. N. Pilipetskii, "Enhancement in performance of long-haul DWDM systems via optimization of long-haul DWDM systems via optimization of the transmitter format," *OFC*, **1**, MF5/1-3, (2001).
- [26] A. Takada, K. Sato, M. Saruwatari, and M. Yamamoto, "Pulse width tunable subpicosecond pulse generation from an actively modelocked monolithic MQW laser/MQW electroabsorption modulator," *Elect Lett.*, **30**, 898-900 (1994).
- [27] S. V. Chernikov, M. J. Guy, J. R. Taylor, D. G. Moodie, and R. Kayhyap, "Duration-tunable 0.2 -20 ps 10 GHz source of transform-limited optical pulses based on an electroabsorption modulator," *Opt Lett.*, **23**, 2399-2402 (1995).
- [28] Z. Jiang, D. E. Leaird, and A. M. Weiner, "Width and wavelength tunable optical RZ pulse generation and RZ-to-NRZ format conversion at 10 GHz using spectral line-by-line control," *Photon. Technol. Lett.*, **17**, 2733-2735 (2005).
- [29] Z. Jiang, D. E. Leaird, and A. M. Weiner, "Spectral line-by-line pulse shaping," *Opt. Lett.*, **17**, **30**, 1557-1559 (2005).

- [30] C. Yu, L. S. Yan, T. Luo, Y. Wang, Z. Pan, and A. E. Willner, "Width-tunable optical RZ pulse train generation based on four wave mixing in highly nonlinear fiber," *Photon. Technol. Lett.*, **17**, 636-638 (2005).
- [31] A. Zhang, H. Liu, M. S. Demokan, and H. Y. Tam, "Width and wavelength tunable optical pulse train generation based on four wave mixing in highly nonlinear photonic crystal fiber," *Photon. Technol. Lett.*, **17**, 2664-2666 (2005).
- [32] K. L. Hall and K. A. Rauschenbach., "100-Gbit/s bitwise logic," *Opt. Lett.*, **23**, 1271-1273 (1998).
- [33] A. J. Poustie, K. L. Blow, A. E. Kelly, and R. J. Manning, "All optical full adder with bit-differential delay," *Opt. Commun.*, **168**, 89-93 (1999).
- [34] A. J. Poustie, K.L. Blow, A. E. Kelly, and R. J. Manning, "All-optical binary half adder with bit-differential delay," *Opt. Commun.*, **156**, 22-26 (1998).
- [35] A. J. Poustie, K.L. Blow, A. E. Kelly, and R. J. Manning, "All-optical parity checker with bit-differential delay," *Opt. Commun.*, **162**, 37-43 (1999).
- [36] B. K. Kang, J. H. Kim, Y. T. Byun, S. Lee, Y. M. Jhon, D. H. Woo, J. S. Yang, S. H. Kim, Y. H. Park and B. G. Yu, "All-optical AND gate using probe and pump signals as the multiple binary points in cross phase modulation," *Jpn. J. Appl. Phys.*, **41**, L568-L570 (2002).

- [37] H. Soto, C. A. Diaz, J. Topomondzo, D. Erasme, L. Schares, and G. Guekos, "All-optical AND gate implementation using cross-polarization modulation in a semiconductor optical amplifier," *Photon. Technol. Lett.*, **4**, 498-500 (2002).
- [38] D. Nasset, M. C. Tatham, and D. Cotter, "High bit rate operation of an all optical AND gate by using FWM in an SLA with degenerate input signals," *OFC*, TuD2, (1995).
- [39] S. Mikroulis, H. Simos, E. Roditi, and D. Syvridis, "Ultrafast all-optical AND logic operation based on four-wave mixing in a passive InGaAsP-InP microring resonator," *Photon. Technol. Lett.*, **17**, 1878-1880 (2003).
- [40] A. Bogoni, L. Poti`, R. Proietti, G. Meloni, F. Ponzini, and P. Ghelfi, "Regenerative and reconfigurable all-optical logic gates for ultra-fast applications," *Electron. Lett.*, **41**, March, (2005).
- [41] J. H. Lee., T. Nagashima, T. Hasegawa, S. Ohara, N. Sugimoto, and K. Kikuchi, "40 Gbit/s XOR and AND gates using polarization switching within 1 m-long bismuth oxide-based nonlinear fibre," *Electron. Lett.*, **41**, sept, (2005).

Chapter 6

Injection Locking in Fabry Pérot laser diodes

6.1 Introduction

Christiaan Huygens in 17th century first observed injection-locking in a mechanical phenomenon: clocks that are in physical proximity can synchronize each other. Later, in the early 20th century, physicists rediscovered this phenomenon in electrical circuits. Since then injection locking has become an area of intense research. Among the various mathematical treatments of injection locking, the method developed by Van der Pol [1] and its extension by Andronov and Witt [2] are very popular. In 1966 Stover and Steier [3] demonstrated, locking a He-Ne laser by injection of another He-Ne laser and measured the locking range of the laser as a function of drive level of the locking signal. Buczek and Freiberg in 1972 [4] showed that carbon dioxide (CO₂) ring laser can be frequency stabilized by injection-locking with a stable low power reference laser. Experimental demonstration of injection-locking in AlGaAs semiconductor lasers was first reported in early 1980's by

Kobayashi and Kimura [5,6]. They studied the Injection locking phenomenon in an AlGaAs double-heterostructure with respect to locking frequency range and locking gain. Experimental results of locking half bandwidth versus the ratio of locked-laser power to injected power agreed well with the theoretical value based on Adler's theory [7].

The injection of single longitudinal mode beam, emitted from a 1.55 μm InGaAsP buried-heterostructure semiconductor laser was studied by Yamada et. al. [8]. Using this light injection technique, single longitudinal mode operation of the directly modulated laser was realized. Without light injection, a single pulse was split into multiple pulses after transmitting through a 44.3 km long single mode fiber. However, when optical beam was injected into the modulated laser, no pulse splitting was observed while passing through the same length of fiber.

Otsuka and Tarucha [9] investigated the injection locking of semiconductor lasers theoretically by numerical analysis. They reported that the frequency tuned weak injection light can effectively suppress the spectral broadening, and results in single-longitudinal oscillation. Lang [10] studied the injection locking in semiconductor lasers taking into consideration the carrier density dependence of the refractive index. The carrier density dependent refractive index causes the locked output versus the detuning to be asymmetric.

The research carried out by Henry et al. [11] on injection-locking of a 1.54 μm wavelength InGaAsP laser also revealed a highly unsymmetrical increase in the slave laser intensity as the master laser was tuned across the tuning range. The physical origin of the instability on the higher end of the locking range is attributed to the change in laser, altering the phase of the laser field relative to that of the injected field [11]. Optical injection both increases the relaxation oscillation frequency and introduces both damping and destabilizing terms, which cause the oscillations to go from strongly damped on the low frequency end of the locking range to unstable on the high frequency end [11].

Kawaguchi et al., [12] reported the theoretical and experimental considerations of the bistability in the locking curve. Bistable characteristics were observed in the locked output versus wavelength detuning curve by varying the master laser temperature. Bistability was also observed in the locking curve by varying the driving current of the master laser. The bistability was based on the wavelength shift caused by the active region temperature change in the master laser.

Li [13] reported the static and dynamic properties of injection locked lasers and concluded that, when a laser is biased far above the threshold or is locked by a large injection power, the influence of the nonlinear gain is significant. In [14] Li studied optical frequency bistability and power bistability using a unified description of

semiconductor lasers with external light injection. Li et al. [15] also studied theoretically the dynamic properties of optically switched bistable semiconductor lasers biased from below to above threshold. A small detuning is desired to reduce the switching-on and switching-off times. The switching-on and switching-off times are related to the laser parameters and the parameters of the input optical signal (optical power and the frequency detune).

Horer and Patzak [16] developed a large signal analysis model of all-optical wavelength conversion using two mode injection locking in a dc biased Fabry Perot laser diode. The conversion mechanism is mainly attributed to the dispersive switching which is shown to be very fast above threshold due to injection locking.

6.2 Applications of Injection Locking

There are numerous applications of injection-locking technique. Examples include, wavelength conversion, 2R regeneration, chirp reduction, partition noise reduction, measurement of linewidth enhancement factor, polarization stabilization, phase shift keying modulation, radio-over-fiber (ROF), mm-wave generation, multicasting, and un-cooled transmitters using tunable vertical cavity surface emitting lasers (VCESLs).

Injection-locking is used for radio-over-fiber applications [17]. A DFB laser

was directly modulated with a 125 Mb/s digital signal multiplexed to an RF carrier of 18 GHz. Due to the injection-locking resonance frequency enhancement, narrow-band transmission at the sharp resonance frequency peak was possible. In a similar approach, injection-locking is applied in a Cable Television (CATV) transmission experiment, demonstrating performance improvement with locking [18]. The external light-injection technique greatly enhanced the frequency response of the laser diode, and thus improved the overall performance of the fiber optical CATV system.

Optical generation of millimeter-waves has been demonstrated by a sideband injection-locking technique [19-20], with sub-Hertz RF line-widths. Recently, it has been implemented in a monolithic two-laser device [21]. The two lasers are biased such that they are unlocked and detuned by 36 GHz. The follower laser is modulated at 12 GHz and has a third harmonic at 36 GHz, which gives rise to locking at this spectral component. Monolithic integration has also shown a resonance frequency enhancement to 21 GHz [22].

Retiming of signals, pulse shaping as well as wavelength conversion over 32 nm is demonstrated at 2.5 and 5 Gbit/s with bi-stable semiconductor lasers. It is also shown that switching is possible at 10 Gbit/s using the same mechanism [23].

A multi-wavelength WDM transmitter for use in multicasting applications was

demonstrated using inter-modal injection-locking, where 8 modes in the FP laser were simultaneously locked [24].

6.3 Semiconductor laser diodes

Semi-conductor lasers have assumed an important technological role since their invention in the early 1960s. Judged by economic impact, semi-conductor lasers have become the most important class of lasers. They are now used in applications such as cable TV signal transmission, telephone and image transmission, computer interconnects and networks, compact disc (CD) players, bar-code readers, laser printers, and many military applications. They are now figuring in new applications ranging from two-dimensional display panels to erasable optical data and image storage. They are also invading new domains such as medical, welding, and spectroscopic applications that are now the captives of solid state and dye lasers. The main reason behind this major surge in the role played by semi-conductor lasers is their continued performance improvements especially in low-threshold current, high speed direct current modulation, ultra-short optical pulse generation, narrow spectral line-width, broad line-width range, high optical output power, low cost, low electrical power consumption and high efficiency [25].

In the FP (Fabry-P erot) resonator, a pair of partially reflecting mirrors are directed towards each other to enclose the cavity. The mirror facets are constructed by making two parallel clefts along natural cleavage planes of the semiconductor crystal. The purpose of these mirrors is to provide strong optical feedback in the longitudinal direction, thereby converting the device into an oscillator with a gain mechanism that compensates for the optical losses in the cavity. The laser cavity can have many resonant frequencies. The device will oscillate at those resonant frequencies for which the gain is sufficient to overcome the losses. The sides of the cavity are simply formed by roughening the edges of the device to reduce unwanted emissions in these directions [26].

The DFB (Distributed Feedback Laser) is designed to overcome the spectral shortcomings of the FP laser. It is very similar to an FP laser with the addition of Bragg reflector structure located near the light-emitting active region. The Bragg reflector grating provides a periodic change in the index of refraction in the wave-guide. Each period of grating reflects a small amount of light back in the opposite direction. The Bragg grating forms an efficient mirror at the wavelength where the grating period is one-half of the wavelength of light in the semiconductor material. The small dimensions of the grating make the device fabrication technology more critical than an FP laser. Extra wafer processing steps are necessary to etch the

Bragg grating into the semiconductor material and to grow new materials on top. This results in a more expensive laser diode. DFB lasers are the industry standard for the use in long-distance fiber-optic links. [27]

The Vertical cavity surface emitting laser (VCSEL) was originally developed as a low-cost alternative to FP and DFB lasers. The first commercial application of these lasers was in the area of high-speed data communication links replacing LEDs. Vertical cavity surface emitting lasers emit perpendicular to the top plane of a semiconductor wafer. The VCSEL uses a multilayer dielectric mirror that is grown directly on the semiconductor surface. This mirror consists of alternations of high and low index of refraction layers to form a Bragg reflector. The distinguishing feature of this structure is its extremely short optical amplifier length (on the order of 100 nm). This length is compared to the 300 μm length typical of an FP or a DFB laser. This short amplifier length limits the available gain from the amplifier to a very small value. The mirror reflectivity is very high so that the low-gain optical amplifier can achieve threshold. Only a single longitudinal mode is available because of the small distance between mirrors [27].

Generally, InGaAsP and GaAlAs semiconductor materials are used to make laser diodes. There are two commonly employed structures to manufacture these types of laser diodes. They are buried hetero (BH) and multi-quantum well (MQW) structures.

MQW lasers offer significant advantages over BH lasers. They offer lower threshold current, higher slope efficiency, low noise, better linearity, and better stability over temperature. One drawback of MQW lasers is their susceptibility to back reflections [26].

The properties and characteristics of Fabry Pérot laser diode (FP-LD) find many promising applications in the field of all-optical signal processing. Here we are using injection locking property in a FP-LD to implement all-optical logic gates and an all-optical bit error monitoring system, which will be discussed in the next chapter.

6.4 Characterization of a Fabry Pérot laser diode

In our work we utilized off-the-shelf FP-LD manufactured by Wuhan Telecommunication Corporation (WTC), Wuhan, China. The FP-LD has a double channel planar buried heterostructure (DC-PBH) and multi-quantum well (MQW) active region with InGaAsP as the active layer surrounded by layers of InP acting as cladding. The FP-LD has a threshold current of ~ 10.8 mA with the longitudinal mode spacing of around 1.1 nm at room temperature.

6.4.1 Light (L) ~ Current (I) relationship of semiconductor Laser

The light (L) emitted by a semiconductor laser is measured as a function of its applied bias current (I). The resulting curve which is strongly temperature dependent is referred to as Light (L) ~ Current (I) curve. The current at which the light output abruptly starts increasing, corresponds to the laser threshold current (I_{th}). The threshold current (I_{th}) is an important laser parameter and its minimization is often sought. In the proximity of the I_{th} , the light increases by several orders of magnitude. When $I < I_{th}$, the light output consists of only spontaneous emission whereas when $I > I_{th}$ stimulated emission dominates. The temperature variation of I_{th} can be approximated by the empirical expression [26]:

$$I_{th}(T) = I_z e^{(T/T_o)} \quad (6.1)$$

where T_o is a measure of the relative temperature insensitivity and I_z is a constant. For the conventional stripe geometry GaAlAs laser diode T_o is typically 120° to 165° C in the vicinity of room temperature. The variation in I_{th} with temperature is 0.8 percent $^\circ$ C. Smaller dependences of I_{th} on temperature have been demonstrated for GaAlAs quantum-well heterostructure lasers. For these devices T_o can be as high as 473° C. The threshold variation of this particular laser type is 0.23 percent $^\circ$ C. The lasing threshold can also change as the laser ages. Consequently, if a constant optical output power level is to be maintained as the temperature of the laser changes or as the laser

ages, it is necessary to adjust the dc bias current level. Possible methods for achieving this automatically are optical feedback schemes, temperature-matching transistors, and threshold-sensing circuits [26]. Figure 6.1 shows the temperature-dependent behavior of the optical output power as a function of operating current of the FP-LD. The threshold current (I_{th}) of the FP-LD (model LDM5S813) at room temperature (25° C) is 10.8 mA. The threshold current (I_{th}) of the FP-LD increases with the operating temperature.

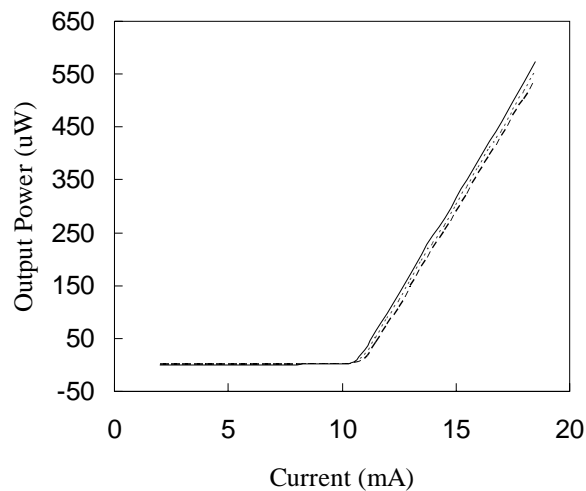


Fig. 6.1 Temperature-dependent behavior of the optical output power as a function of the bias current for the FP-LD for three different temperatures, 20° C (solid line), 25° C (dotted line) and 30° C (dashed line)

6.4.2 Effect of operating current on FP-LD

The spectral output of a solitary FP-LD is affected by its operating current. In fact, the whole FP-LD spectrum is red-shifted (longer wavelength) with an increase in its operating current. The total output power as well as the power of individual longitudinal mode is larger at higher operating currents.

Figure 6.2 shows the solitary FP-LD spectra at different biasing currents. On a 30 nm span of optical spectrum analyzer (OSA) with a resolution of 0.1 nm, when the FP-LD operates at $1.1 I_{th}$ the main mode would be the 13th mode (counting from the left side of the spectrum), and it would be 15th mode when the FP-LD is operated at $1.5 I_{th}$. The FP-LD shows broadband lasing of the cavity modes within the gain spectrum.

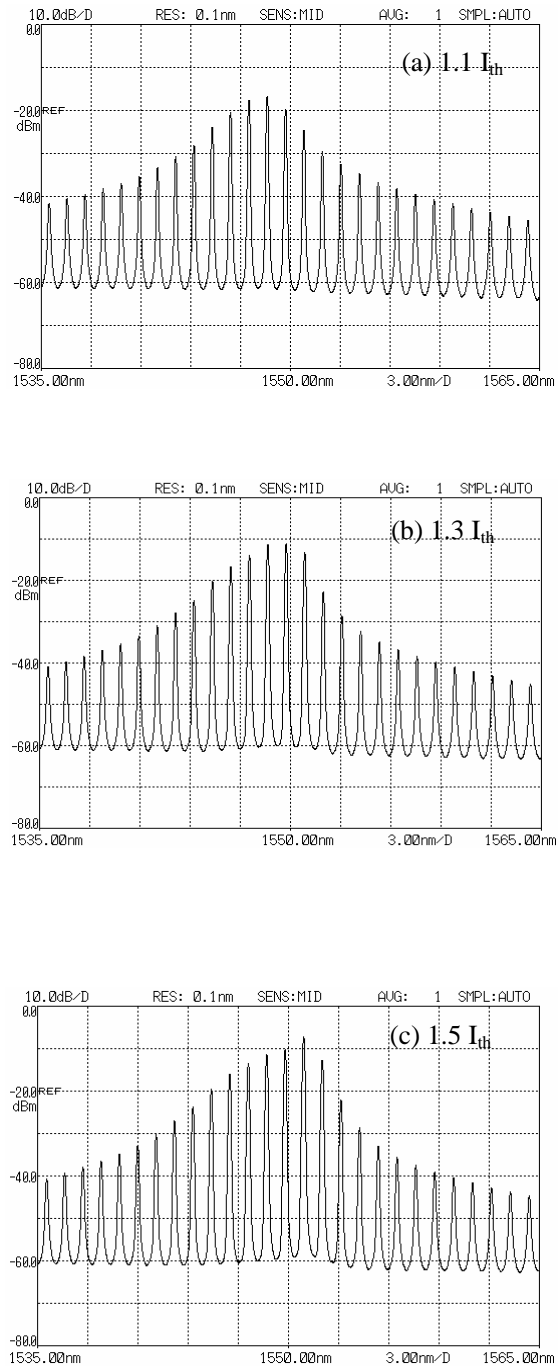


Fig. 6.2 Free running FP-LD longitudinal modes under different bias conditions, (a) $1.1 I_{th}$, (b) $1.3 I_{th}$ and (c) $1.5 I_{th}$.

6.5 Single mode injection locking in FP-LD

Injection-locking occurs when an external optical signal called the master signal is injected into the resonant cavity called the slave laser within a well-defined range called the locking range around the laser's free running frequency. The injected light is resonantly amplified and all the other laser modes are strongly suppressed and hence the master light controls the subsequent behavior of the slave laser.

Figure 6.3(a,b,c) shows the spectra of single-mode injection locked FP-LD for 3 different longitudinal modes in the wavelength range from 1535 nm to 1565 nm.

Figure 6.4 shows the side mode suppression ratio (SMSR) under single mode injection locking from 1535 to 1565 nm. The SMSR is mostly above 40 dB along this span for a fixed input power of 0 dBm from the tunable laser.

The factors that affect the spectral output of single mode injection locking are (i) biasing current applied to the FP-LD (ii) operating temperature of the FP-LD (iii) wavelength detune (wavelength difference between the injected signal and the respective FP-LD longitudinal mode) (iv) injected signal power to the FP-LD (v) selection of the longitudinal mode of FP-LD. An increase in FP-LD bias current would shift the entire spectrum of the solitary FP-LD towards the red side (longer wavelength) of the spectrum as well as causes an increase in output power. The

injection-locking of FP-LD would also shift the longitudinal modes towards the red side of the spectrum (longer wavelength side).

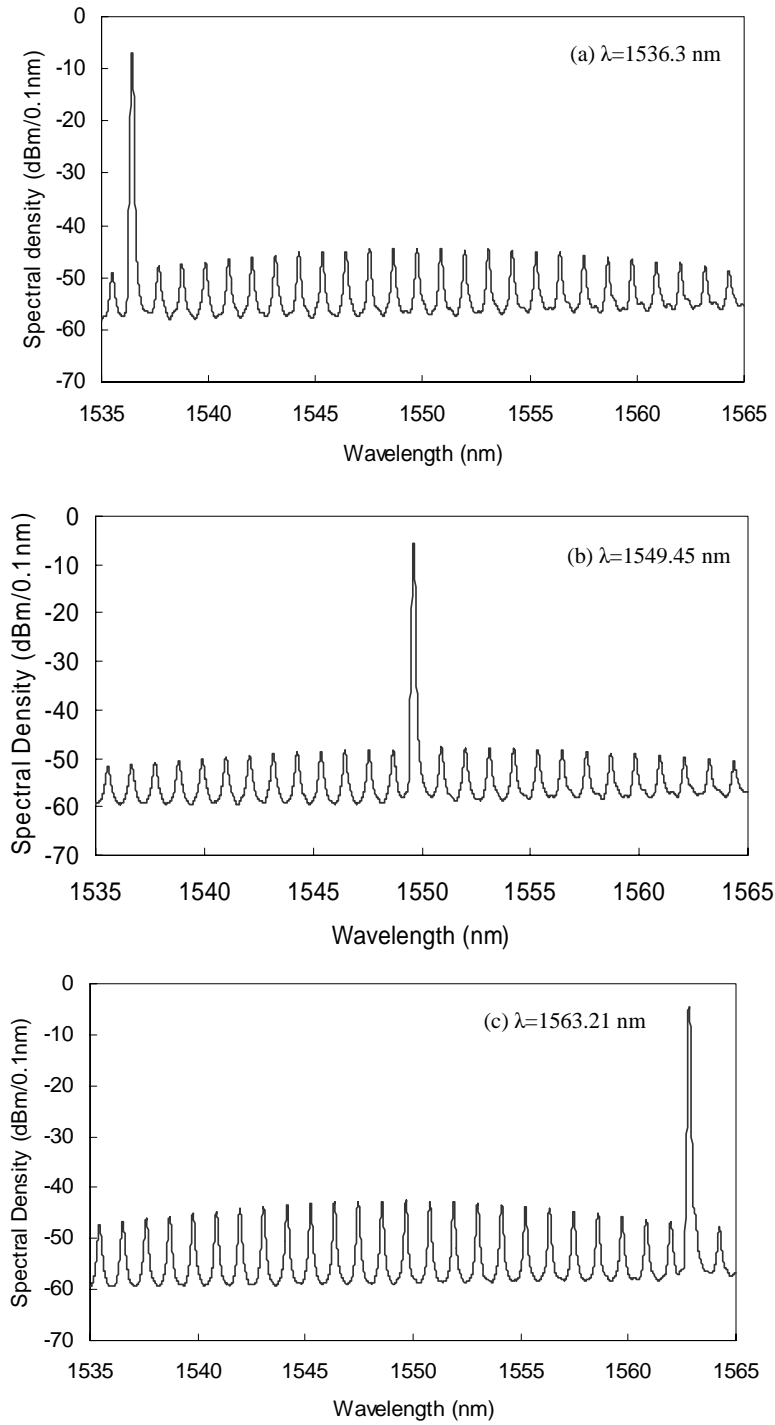


Fig. 6.3 Injection-locking at three different FP-LD modes, (a) 1536.3 nm (b) 1549.45 nm (c) 1563.21 nm

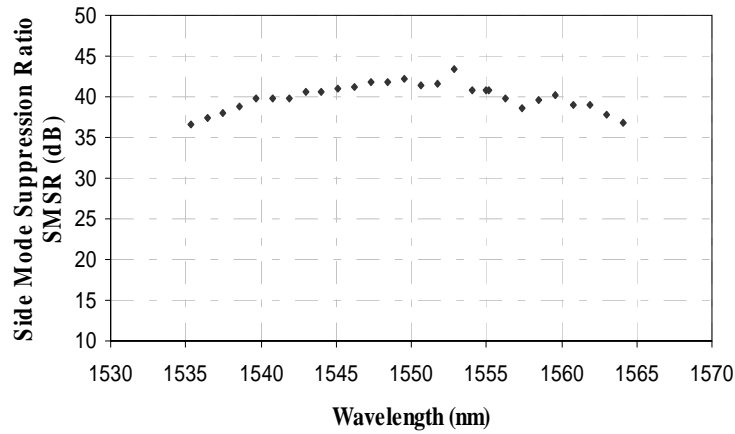


Fig. 6.4 Side mode suppression ratio for single mode injection locking

Figure 6.5(a) shows five modes of the free running FP-LD at a biasing current of $1.3I_{th}$. The longitudinal mode at 1548.75 nm is injection locked. Figure 6.5(b) shows the spectrum of injection locked FP-LD. The master signal is injected with a wavelength detune of 0.18 nm using a tunable laser. The injection locked mode along with the suppressed side modes are red shifted by 0.25 nm. A SMSR of around 45 dB is also observed. This phenomenon of mode-shift over shooting detune ($\lambda_{shift} > \lambda_{detune}$) has been reported in [28,29].

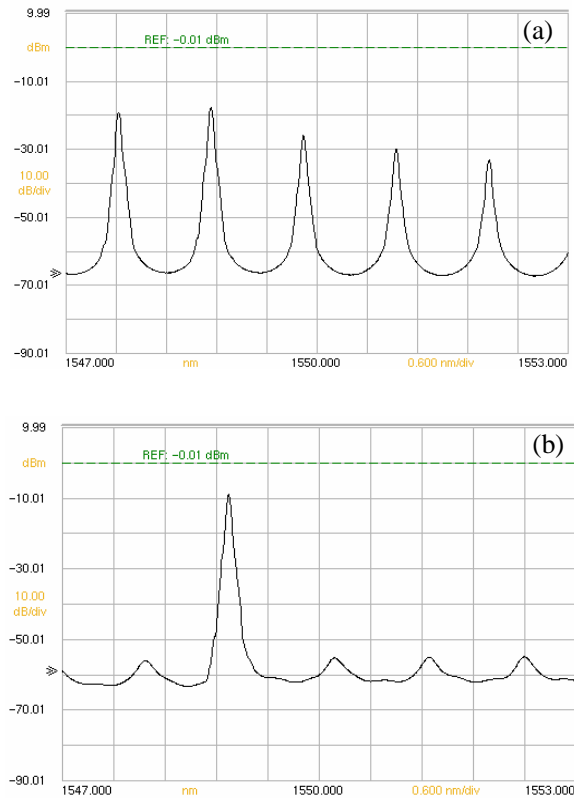


Fig. 6.5 (a) Five modes of the free running FP-LD (b) injection-locked mode

The experimental configuration shown in Figure 6.6 was used to characterize the injection locking phenomenon, to investigate the polarization effect on injection locking and also to observe the asymmetric injection locking curve.

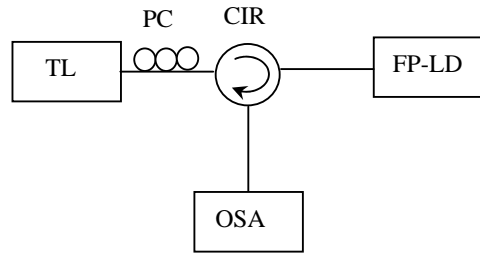


Fig. 6.6 Experimental setup for investigating injection locking of a FP-LD and its polarization characteristics.

The master laser used in the experiment was a tunable external cavity laser with wavelength tuning resolution of 10 pm. Port 1 and 2 of the polarization insensitive circulator were used to direct the power of the tunable laser to the FP-LD, the output of the FP-LD was monitored by an OSA through port 3 of the circulator. The bias current of the FP-LD was set to 12.96 mA ($1.2 I_{th}$). The polarization controller (PC) inserted after the tunable laser was used to align the polarization of tunable laser to the TE polarization of FP-LD. All the fibers used in the experiment were fixed on the optical table to avoid changes of the polarization state during the experiment. The tunable laser was turned on with an output power of 0 dBm, and PC was adjusted to optimize the output power of the tunable laser to the FP-LD by monitoring the OSA, i.e., aligning the polarization of the tunable laser to the FP-LD. This procedure

ensured that the output power of the tunable laser is injected to the TE mode of the FPLD. The tunable laser was scanned across the wavelength from 1554 nm to 1559 nm while being measured by the OSA. The OSA was set to the hold maximum mode such that the higher amplitude points of the spectrum were held during the sweep. Figure 6.7 (a) shows the free running spectrum of FP-LD. Figure 6.7 (b) shows the measured output spectrum. Injection locking was clearly observed at all the five cavity longitudinal modes of the FP-LD for TE injection. The injection locking range was 0.28 nm and was asymmetric because of the change in refractive index with carrier density due to optical injection [12]. The output power at unlocked and locked state were -24.5 dBm and -14.35 dBm, respectively, which implied 10.15 dB gain was obtained by the injection locking effect as shown in Fig. 6.7 (c).

The polarization dependent injection locking behavior can be explained by the fact that the FP-LD is an internally strained semiconductor laser operating in single TE mode (electric field parallel to the junction) because of higher mirror reflectivity of TE mode compared to that of TM mode (electric field normal to the junction) [30,31]. When the output of the tunable laser was aligned to the TE mode of the FP-LD, it will be strengthened resonantly by the injection locking effect whereas the orthogonally aligned polarized TM component will be strongly suppressed because of its lower gain and higher loss coefficient [32]. Therefore, the FP-LD in this experiment acts as a

polarization filter as well as an amplifying medium for the tunable laser when it is injection locked. Figure 6.7 (a,b) show that the output power from the port 3 of the circulator was -24.5 dBm when the wavelength of tunable laser is not matched with the TE and TM resonant modes. The insertion loss of the forward path, i.e., PC1 plus port 1 to port 2 of the circulator was measured to be 1.8 dB, while the insertion loss of the backward path, port 2 to port 3 of the circulator was 0.9 dB. Since the output power of the tunable laser was fixed at 0 dBm, the power loss of this injection locking technique is therefore about 21.8 dB. This significant loss is mainly caused by the high coupling loss for the light injected to the pigtailed FP-LD.

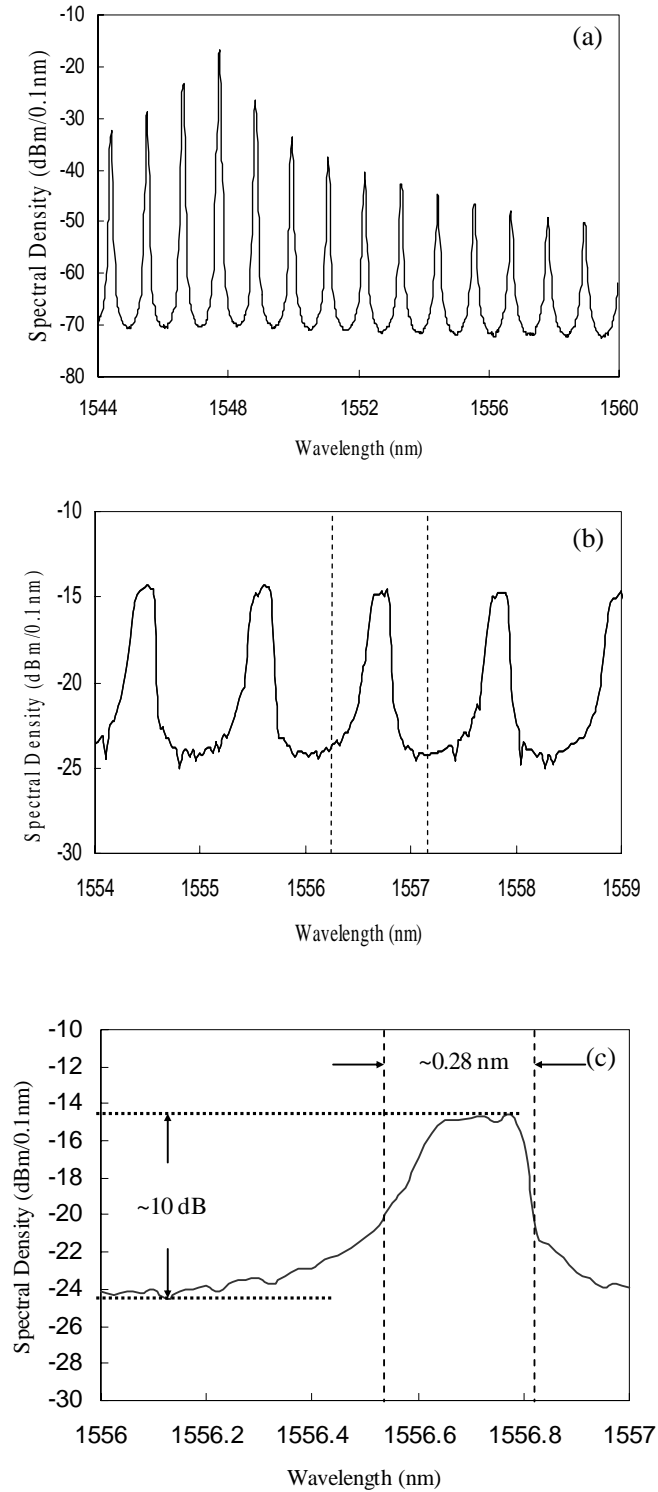


Fig. 6.7 (a) Optical spectrum of free running FP-LD (b) Optical spectrum measured at port 3 of the circulator by scanning the tunable laser aligned to TE mode using maximum hold function of the OSA (c) Magnified portion of (b)

6.5.1 Effect of wavelength detune on injection locking threshold power

If an external optical signal is injected at a given detune from the closest free-running mode of an FP-LD, there exists a threshold of the injected light power beyond which the external signal would injection lock the FP-LD and force it to operate at single wavelength at a constant output power. If the power of the external signal is below the injection locking threshold, the injected signal will experience loss.

This threshold power P_{th} is expressed as [33]

$$P_{th} = \frac{(2\pi\tau_d\Delta f)^2 P_i}{(1 + \alpha)} \quad (6.2)$$

where τ_d is the photon life time, Δf is the detune, P_i is the output power of one of the longitudinal modes of the FP-LD at the free running state, α is the linewidth enhancement factor. It is evident from (6.2) that the wavelength detune along with injection power of the master signal affects the injection locking mechanism. The larger wavelength detune requires greater injection power to attain injection locking. In order to study the effect of different wavelength detunes on the injection locking threshold power, the input-output characteristics of single mode injection locking were performed. These characteristics were obtained by varying the input power in steps of 0.05 dB. For any specific longitudinal mode of FP-LD, with a fixed wavelength detune of the external injected light, as the input power is increased the output power also increases. However, after further increase output power suddenly jumps to a

higher power level at a particular input power level, known as the threshold power (P_{th}) as expressed in equation (6.2). At this point the injection locking has initiated and the output is clamped to another higher output level. This is called intensity stabilization. Figure 6.8 depicts the input versus output power relationship for single mode of FP-LD when injected by an external signal at wavelength detunes of respectively 0.03 nm and 0.06 nm. The FP-LD was biased at $1.2 I_{th}$. When the wavelength detune is 0.03 nm, the output power rise by 10 dB, however for the larger wavelength detune of 0.06 nm, the output power rise by only 6 dB. Hence we can conclude that when the wavelength detune is increased, the injection locking threshold power P_{th} is also increased and the power rise reduces.

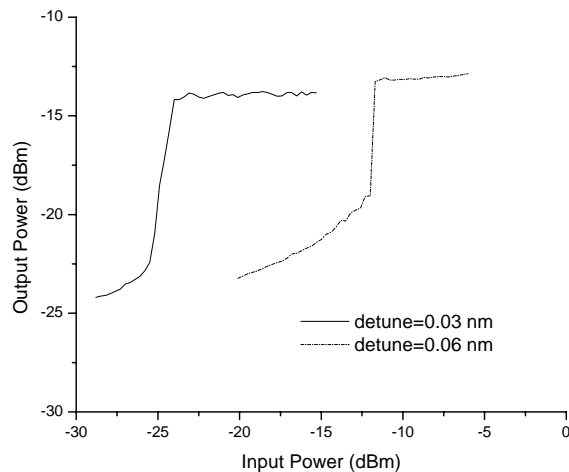


Fig. 6.8 Input-output characteristics for different detunes.

6.6 Optical bistability and hysteresis

Optical bistability, as the term implies, refer to the situation in which two stable output states are associated with a single input state. The existence of bistability depends on an appropriate system parameter, such as absorption coefficient or refractive index, which depend on the optical input intensity. Laser diodes that include saturable absorbers in their cavity show bistability in the optical-output-versus-current (L-I) curve and in the optical-output-versus-optical-input curve [34]. A saturable absorber is defined as a material whose absorption decreases with the increase in the incident radiation intensity. In the OFF state, there is only spontaneous emission from the gain region. Since the light level is low, light traveling in the waveguide between the reflecting ends will be strongly absorbed and there will be no laser action. In the ON state, the device operates as a laser. The population in the absorber is inverted by optical pumping from the gain region so that it is essentially transparent to the laser radiation. Chen and Liu [35-38] observed a new kind of optical bistability, called polarization bistability in semiconductor lasers. This phenomenon was observed in buried heterostructure InGaAsP/InP lasers operating near polarization transition temperature [36]. This temperature dependent behavior is attributed to the internal thermal stresses in the active layer, which modifies the band structure and thereby changes the optical gain of TM mode relative

to that of TE mode [36]. Switching between TE and TM states at the output of the semiconductor laser was experimentally obtained from an external TM polarized radiation [39]. Mori [39-40] found that the TE mode oscillation occurred when the semiconductor laser was biased slightly above the threshold current. When the TM polarized light was injected into the active layer of the laser, two different types of hysteresis loops were simultaneously observed in the input versus output characteristics. The switching times obtained were less than 1 ns for both switch-up and switch-down [40]. Fujita et al. [41] suggested that the underlying physical basis of this polarization bistability is the nonlinear gain saturation.

We also observed hysteresis behavior in the FP-LD, i.e., after injection locking the FP-LD (while output power is high) when the input power is decreased, the output power is still maintained at the same value for a significant decrease in input power and finally the output falls to a lower level on further decrease in input power. It is also worth mentioning that in the forward direction (while increasing the input power) the threshold (P_{th}) is reached at a higher input power than in the reverse direction (while decreasing the input power) where the output reduces to a lower power only when the input power is much smaller. Experiments were conducted to study the hysteresis phenomenon using single mode injection locking of FP-LD. Hysteresis effect was studied for different wavelength detunes of the injected signal as well as

under different biasing current applied to the FP-LD. Figure 6.9 depicts the hysteresis characteristics for different wavelength detunes of the injected signal. The FP-LD is biased at $1.5 I_{th}$. We observed the hysteresis width to be ~ 2 dB for a wavelength detune of 0.12 nm, which increases to ~ 4 dB when the wavelength detune is increased to 0.16 nm. The output power after injection locking is maintained at -7.6 dBm. At larger wavelength detunes of (> 0.2 nm) no significant jump in the output power was seen. For these detunes the output power increases gradually as the input power is increased and finally reaches a constant level without experiencing a jump in power.

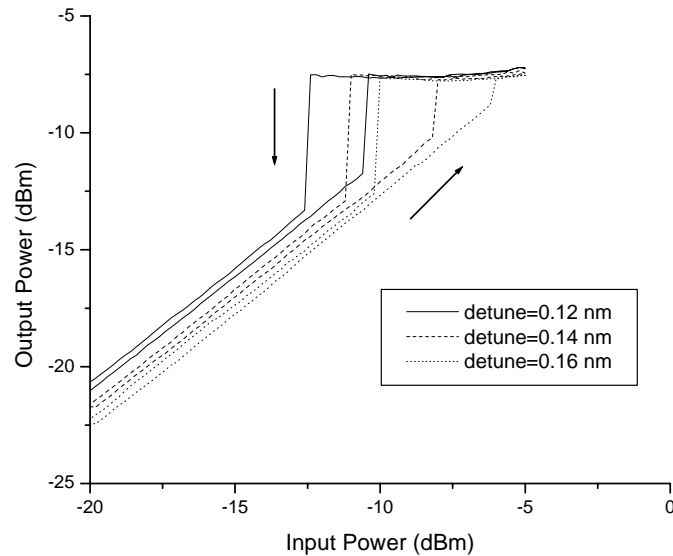
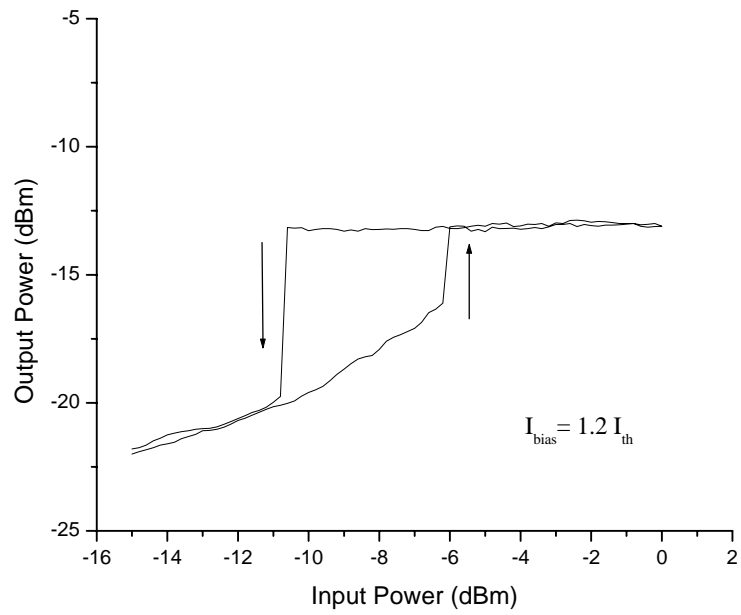


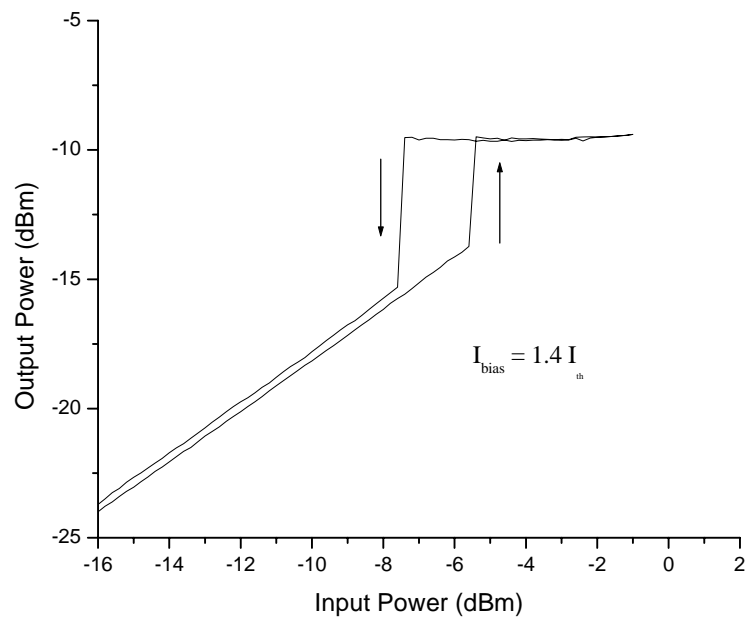
Fig. 6.9 Effect of different detunes on hysteresis during single mode injection locking of FP-LD.

Next we studied the effect of different biasing current applied to the FP-LD on hysteresis parameters. Figure 6.10 shows that the hysteresis width is 4.5 dB when the

FP-LD is biased at $1.2 I_{th}$. The output power once injection locking has achieved is -13.25 dBm and the input threshold power (P_{th}) is -6.1 dBm. The jump (from unlocked to locked state) is 3 dB. However, when the FP-LD is biased at $1.4 I_{th}$ the hysteresis width is reduced to 2 dB while the output power increases to -9.5 dBm. Hence it can be deduced from this comparison that the P_{th} is larger when the FP-LD is operated at larger biasing current. The output power once the laser is injection locked is also larger when operated at higher biasing current. Nevertheless, the hysteresis width reduces when the FP-LD is operated at higher biasing current. During this comparison the same FP-LD mode and wavelength detune of the injected signal were used. The wavelength detune used was 0.12 nm.



(a)



(b)

Fig. 6.10 Effect of operating current on hysteresis during injection locking of FP-LD.

6.7 Chapter Summary

In this chapter a background review of injection-locking of lasers was presented. The underlying principles and properties of injection-locking a Fabry Pérot laser diode were delineated. The results of experimental characterization of a single mode injection-locking were also reported. Bistability and hysteresis property in the semiconductor laser diodes was also described. The principle of injection -locking of the FP-LD is used for the proposed all-optical logic gates and a real time all-optical bit error monitoring system which will be discussed in the next chapter.

References

- [1] B. Van der Pol, “Forced oscillations in a circuit with nonlinear resistance”. *Phil. Mag.*, **3**, 65–80 (1927).
- [2] A. A. Andronov, A. A. Vitt, and S. E. Khaikin, “*Theory of Oscillators*” Oxford, (1966).
- [3] H. L. Stover and W. H. Steier, “Locking of laser oscillations by light injection,” *Appl. Phys. Lett.*, **8**, 91-93 (1966).
- [4] C. J. Buczek and R. J. Frieberg, “Hybrid injection locking of higher power CO₂ lasers,” *IEEE J. Quantum Electron.*, **QE-8**, 641-650 (1972).
- [5] S. Kobayashi and T. Kimura, “Injection locking characteristics of an AlGaAs semiconductor laser,” *IEEE J. Quantum Electron.*, **QE-16**, 915-917 (1980).
- [6] S. Kobayashi and T. Kimura, “Injection locking in AlGaAs semiconductor laser by injection locking,” *IEEE J. Quantum Electron.*, **QE-17**, 681-689 (1981).
- [7] R. Adler, “A study of locking phenomena in oscillators,” *Proc. IRE*, **34**, 351-357 (1946).
- [8] J. Yamada, S. Kobahashi, H. Nagai, and T. Kimura, “Modulated single longitudinal mode semiconductor laser and fiber transmission characteristics at 1.55 μm ,” *IEEE J. Quantum Electron.*, **QE-17**, 1006-1009 (1981).
- [9] L. Otsuka and S. Tarucha, “Theoretical studies on injection locking and injection -induced modulation of laser diodes,” *IEEE J. Quantum Electron.*, **QE-17**, 1515-1521 (1981).
- [10] R. Lang, “Injection locking properties of semiconductor lasers,” *IEEE J. Quantum Electron.*, **QE-18**, 976-983 (1982).

- [11] C. H. Henry, N. Olsson, and N. K. Dutta, "Locking range and stability of injection locked 1.54 μ m InGaAs semiconductor lasers," *IEEE J. Quantum Electron.*, **QE-21**, 1152-1156 (1985).
- [12] H. Kawaguchi, K. Inoune, T. Matsuoka, and K. Otsuka, "Bistable output characteristics in semiconductor laser injection locking," *IEEE J. Quantum Electron.*, **QE-21**, 1314-1317 (1985).
- [13] L. Li, "Static and dynamic properties of injection-locked semiconductor lasers," *IEEE J. Quantum Electron.*, **QE-21**, 1701-1708 (1994).
- [14] L. Li, "Optical frequency bistability and power bistability in semiconductor lasers," *IEEE J. Quantum Electron.*, **QE-31**, 233-239 (1995).
- [15] L. Li, "Dynamic properties of optically switched bistable semiconductor lasers," *IEEE J. Quantum Electron.*, **QE-32**, 1009-1014 (1996).
- [16] J. Hörer and E. Patzak, "Large-signal analysis of all-optical wavelength conversion using two-mode injection-locking in semiconductor lasers," *IEEE J. Quantum Electron.*, **QE-33**, 596-607 (1997).
- [17] A. Kaszubowska, P. Anandarajah, and L. P. Barry, "Improved performance of a hybrid radio/fiber system using a directly modulated laser transmitter with external injection," *IEEE Photon Technol Lett*, **14**, 233-235 (2002).
- [18] L. Hai-Han, H. Hsu-Hung, S. Heng-Sheng, and W. Ming-Chuan, "Fiber optical CATV system-performance improvement by using external light-injection technique," *IEEE Photon Technol Lett*, **15**, 1017-1019 (2003).
- [19] A. M. Yurek, L. Goldberg, H. F. Taylor, and J. F. Weller, "Millimeter-wave signal generation with an injection-locked laser diode," *IOOC-ECOC*, 1, 791-794,

- Italy, (1985).
- [20] M. Al-Mumin, W. Xinhong, M. Weiming, S. A. Pappert, and L. Guifang, “Optical generation and sideband injection locking of tunable 11-120 GHz microwave/millimetre signals,” *Electron Lett*, **36**, 1547-1548 (2000).
- [21] H.-K. Sung, T. Jung, M. C. Wu, D. Tishinin, K. Y. Liou, and W. T. Tsang, “Optical generation of millimeter-waves using monolithic sideband injection locking of a two-section DFB laser,” *LEOS*, **2**, 1005-1006, Arizona, (2003).
- [22] T. Jung, “Demonstration of monolithic optical injection locking using a two section DFB laser,” *CLEO*, CThC4, (2003).
- [23] K. Weich, E. Patzak, and J. Horner, "Fast all-optical switching using two-section injection-locked semiconductor lasers," *Electron Lett*, **30**, 493-495 (1994).
- [24] C. W. Chow, C. S. Wong, and H. K. Tsang, “All-optical modulation format conversion and multicasting using injection-locked laser diodes,” *IEEE J. of Lightw Technol*, **22**, 2386-2392 (2004).
- [25] E. Kapon, “*Semiconductor Lasers I*”, Academic press, San Diego, (1999).
- [26] G. Keiser, “Optical fiber communication”, McGraw Hill, Boston, (2000).
- [27] D. Derickson, “Fiber optic test and measurement”, Prentice Hall, New jersey, (1998).

- [28] T. B. Simpson, J. M. Lui, K. F. Huang, and K. Tai, “Nonlinear dynamics induced by external optical injection in semiconductor lasers,” *Quantum semiclass. Opt*, **9**, 765-784 (1997).
- [29] A. Murakami, K. Kawashima, and K. Atsuki, “Cavity resonance shift and bandwidth enhancement in semiconductor lasers with strong light injection,” *EEE J. Quantum Electron.*, **QE-39**, 1196-1204 (2003).
- [30] J. Liu and Y. Chen, “Compensation of internal thermal stresses in InGaAsP/InP lasers for polarization stabilization,” *IEEE J. Quantum Electron.*, **QE-21**, 271-277 (1985).
- [31] G. Ropars, A. Floch, G. Jezequel, R. Naour, Y. Chen, and J. Liu, “The inhibition mechanism in polarization semiconductor lasers,” *IEEE J. Quantum Electron.*, **QE-23**, 1027-1032 (1987)
- [32] B. M. Yu and J. M. Liu, “Polarization-dependent gain, gain nonlinearities, and emission characteristics of internally strained InGaAsP/InP semiconductor lasers,” *J of Appl Phys*, **69**, 7444-7459 (1991).
- [33] L. Xu, W. H. Chung, L. Y. Chan, L. F. K. Lui, P. K. A. Wai, and H. Y. Tam, “Simultaneous all-optical reshaping of two 10 Gb/s signals using a single injection-locked Fabry Perot laser diode,” *IEEE Photon Technol Lett*, **16**, 1537-1539, (2004).
- [34] H. Kawaguchi, “*Bistabilities and nonlinearities in laser diodes*”, Artech House, Inc. Boston (1994).

- [35] Y. C. Chen and J. M. Liu, "Direct polarization switching in semiconductor lasers," *Appl. Phys. Lett.*, **45**, 604-606 (1984).
- [36] Y. C. Chen and J. M. Liu, "Temperature-dependent polarization behavior of semiconductor lasers," *Appl. Phys. Lett.*, **45**, 731-733 (1984).
- [37] Y. C. Chen and J. M. Liu, "Polarization bistability in semiconductor lasers," *Appl. Phys. Lett.*, **46**, 16-18 (1985).
- [38] Y. C. Chen and J. M. Liu, "Polarization bistability in semiconductor laser: Rate equation analysis," *Appl. Phys. Lett.*, **50**, 1406-1408 (1987).
- [39] Y. Mori, "Dynamic properties of transverse-magnetic wave injected semiconductor lasers," *IEEE J. Quantum Electron.*, **QE-27**, 2415-2421, (1991).
- [40] Y. Mori and J. Shibata, "Optical polarization bistability in TM wave injected semiconductor lasers," *IEEE J. Quantum Electron.*, **QE-25**, 265-272 (1989).
- [41] T. Fujita, A. Schremer, and C. L. Tang, "Polarization bistability in external cavity semiconductor," *Appl. Phys. Lett.*, **51**, 392-394 (1987).

Chapter 7

All optical logic gates and a signal quality monitoring system

7.1 Introduction

As electronic circuits are anticipated to confront the speed limitation barrier, efforts to realize all-optical logic systems are starting to increase. Therefore, all-optical binary logic gates are expected to become key building blocks in signal processing and communication networks in the near future. The optical logic gates must have the following characteristics:

- High speed: (faster than the comparable electronic switches)
- Full Boolean logic capability: The optical logic technology must be capable of performing the complete set of Boolean logic functions.
- Cascadability: The output of the logic gate must be able to be used as the input for the next stage of logic gates. With amplification, it must be capable of fanning out to provide input to multiple logic gates.

- Capability of high-density integration: For this, the individual gate must be very compact.

Many researchers have directed their efforts towards implementing all-optical logic devices with various methods. As discussed in chapter 4, the logic devices of major interest can be classified depending on the methodology used to achieve the nonlinear operation of the logic devices: the fiber nonlinearity-based logic gates [1-3] and the semiconductor-optical-amplifier (SOA) based logic gates [4-31]. The all-optical logic gates based on the nonlinearities of the optical fiber has the potential of operating at terabits per second due to very short relaxation times (<100 fs) of its nonlinearity. The downside of optical fiber is that its nonlinearity is weak and hence long interaction length or very high control energy is required to achieve reasonable switching efficiency.

The SOA-based optical logic gates where the intensity dependent refractive index is orders of magnitude larger than that of fiber are attractive due to possibility of device compactness and manufacturability resulting from monolithic integration. The first reports of optically controlled SOA gates were made in [14] and [15]. In both cases, cross-gain modulation (XGM) was explored. The input signal is used to saturate the gain and thereby modulate a CW signal (probe) at the desired output wavelength. The cross-gain modulated (XGM) gate is extremely simple to assemble. It is polarization

insensitive because of polarization-independent SOA gain, and it is very power efficient. It also turned out that the gate can be extremely fast, and, by 1998, bit rate capabilities of 100 Gb/s were reported [16-17]. At first glance, it seems impossible to reach this speed due to the relatively slow carrier dynamics with lifetimes in the order of 100 ps [18]. Detailed analyzes can, however, explain the significant role of gain saturation in achieving high speed [19]. The prospects of achieving even higher bit rates look fine with the use of quantum dot material. Pump-probe experiments reveal very fast gain dynamics [20] in amplifiers made from this material. Nevertheless, the XGM gate has a number of shortcomings, such as inversion of the input-control signal, the relatively large chirp of the output signal due to the large gain modulation and pattern dependence.

Gates with better performance are achieved by placing SOAs in interferometric configurations. In these gates, the optical input signal controls the phase difference between the interferometer arms through the relation between the carrier density and the refractive index in the SOAs through cross-phase modulation (XPM); thereby a CW light or a pulse train can be gated [21] or control pulses can be used to gate the input signal. For stable operation, the XPM converters must be integrated. The first monolithic structures reported [22] were based on Michelson interferometers, realized by cutting sections out of the 4×4 space switch with SOAs [23]. An early realization

of a two-port Mach–Zehnder structure was based on a back-to-back coupling of the Y-lasers [24]. Following these early versions of XPM gates, an impressive activity on monolithic integration of interferometric gates has taken place [25-28], making these gates one of the test grounds for monolithic integration of active optical elements. Only small input-signal levels are needed to introduce a phase difference between the interferometer arms. Because of the small modulation associated with the phase shift, the frequency chirp of the output signal will also be small compared to XGM based gates [22], [29].

Instead of the cross-gain and cross-phase modulation in SOAs, it is also possible to utilize four-wave mixing (FWM) [30-31]. The input-to-output signal efficiency of the gate decreases with the wavelength separation of the pump and the input signal, but experiments using SOA gates with very long cavities have resulted in conversion efficiencies approaching 0 dB [32], which is important for good optical SNR at the output.

All optical logic gates using planar waveguide devices such as nonlinear Mach-Zehnder interferometers and distributed Bragg gratings have also been reported [33-34]. Microring resonators can also be employed to realize logic functions with the added advantage of enhanced switching thresholds and compact size. Switching in these devices is accomplished due to intensity-dependent nonlinear effects [35].

Injection-locking a slave laser to a master laser is a well established technique that has been proposed in the literature to realize all optical signal processing functions [36-40]. The reason which makes these semiconductor lasers work as the building block for all optical signal processing devices is the existence of optical threshold. If the injected power of the master laser is above this threshold the slave laser gets locked, otherwise it remains unlocked. Hence the injection locked semiconductor lasers based devices are very compact, robust, and can operate at low powers. In our works, we are also utilizing the property of optical threshold in FP-LD to realize different kinds of all-optical logic gates and to demonstrate a signal quality monitoring system by combining two logic functions.

7.2 Two mode injection locking

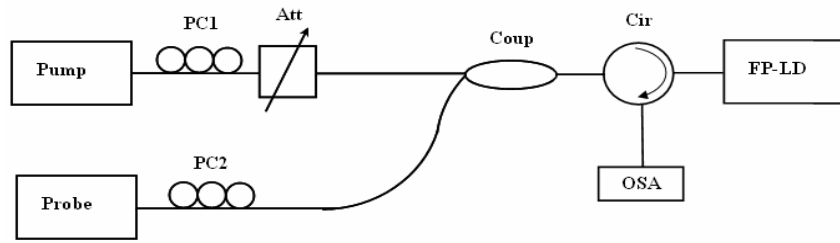
As discussed previously in section 6.4, if the optical frequency of the injected light is close to the lasing frequency of the unperturbed laser, the laser will adjust its frequency and coherence properties to that of injected light. This is termed as stimulated emission and is attributed to the fact that as the injected signal power increases, the carrier density inside the active region of the FP-LD decreases, thereby increasing the refractive index and causing a red-shift in the longitudinal modes of the FP-LD [36-37].

When two light signals are injected into the FP-LD they influence each other. A competition takes place to share the carrier density in the active region. The wavelength detunes and the injected powers contribute to the gain competition. If one of the signals with relatively small wavelength detune is aligned close to one of the modes of the FP-LD, it will injection-lock the FP-LD and suppress all the other modes of the FP-LD. The injected power required to injection lock a FP-LD is proportional to the wavelength detune. If a second signal with a relatively larger detune, is injected in another mode of the FP-LD with an appropriate injected power, it will produce a red-shift in the FP-LD mode comb. This red-shift in the FP-LD will pull the FP-LD mode away from the previously injected signal. Hence in the presence of the second signal the first signal is suppressed and in the absence of the second signal

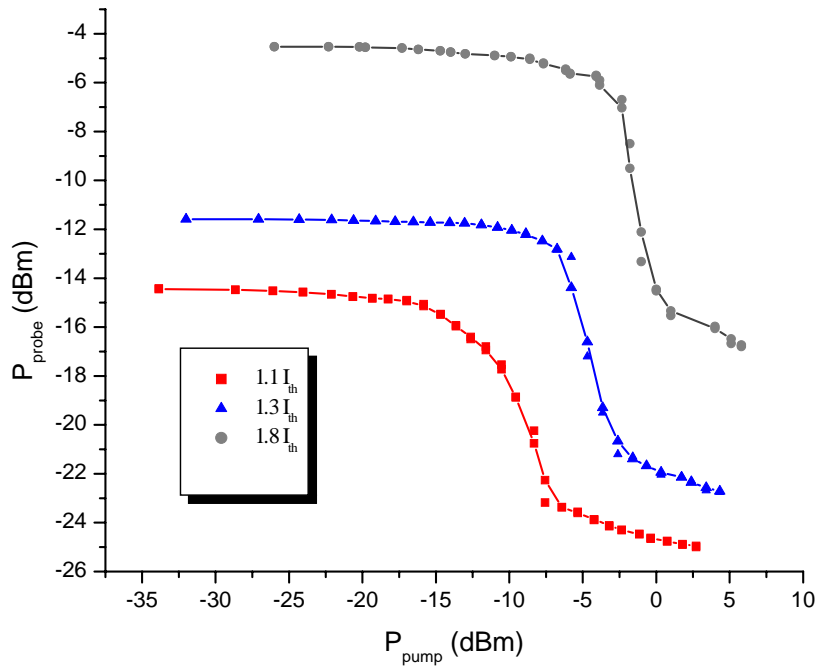
the first signal is amplified. This two mode injection locking principle is extensively used for various applications [37-40]. This is also the working principle of our proposed all-optical NOT gate. The all-optical NOT gate with variable threshold is detailed below.

7.3 All optical NOT gate with variable threshold

The pump-probe experiment shown in Fig. 7.1(a) is conducted to characterize the thresholding behavior in FP-LD. Two tunable lasers provide the pump and probe signals and an attenuator is used to adjust the power of the pump laser. First we study the case when only probe beam is injected into the FP-LD with a fixed wavelength detune. Strong amplification takes place which reduces the carrier density in the active region due to stimulated emission, and causes an increase in the refractive index. The injected light is resonantly amplified and all the other longitudinal modes of the laser are strongly suppressed. The mode comb is slightly red-shifted compared to its position when no light is injected. Within a small wavelength window, the stimulated recombination due to probe amplification is strong enough to reduce the carrier density. This range is called the injection locking range. The width of this locking range depends on the ratio of the injected power relative to the power of the unlocked slave laser [17].



(a)



(b)

Fig. 7.1 (a) Configuration of Pump/probe experiment. (b) Pump/probe characteristics of the NOT gate under two-mode injection locking in an FP-LD. (Note: I_{th} = threshold current of FP-LD)

The pump signal at a relatively larger detune is later injected into another longitudinal mode of this slave laser and its power is increased via an attenuator as shown in Fig. 7.1(a). At a certain input power, known as threshold power (P_{th}) of pump beam the probe beam suddenly jumps to a lower power level. The pump signal at this power gets resonantly amplified, decreases the carrier density and increases the refractive index. Now the FP mode comb is further red-shifted resulting in low probe output power. Figure. 7.1(b) shows the relationship between the pump and probe beam powers at different biasing current of FP-LD. It is interesting to note that the P_{th} changes with an increase in the biasing current of the FP-LD. When the bias current of the FP-LD is $1.1 I_{th}$, the probe beam drops by 7 dB for an increase of 5 dB pump power whereas for a higher bias current of $1.8 I_{th}$ the probe beam drops by 9 dB for an increase of 2.5 dB in pump power.

We utilize the two-mode injection locking property in a dc driven FP-LD for all optical variable threshold NOT gate. The 10 Gb/s NRZ data signal and the CW signal are injected into two different longitudinal modes of the FPLD. The output at the wavelength of the CW light is switched by the data signal light, and thereby the information is transferred from the data signal to the CW light beam. The light is digitally switched by light. When the input bit in data signal is logic “1” the power is high and the depletion occurs due to stimulated emission that blocks the CW

wavelength, hence the CW beam is at logic “0”. Whereas when the bit in data signal is logic “0” (low power), depletion does not occur and CW signal passes at full power, hence CW beam is at logic “1”. Thus the FP-LD at $\lambda_{\text{NOT}}(\text{CW})$ exhibits the logic NOT. The operation of this gate is based on the observation that the working threshold (P_{th}) of FP-LD can be tuned by varying the wavelength detune, injection power of the signals, and the biasing current of the FP-LD as shown in Fig. 7.2.

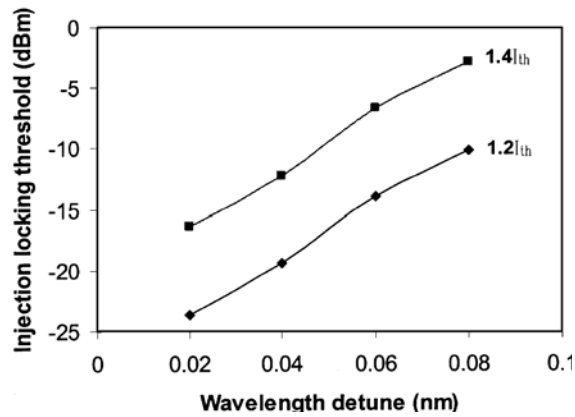


Fig. 7.2 Injection locking threshold versus wavelength detune for two different FP-LD biasing currents. (Note: I_{th} = threshold current of FP-LD).

7.3.1 Experimental Results and Discussions

Figure. 7.3 shows the experimental setup to demonstrate the all-optical threshold variable NOT gate. The NOT gate consists of a CW tunable laser which provides the probe beam, polarization controllers PC (1 ~ 4), 3 dB coupler, circulator, tunable band pass filter (BPF) with a FWHM of 0.7 nm, and an FP-LD. The working threshold level of the NOT gate is represented by Γ . The threshold level is the intensity decision level that is used to define the input data as a bit “1” or a bit “0” respectively when the intensity is above or below this level. The NOT gate can work at variable thresholds i.e, Γ_{low} and Γ_{high} , where $\Gamma_{high} > \Gamma_{low}$.

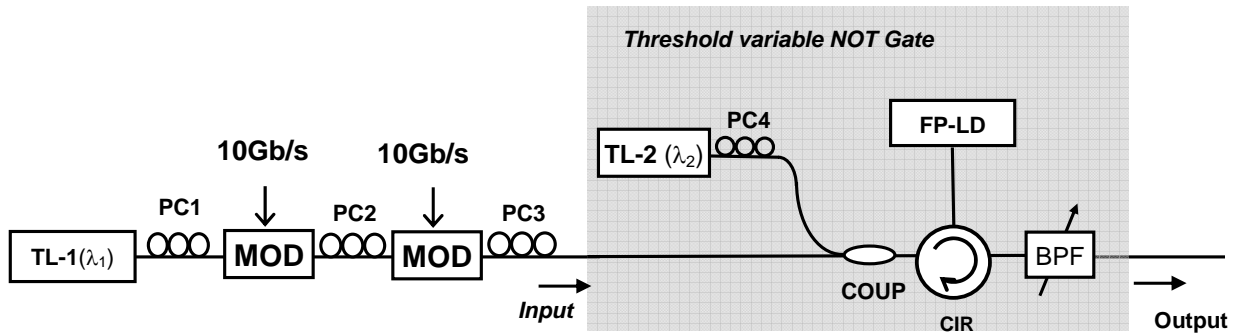


Fig. 7.3 Experimental setup for the all-optical threshold variable NOT gate.
 Note: TL – tunable laser; PC – polarization controller; MOD – modulator;
 COUP – coupler; CIR – circulator; and BPF – tunable bandpass filter.

The 10 Gb/s NRZ data signal at 1542.67 nm (λ_1) was generated by using two 10 Gb/s modulators on the output of a tunable laser (TL-1). By operating the modulators at different extinction ratios, we introduced three level data signal to study the effect of different threshold levels. The NRZ data signal was injected into the FP-LD which functions as an inverted wavelength converter, a thresholder and an NOT gate simultaneously. Besides a 10 Gb/s input data signal we also injected a CW signal at 1548.32 nm (λ_2) into FP-LD. The 10 Gb/s data and the CW signals were wavelength detuned from two different longitudinal modes of FP-LD at the longer wavelength side with values of +0.12 nm and +0.05 nm respectively. First the FP-LD was biased at $1.1 I_{th}$ where I_{th} is the threshold current of FP-LD and the threshold level for FP-LD is set to Γ_{low} . The powers of the data and CW signals were chosen such that a '1' bit or the intermediate amplitude data bits would injection-lock the FP-LD. Thus the inverted data signal obtained at 1548.32 nm had all the intermediate amplitude bits as well as true '1' bits converted to '0' bits. Now the threshold of the NOT gate was set to Γ_{high} by changing the operating current of the FP-LD to $1.3 I_{th}$. The powers of the data and the CW signals were selected in such a way that only true '1' bits would injection lock the FP-LD.

Figure 7.4 summaries the operation of the threshold variable NOT gate. Figure 7.4(a) depicts the 10 Gb/s NRZ signal with some bits having an intermediate intensity.

Figure 7.4(b) shows the inverted and wavelength converted signal when the FP-LD was operated at Γ_{low} . Note that all the intermediate intensity bits (between the two thresholds) in the original signal are now converted to zeroes. Figure 7.4(c) shows the inverted and wavelength converted signal when the FP-LD was operated at Γ_{high} .

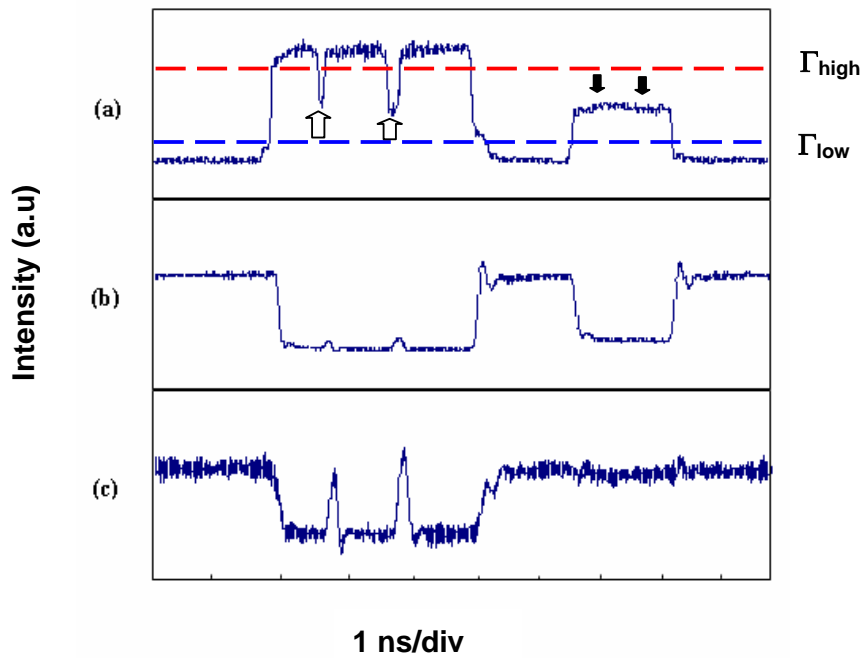


Fig. 7.4 Temporal profiles of (a) the input 10 Gb/s NRZ signals with low intensity single bits and burst distortion (b) the inverted λ -converted signal when the NOT gate is working at Γ_{low} (c) the inverted λ -converted signal when the NOT gate is working at Γ_{high} .

7.4 All-optical NOR gate

Hitherto, a variety of schemes have been reported to realize all optical logic NOR gates [7-10,12,13]. Sharaiha et al. [7] demonstrated an all optical NOR gate utilizing gain saturation along with wavelength conversion in a semiconductor laser amplifier (SLA). A switching time of ~300 ps for the rise time and 100 ps for the fall time predicts the setup to operate up to 2.5 Gb/s.

Patel et al. [8,9] reported a semiconductor optical amplifier (SOA) based ultrafast nonlinear interferometer (UNI) gate. The scheme utilized cross phase modulation (XPM) and cross gain saturation (XGS) in conjunction with interferometric structure to obtain a variety of logic functions. NOR operation was demonstrated at 10 Gb/s.

NOR logic gate based on cross polarization modulation (XPolM) effect [10] in an SOA was reported by Soto et al. [11]. The gate utilizes a single SOA and does not require an additional synchronized clock. The gate can work for two as well as for three inputs and was demonstrated with the input logic signals modulated at 2.5 Gb/s.

In [12] NOR logic gate using two cascaded SOAs in a counterpropagating feedback configuration was suggested. However, the interconnection distance between the two SOAs limits the operable rate of this configuration to below GHz range.

Recently, an all optical NOR gate working at 10 Gb/s was reported by Zhao et al. [13]. The reported configuration utilizes an SOA fiber ring laser which replaces the continuous wave (CW) light required in many other schemes.

In our work we have utilized three-mode injection locking in a FP-LD to realize an all optical NOR gate. The three-mode injection locking is a totally different scenario when compared to two mode injection locking, since the number of parameters to handle increases. The wavelength detunes of the three injected signals, the injected powers of the three signals, the operating current and temperature of the FP-LD are crucial. The operation principle of this logic gate is that either the presence of a single or both data beams will injection lock the FP-LD and thus suppresses the FP-LD at λ_{NOR} . The absence of both data beam will cause the CW beam to injection lock the FP-LD, hence depicting the logic NOR.

7.4.1 Experimental Results and Discussions

Figure 7.5 shows the schematic of the experimental setup to demonstrate the all-optical NOR gate. Two separate 10 Gb/s NRZ pulses of 2^{31} -1 pseudorandom bit sequences (PRBS) generated with two tunable laser sources (TL-1 and TL-2) and two LiNbO₃ modulators (MOD1) and (MOD2), are used as inputs to the NOR gate. A variable optical delay line (ODL) is used to synchronize the two inputs into the FP-LD. The ODL provided a maximum delay of 330 ps. The polarization controllers PC (1~4) are adjusted to ensure that the injected light is TE polarized. The NOR gate consists of a tunable laser (TL-3), a FP-LD, a circulator, two 3 dB couplers and a band pass filter. The FP-LD is biased at $1.2 I_{th}$ where I_{th} is the threshold current. The powers and detunes of the three inputs to FP-LD are chosen such that the output from TL-3 injection-locked FP-LD only when both the input data signal output were low, i.e., zero. The band pass filter having FWHM of 0.7nm selects the wavelength of TL-3 at the output port of the circulator which gives the output of the NOR gate.

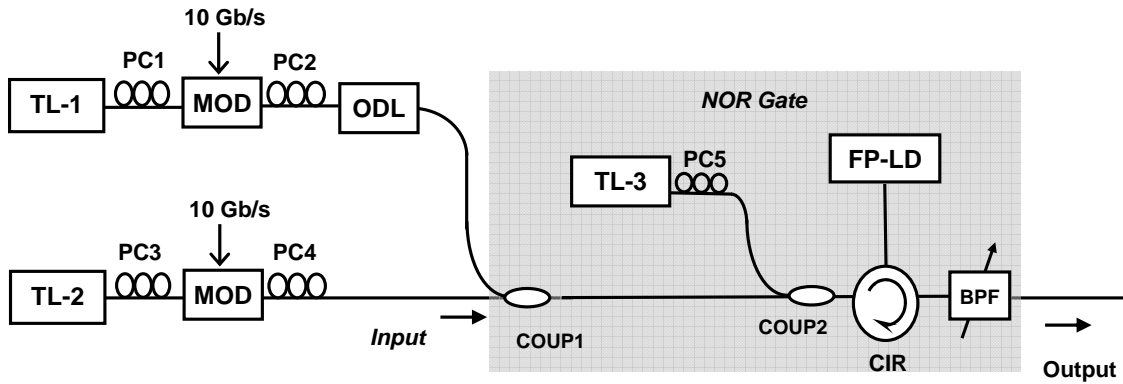


Fig. 7.5 Experimental setup of an all-optical NOR gate. Note: TL – tunable laser; PC – polarization controller; MOD – modulator; COUP – coupler; CIR – circulator; ODL – Optical Delay Line. and BPF – tunable bandpass filter.

The FP-LD is first injection locked by coupling the CW output of a tunable laser (TL-3) at wavelength 1547.16 nm (λ_{NOR}) with a power at -7 dBm, which is detuned at $+0.05$ nm of one of the longitudinal modes of the FP-LD. Later, the two 10 Gb/s NRZ data signals with wavelengths of 1544.35 nm (λ_1) and 1551.73 nm (λ_2) are injected into FP-LD. These two data streams are wavelength detuned at $+0.12$ nm with two different longitudinal modes of the FP-LD. The output of the NOR gate is obtained by filtering out the wavelength at λ_{NOR} using a band pass filter. Figure 7.6(a) shows the temporal profile of the input 1 at (λ_1). Figure 7.6(b) shows the temporal profile of the input 2 at (λ_2). Figure 7.6(c) shows the temporal profile of the NOR output at (λ_{NOR}). The input data signals and the output NOR signal are observed

using a 50 GHz sampling oscilloscope. In the next section we propose and demonstrate an all-optical signal quality monitoring system using cascaded optical NOT and NOR gates.

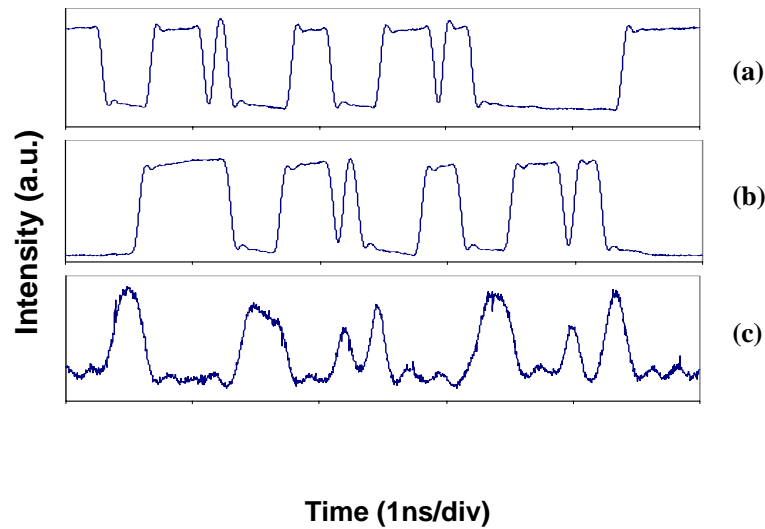


Fig. 7.6 Temporal profiles of (a) the first 10 Gb/s NRZ input signal (b) the second 10 Gb/s NRZ input signal (c) the NOR output signal.

7.5 All-optical signal quality monitoring system

Service providers must guarantee data integrity to their clients, and the bit-error rate measurement is used to measure it. The signal quality monitoring circuitry plays an integral role in a SONET/SDH (Synchronous Optical Network/Synchronous Digital Hierarchy) system. The typical signal quality monitoring systems are very expensive and bulky so it is extremely difficult to use these electrical BERTS (Bit Error Rate Test Sets) in multi-channel optical networks such as WDM systems. Since, Quality of Service (QoS) management, performance monitoring, and signal failure location detection in the optical domain are tedious with the current state-of-the-art techniques hence real time bit-error rate monitoring could perform an essential role in fault management to create large scale robust transport networks [42]. The optical layer protection of gigabit-ethernet system is of paramount importance since it does not have BER-indicating bits and hence a mechanism to ensure quality of service by monitoring optical signal quality is required [43]. Real time monitoring of optical signals could also be utilized for eye monitoring for adaptive polarization-mode dispersion (PMD) compensation [44] in high capacity transport and access networks. Real time monitoring is difficult because of the limited signal processing capabilities of the presently available all-optical devices. Typical signal quality monitoring schemes require expensive optical-electrical conversions and high speed large scale integration

chips [45]. We have proposed an all-optical signal quality monitoring system (SQMS) working at 10 Gb/s utilizing the mutual injection locking property in two Fabry Perot laser diodes (FP-LDs).

7.5.1 Operation principle

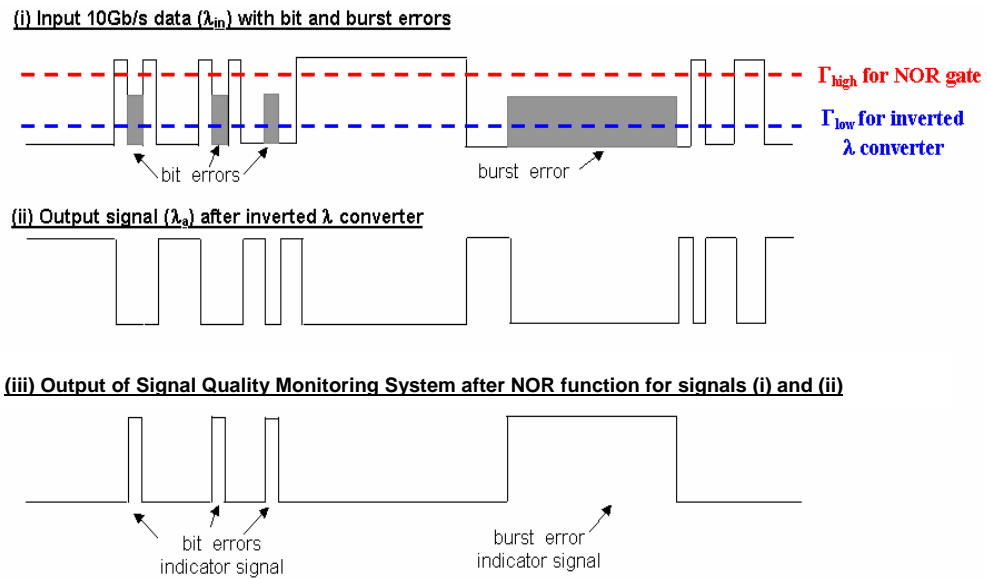
The all-optical SQMS monitoring system is realized using two stages of all-optical processes: a NOT gate to perform an inverted wavelength conversion of the input signal and a NOR operation for the wavelength converted signal and the original signal. In the proposed scheme we identify an error using two optical threshold levels Γ_{low} and Γ_{high} , where $\Gamma_{\text{high}} > \Gamma_{\text{low}}$ [Fig. 7.7(b)]. If the optical intensity in a bit period is above Γ_{high} (below Γ_{low}), the bit period is assumed to contain a correct '1' ('0') bit. If the optical intensity falls in between the two threshold levels, the bit period is assumed to contain an error bit. Thus the data bit p in any signal can be classified to be in one of the three states; 0 , 1 , E , where state E represents an error bit of value between 0 and 1. The proposed scheme only identifies amplitude jitters in the signal and cannot identify errors due to timing jitters. The detection of amplitude jitter is based on intensity threshold, whereas the detection of timing jitters requires the implementation of timing threshold which is not possible in the current scheme. As the thresholding function is the key for realization of this type of system, hence we have to employ a device which can provide nonlinear interaction and thresholding function

simultaneously or otherwise separate devices have to be engaged for logical processing and thresholding purposes, which may complicate the entire system. It is interesting to note that the NOT, NOR logic and thresholding can be easily realized respectively using dual mode and multimode injection locking in a FP-LD, hence we implemented the SQMS using the logic function $\text{NOR}\{\text{NOT}[\text{TH}_1(p)], \text{TH}_2(p)\}$, where TH_1 and TH_2 are threshold decision functions using the logical threshold levels γ_{low} and γ_{high} respectively. The γ_x is the logical value corresponding to the optical intensity Γ_x where $x = \text{low, high}$ and $0 < \gamma_{\text{low}} < \gamma_{\text{high}} < 1$. That is, $\text{TH}_i(p) = 1$ if $p \geq \gamma_x$ and $\text{TH}_i(p) = 0$ if $p < \gamma_x$ where $i = 1, 2$, and $x = \text{low, high}$. The logical threshold levels are chosen such that $\gamma_{\text{low}} < E < \gamma_{\text{high}}$. These two logical threshold levels, γ_{low} and γ_{high} , correspond to the operation thresholds for the NOT gate (Γ_{low}) and optical NOR gate (Γ_{high}) respectively. Figure 7.7(a) shows the truth table of the logic operation, $\text{NOR}\{\text{NOT}[\text{TH}_1(p)], \text{TH}_2(p)\}$ by the SQMS. Figure 7.7 (b) shows a 10-Gb/s data signal at wavelength λ_{in} . The shaded bits identify both bit and burst errors. The 10-Gb/s corrupted data is then split into two portions, one of which undergoes inverted wavelength conversion and the other portion remains unchanged. Fig. 7.7(b-ii) shows the output of the inverted wavelength converter, i.e., the NOT gate, which performs the logic functions NOT. The wavelength converted signal is then combined synchronously with the unmodified portion of the original corrupted

10-Gb/s signal and fed into the optical NOR gate as shown in Fig. 7.7(b-iii). After the NOR operation, the output signal identifies the position and duration of the error bits. The nature of the errors, bit or burst, are given by the duration of the output signal. In the experiment, the monitoring system was realized using two injection-locked FP-LDs which functioned as the inverted wavelength converter and the optical NOR gate. The decision thresholds can be tuned by varying the wavelength detunes (the wavelength differences between the signal and the FP longitudinal modes) and the bias current of the FP-LDs.

p	Optical NOT gate		Optical NOR gate	
	$TH_1(p)$	$NOT[TH_1(p)]$	$TH_2(p)$	$NOR[NOT[TH_1(p)], TH_2(p)]$
1	1	0	1	0
E	1	0	0	1
0	0	1	0	0

(a)



(b)

Fig. 7.7 (a) The truth table of the logical function $NOR\{NOT[TH_1(p)], TH_2(p)\}$ implemented by the SQMS. The input p takes on values 0, 1, and E where $0 < E < 1$ represents an error bit. (b) The basic principle of all-optical SQMS. (i) A 10 Gb/s input signal with the error bits in grey. (ii) The ideal inverted wavelength converter output. (iii) The ideal output of the monitoring system.

7.5.2 Experimental Results and Discussions

Figure 7.8 shows the schematic of the experimental setup to demonstrate the all-optical SQMS. The corrupted 10 Gb/s NRZ data signal was generated using two 10 Gb/s modulators on the output of a tunable laser (TL_1). Data 1 and Data 2 are the two 10 Gb/s data sequences that fed into the two modulators. Data 2 is a delayed copy of the complement of Data 1. By operating the modulators at different extinction ratios, we could vary the intensities of individual bits. The bits with intensities between the two threshold levels were considered as error bits. We introduced both single-bit errors and burst errors. The errors in the corrupted signal are due to amplitude jitters only. We did not consider other source of signal degradation such as SNR degradation, waveform deformation and error due to timing jitters. We then split the corrupted signals into two parts. One part was injected into a Fabry-Perot laser diode (FP-LD_1) which worked as an inverted wavelength converter. FP-LD_1 implemented the operation of TH₁ and the NOT gate using dual wavelength mutual injection-locking [38].

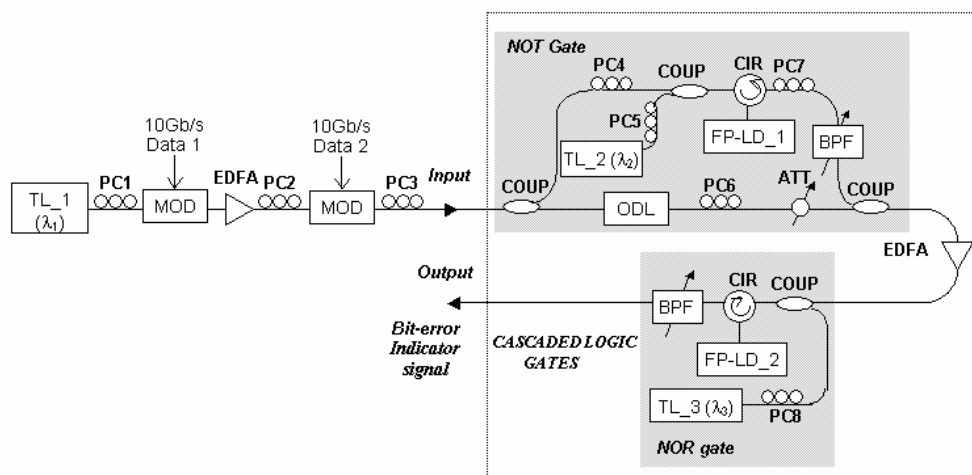


Fig. 7.8 Experimental setup for the all-optical signal quality monitoring system (SQMS). Note: TL – tunable laser; PC – polarization controller; MOD – modulator; COUP – coupler; ODL – optical delay line; ATT – variable attenuator; CIR – circulator; and BPF – tunable bandpass filter.

Besides the input 1542.67 nm (λ_{in}) 10 Gb/s data signal, we also injected a CW signal at 1548.32 nm (λ_a) into FP-LD₁. The 10 Gb/s data and the CW signal were wavelength detuned from two different longitudinal modes of FP-LD₁ at the longer wavelength side with values of +0.18 nm and +0.06 nm respectively. The biasing current of FP-LD₁ is $1.3 I_{th_1}$ where I_{th_1} is the threshold current of FP-LD₁. The threshold level for FP-LD₁ was set to Γ_{low} such that an error bit in the data signal was treated as a '1'. The powers of the data and CW signals were chosen such that a '1' bit or an error bit in the data signal would injection-lock FP-LD₁. Thus the inverted data signal obtained at 1548.32 nm in the output of FP-LD₁ had all the error bits converted to zeroes. The other part of the original 10 Gb/s corrupted data signal was injected into another Fabry-Perot laser diode (FP-LD₂) together with the 1548.32 nm output from FP-LD₁ which was synchronized to the 10 Gb/s data signal by the variable delay line (ODL). We also injected a CW signal at 1546.11nm (λ_m) into FP-LD₂. FP-LD₂ realized the logic operations TH₂ and the NOR gate using multi-wavelength injection locking. The biasing current of FP-LD₂ is $1.1 I_{th_2}$ where I_{th_2} is the threshold current of FP-LD₂. Note that because the overall injected powers into FP-LD₂ is smaller than that of FP-LD₁, the biasing current required for FP-LD₂ ($1.1 I_{th_2}$) to set a high threshold (Γ_{high}) is smaller than the biasing current for FP-LD₁ ($1.3 I_{th_1}$) to set a low threshold (Γ_{low}). The threshold level for FP-LD₂

was set such that an error bit in the data was treated as a '0.' The powers and detunes (wavelength differences between the signals and the respective FP-LD longitudinal modes) of the three inputs to FP-LD_2 were chosen such that the 1546.11 nm CW beam injection-locked FP-LD_2 only when both the data signal and the FP-LD_1 output were low, i.e., zeroes. The incident powers for λ_{in} , λ_a , and λ_m at the NOR gate were 1.43 dBm, 0.3 dBm, and -3.13 dBm respectively. Consequently, the '1' bits at 1546.11 nm in the output of FP-LD_2 indicated both the position and duration of any errors in the original signal. Figure 7.9(a) and 7.9(b) show the spectra of the NOT gate (FP-LD_1) and the NOR gate (FP-LP_2) output respectively. The operation range of the proposed SQMS is limited. The input NRZ corrupted signal should be within ± 0.02 nm of the 0.18 nm detune used in this experiment. The tolerance in power is around ± 2.5 dB.

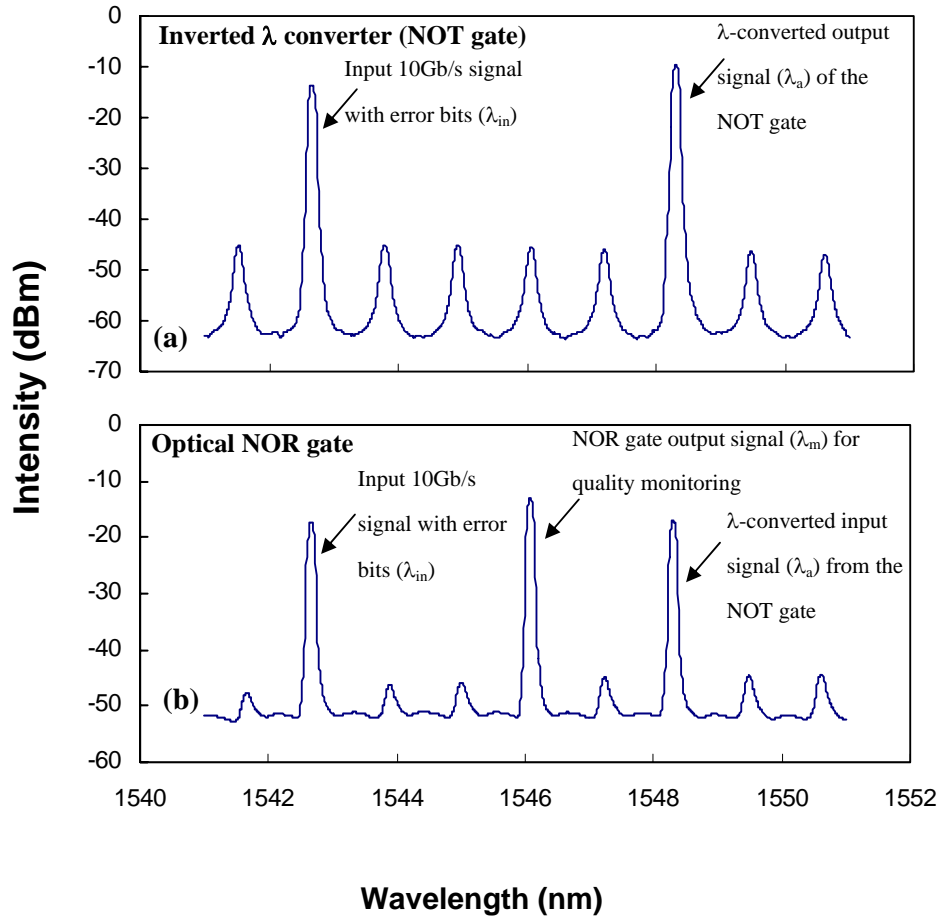


Fig. 7.9 Output spectra of (a) the inverted wavelength converter (FP-LD_1) and (b) the optical NOR gate (FP-LD_2) under injection-locking in SQMS.

Figure. 7.10, depicts the operation of the SQMS. Figure 7.10(a) depicts the 10 Gb/s corrupted NRZ signal. The solid arrows identify single bit errors while the open arrows identify burst errors. Fig. 7.10(b) shows the inverted and wavelength

converted data output signal of FP-LD₁ at 1548.32 nm. Note that all the error bits in the original signals are now converted to zeroes. Fig. 7.10(c) gives FP-LD₂ output at 1546.11 nm. All the error bits in the original signals now appear as '1' bits. The proposed scheme is sensitive to the polarization of the input signals because the scheme utilizes the injection-locking mechanism in FP-LD. Previous experiments show that an injection-locked FP-LD is both wavelength and power stable; we observe wavelength and power fluctuations of less than 0.01 nm and 0.5 dB respectively in a 3-day continuous control. The noise in the final output as observed in Fig. 7.10(c) is due to stringent requirement of mode matching of the two laser diodes, since perfect mode matching is essential for optimized operation of SQMS and also due to the ASE noise introduced by the two EDFA's. High speed monitoring system at 40 Gb/s and beyond should be possible by replacing the FP-LDs with high-speed multi quantum well FP-LDs [46].

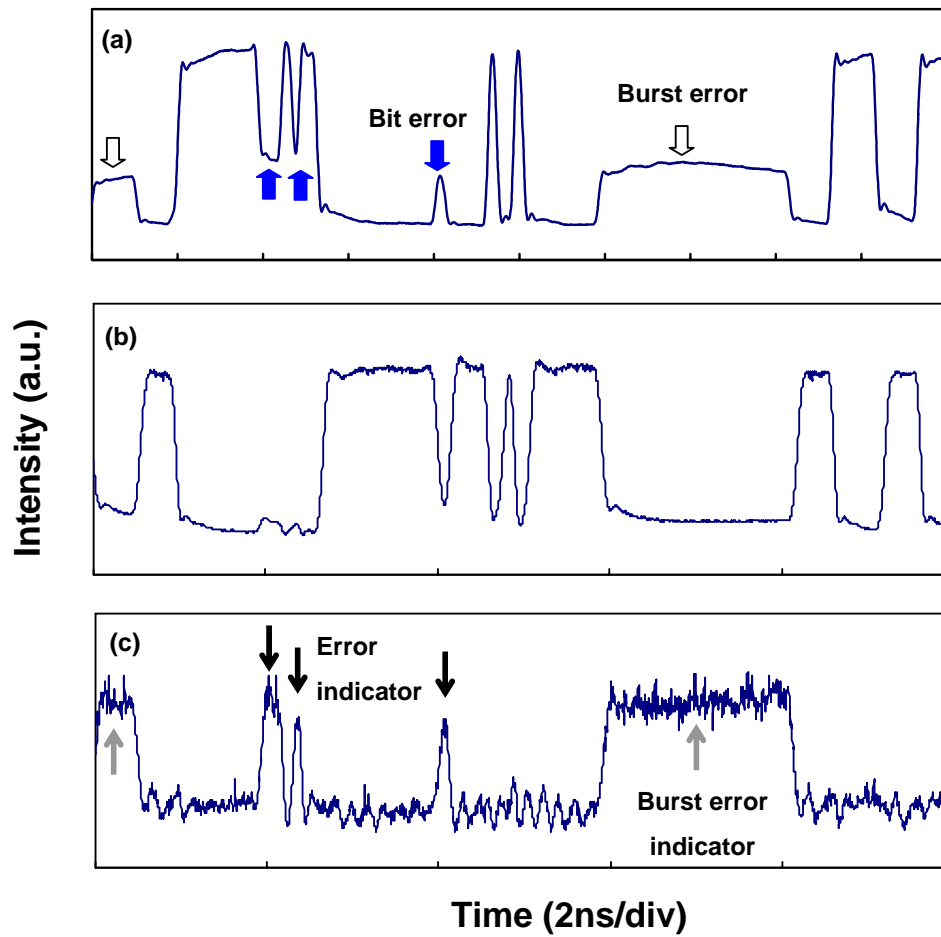


Fig. 7.10 Synchronized temporal profiles of (a) the input 10 Gb/s NRZ signals at 1542.67 nm with both bit and burst errors, (b) the inverted λ -converted signal at 1548.32 nm, and (c) the error indicator signals generated by the SQMS at 1546.11 nm.

7.6 Chapter Summary

In this chapter the literature on all-optical logic gates was reviewed. An all-optical NOT gate and NOR gate were proposed and demonstrated using injection locking principle in a Fabry Perot laser diode. Later a signal quality monitoring system which consists of a cascaded all optical NOT and NOR gates was proposed and demonstrated. These all optical logic devices will play an important role in the future all optical signal processing systems and all optical networks based on Fabry Perot laser diodes.

References

- [1] M. N. Islam, "All optical cascadable NOR gate with gain," *Opt. Lett.*, **15**, 417-419 (1990).
- [2] M. Jinno and T. Matsumoto, "Nonlinear sagnac interferometer switch and its applications," *J. Quantum Electron.*, **28**, 875-882 (1992).
- [3] A. Bogoni, L. Poti, R. Proietti, G. Meloni, F. Ponzini, and P. Ghelfi, "Regenerative and reconfigurable all-optical logic gates for ultra-fast applications," *Electron. Lett.*, **41**, March, (2005).
- [4] T. Houbavlis, K. Zoiros, K. Vlachos, T. Papakyriakopoulos, H. Avramopoulos, F. Girardin, G. Guekos, R. Dall'Ara, S. Hansmann, and H. Burkhard, "All-Optical XOR in a Semiconductor Optical Amplifier-Assisted Fiber Sagnac Gate," *IEEE Photon. Technol. Lett.*, **11**, 334-336 (1999).
- [5] T. Fjelde, D. Wolfson, A. Kloch, B. Dagens, A. Coquelin, I. Guillemot, F. Gaborit, F. Poingt and M. Renaud, "Demonstration of 20Gbit/s all-optical logic XOR in integrated SOA-based interferometric wavelength converter," *Electron. Lett.*, **36**, 1863-1864 (2000).
- [6] T. Fjelde, D. Wolfson, A. Kloch, C. Janz, A. Coquelin, I. Guillemot, F. Gaborit, F. Poingt, B. Dagens and M. Renaud, "10Gbit/s all-optical logic OR in monolithically integrated interferometric wavelength converter," *Electron. Lett.*, **36**, 813-815 (2000).

- [7] A. Sharaiha, H. W. Li, F. Marchese, and J. Le. Bihan, "All-optical NOR gate using a semiconductor laser amplifier," *Electron. Lett.*, **33**, 323-325, (1997).
- [8] N. S. Patel, K. L. Hall, and K. A. Rauschenbach, "40-Gbits cascable all-optical logic with an ultrafast nonlinear interferometer," *Optics Lett.*, **21**, 1466-1468 (1996).
- [9] N. S. Patel, K. L. Hall, and K. A. Rauschenbach, "Interferometric all-optical switches for ultrafast signal processing," *App. Optics.*, **37**, 2831-2841, (1998).
- [10] H. Soto, D. Erasme, and G. Guekos, "Cross-polarization modulation in semiconductor optical amplifiers," *IEEE Photon. Technol. Lett.*, **11**, 970-973 (1999).
- [11] H. Soto, J. D. Topomondzo, D. Erasme, and M. Castro, "All-optical NOR gates with two and three input logic signals based on cross-polarization modulation in a semiconductor optical amplifier," *Opt. Comm.*, **218**, 243-247 (2003).
- [12] A. Hamie, A. Sharaiha, M. Guegan, and B. Pucel, "All-optical NOR gate using two cascaded semiconductor optical amplifiers," *IEEE Photon. Technol. Lett.*, **14**, 1439-1441 (2002).
- [13] C. Zhao, Z. Zhang, H. Liu, D. Liu, and D. Huang, "Tunable all-optical NOR gate at 10 Gb/s based on SOA fiber ring laser," *Opt Express.*, **13**, 2793-2798 (2005).

- [14] T. Durhuus, B. Fernier, P. Garabedian, F. Leblond, J. L. Lafrayette, B. Mikkelsen, C. G. Joergensen, and K. E. Stubkjaer, "High speed all-optical gating using two-section semiconductor optical amplifier structure," in *Proc. CLEO'92*, Anaheim, CA, 552–554.(1992).
- [15] B. Glance, J. M. Wiesenfeld, U. Koren, A. H. Gnauck, H. M. Presby, and A. Jourdan, "High performance optical wavelength shifter," *Electron. Lett.*, **28**, 1714–1715 (1992).
- [16] A. D. Ellis, A. E. Kelly, D. Nasset, D. Pitcher, D. G. Moodie, and R. Kashyap, "Error free 100 Gb/s wavelength conversion using grating assisted cross gain modulation in a 2 mm long semiconductor amplifier," *Electron. Lett.*, **34**, 1958–1959 (1998).
- [17] K. L. Hall and K.A. Rauschenbach, "Fiber optics and optical communications-100-Gb/s bitwise logic," *Opt Lett.*, **23**, 1271–1273 (1998).
- [18] N. Storkfelt, B. Mikkelsen, D. S. Olesen, M. Yamaguchi, and K. E. Stubkjaer, "Measurement of carrier lifetime and linewidth enhancement factor for 1.5- μ m ridge-waveguide laser amplifier," *IEEE Photon. Technol. Lett.*, **3**, 632–634 (1991).
- [19] T. Durhuus, B. Mikkelsen, C. Joergensen, and K. E. Stubkjaer, "All optical wavelength conversion by semiconductor optical amplifiers," *J. of Lightwave*

- Technol.*, **14**, 942–954, (1996).
- [20] F. Romstad, P. Borri, S. Bischoff, J. Mørk, W. Langbein, and J. M. Hvam, “Sub-picosecond pulse distortion in an InGaAsP optical amplifier,” in *Proc. European Conf. Optical Communication (ECOC)*, **II**, Nice, France, 28-29 (1999).
- [21] T. Durhuus, C. Joergensen, B. Mikkelsen, R. J. S. Pedersen, and K. E. Stubkjaer, “All optical wavelength conversion by SOAs in a Mach–Zehnder configuration,” *IEEE Photon. Technol. Lett.*, **6**, 53–55 (1994).
- [22] B. Mikkelsen, T. Durhuus, C. Joergensen, R. J. S. Pedersen, S. L. Danielsen, K. E. Stubkjaer, M. Gustavsson, W. van Berlo, and M. Janson, “10 Gb/s wavelength converter realized by monolithic integration of semiconductor optical amplifiers and Michelson interferometer,” in *Proc. ECOC*, 4, Florence, Italy, 67–70. (1994).
- [23] M. Gustavsson, B. Lagerstrom, L. Thylen, M. Janson, L. Lundgren, A.-C. Morner, M. Rask, and B. Stoltz, “Monolithically integrated 4×4 InGaAsP/InP laser amplifier gate switch arrays,” *Electron. Lett.*, **24**, 2223–2225 (1992).
- [24] M. Schilling, T. Durhuus, C. Joergensen, E. Lach, D. Baums, K. Daub, W. Idler, D. Laube, K. Stubkjaer, and K. Wünnstiel, “Monolithic Mach–Zehnder interferometer based optical wavelength converter operated at 2.5 Gb/s with

- extinction ratio improvement and low penalty,” in *Proc. ECOC*, **2**, Florence, Italy, 647–650.(1994).
- [25] N. Vodjdani, F. Ratovelomanana, A. Enard, G. Glastre, D. Rondi, R. Blondeau, T. Durhuus, C. Joergensen, B. Mikkelsen, and K. E. Stubkjaer, “All optical wavelength conversion with SOAs monolithically integrated in a passive Mach–Zehnder interferometer,” in *Proc. ECOC*, vol. 4, Florence, Italy, 95–98 (1994).
- [26] M. Schilling, K. Daub, W. Idler, D. Baums, U. Koerner, E. Lach, G. Laube, and K. Wunstel, “Wavelength conversion based on integrated all-active three-port Mach–Zehnder interferometer,” *Electron. Lett.*, **30**, 2128–2130 (1994).
- [27] F. Ratovelomanana, N. Vodjdani, A. Enard, G. G. A. D. Ellis, A. E. Kelly, D. Nasset, D. Pitcher, D. G. Moodie, and R. Kashyap, “An all-optical wavelength-converter with semiconductor optical amplifiers monolithically integrated in a asymmetric passive Mach–Zehnder interferometer,” *IEEE Photon. Technol. Lett.*, **7**, 992–994 (1995).
- [28] E. Jahn, N. Agrawal, W. Pieper, H.-J. Ehrke, D. Franke, W. Fürst, and C. M. Weinert, “Monolithically integrated nonlinear Sagnac interferometer and its application as a 20 Gb/s all-optical demultiplexer,” *Electron. Lett.*, **32**, 782–783 (1996).

- [29] W. Idler, M. Schilling, K. Daub, D. Baums, U. Korner, E. Lach, G. Laube, and K. Wunstel, "Signal quality and BER performance improvement by wavelength conversion with an integrated three-port Mach-Zehnder interferometer," *Electron. Lett.*, **31**, 454-455 (1995).
- [30] D. Nasset, M. C. Tatham, L. D. Westbrook, and D. Cotter, "Degenerate wavelength operation of an ultrafast all-optical AND gate using four wave mixing in a semiconductor laser amplifier," *Electron. Lett.*, **30**, 1938-1940 (1994).
- [31] D. Nasset, M. C. Tatham, and D. Cotter, "All-optical AND gate operating on 10 Gbit/s signals at the same wavelength using four wave mixing in a semiconductor laser amplifier," *Electron. Lett.*, **31**, 896-897 (1995).
- [32] F. Martelli, "Semiconductor optical amplifiers for very efficient frequency conversion by four-wave mixing," presented at IQEC '96, ThN2, Sydney, Australia, (1996).
- [33] G. I. Stegeman and C. T. Seaton, "Nonlinear integrated optics," *J. Appl. Phys.*, **58**, R57-R78 (1985).
- [34] S. D. Smith, "Optical bistability, photonic logic, and optical computation," *Appl. Opt.*, **25**, 1550-1564 (1986).

- [35] V. Van, T.A. Ibrahim, P.P. Absil, F.G. Johnson, R. Grover, and P.T. Ho, “Optical signal processing using nonlinear semiconductor microring resonators,” *IEEE J. Sel. Top. Quantum Electron.*, **8**, 705-713 (2002).
- [36] R. Lang, “ Injection locking properties of semiconductor lasers,” *IEEE J. Quantum Electron.*, **QE-18**, 976-983 (1982).
- [37] H.K. Tsang, L.Y. Chan, S.P. Yam, and C.Shu, “ Experimental characterization of dual-wavelength injection-locking of a Fabry-Perot laser diode,” *Optics Comm.*, **156**, 321-326 (1998).
- [38] J. Hörer and E. Patzak, “Large-signal analysis of all-optical wavelength conversion using two-mode injection-locking in semiconductor lasers,” *IEEE J. QuantumElectron.*,**33**, 596-608 (1997).
- [39] Lixin Xu, W.H. Chung, L.Y. Chan, L.F.K. Lui, P.K.A. Wai and H.Y. Tam, “Simultaneous all-optical waveform reshaping of two 10-Gb/s signals using a single injection locked fabry-pérot laser diode ,” *IEEE Photon. Technol. Lett.*, **16**, 1537-1539 (2004).
- [40] L. Y. Chan, P. K. A. Wai, L. F. K. Lui, B. Moses, W. H. Chung, H. Y. Tam, and M. S. Demokan, “Demonstration of an all-optical switch by use of a

- multiwavelength mutual injection-locked laser diode,” *Opt. Lett.*, 28, 837-839 (2003).
- [41] A. Murakami, K. Kawashima, and K. Atsuki, “Cavity resonance shift and bandwidth enhancement in semiconductor lasers with strong light injection,” *IEEE J. Quantum Electron.*, **QE-39**, 1196-1204 (2003).
- [42] S. Okamoto, “Photonic transport network architecture and OA&M technologies to create large scale robust networks,” *IEEE J. Sel. Areas Commun.*, **SAC-16**, 995-1007 (1998).
- [43] S. Shin, B. Ahn, M. Chung, S. Cho, D. Kim, and Y. Park, “Optics layer protection of Gigabit-Ethernet system by monitoring optical signal quality,” *Electron. Lett.*, **38**, 1118-1119 (2002).
- [44] F. Buchali, W. Baumert, H. Bülow, J. Poirrier, S. Lanne, “A 40 Gb/s eye monitor and its application to adaptive PMD compensation,” Tech. Digest. OFC, WE6, 202-203 (2002).
- [45] K. Kwai and H. Ichino, “250 mW 2.488 Gbit/s and 622 Mbit/s SONET/SDH bit error monitoring LSI,” *Electron. Lett.*, **35**, 914-915 (1999).

- [46] Y.Matsui, H. Murai, S. Arahira, S. Kutsuzawa, and Y. Ogawa, “ 30 GHz bandwidth 1550 nm strain-compensated InGaAlAs-InGaAsP MQW laser,” *IEEE Photon. Technol. Lett.*, **9**, 25-27 (1997).

Chapter 8

Research Summary and Future Work

8.1 Research Summary

In this thesis, we have reported the results of our research study on tunable semiconductor fiber ring lasers and multiwavelength semiconductor fiber ring lasers. A tunable semiconductor fiber ring laser with a wide tuning range of over 90 nm was demonstrated. A stable multiwavelength semiconductor fiber ring laser with more than 38 lasing lines at room temperature with a channel spacing of 0.8 nm was also constructed. We also investigated all optical signal processing devices, for instance: a tunable pulsewidth generator, an all-optical on-off switch and an all-optical AND gate using a new type of Bi_2O_3 based highly nonlinear fiber. In addition all-optical logic devices were also implemented using injection locking in a Fabry P erot laser diode. Finally, a novel all-optical signal quality monitoring system was proposed and experimentally demonstrated using cascaded all optical NOT and NOR logic gates.

In the project a newly introduced optical amplifiers called linear optical amplifiers (LOAs) were investigated for construction of widely tunable semiconductor fiber ring lasers and multiwavelength semiconductor fiber ring lasers. The LOA is a metal organic vapor deposition grown InP-based semiconductor device that integrates an active waveguide and a vertical cavity surface emitting laser (VCSEL) on the same chip. The VCSEL lases orthogonally to the signal direction, acting as an optical feedback to prevent carrier depletion during the changes of input signal power level. The LOA exhibits a flat gain over a wide range. This property was utilized to construct a widely tunable semiconductor fiber ring laser with over 90 nm tuning range using a scanning Fabry Perot filter. LOA was also employed to construct a stable multiwavelength semiconductor fiber ring laser. Over 38 lasing lines were observed with a channel spacing of 0.8 nm. The stability test of a single channel revealed that the power fluctuation was within 0.15 dB over 2-hours. A gain clamped SOA was also realized using optical feedback. This gain clamped SOA was also employed to construct a multiwavelength laser source.

A new type of bismuth oxide based highly nonlinear fiber was investigated for implementation of all-optical devices. Bi-HNLF has a very high nonlinearity of $\sim 1000 \text{ W}^{-1}\text{Km}^{-1}$, which is about 100 times more than the conventional nonlinear

dispersion shifted fiber. Only 1.9 m long Bi-HNLF was used to realize all optical devices based on four wave mixing. A tunable pulsewidth generator was proposed and demonstrated. The pulsewidth was tunable from ~ 86 to ~ 19 ps for a repetition rate of 5 GHz, whereas the pulsewidth was tunable from ~ 38 to ~ 19 ps for a repetition rate of 10 GHz. An all-optical on-off switch was also proposed and experimentally demonstrated. The switch was able to switch the data packet during the ON interval of the control signal, whereas it blocked the data signal during its OFF interval. An open eye of the switched signal was observed. Using the same fiber an all-optical AND gate was also proposed and experimentally demonstrated.

Injection locking of a slave laser by a master laser is a well known technique and is used for various applications. Injection locking occurs when the master laser is within the locking range of the slave laser (in our case a Fabry Pérót laser diode) and hence controls the subsequent behavior of the slave laser. A mode shift occurs when the injection locking takes place. Using this principle an all-optical NOT gate has been demonstrated using two mode injection-locking. An all-optical NOR gate has also been demonstrated using three mode injection locking. In the absence of data signals the CW beam will injection lock the FP-LD, whereas in the presence of any one or both data signals, the CW signal will be unlocked. We have also proposed and

experimentally demonstrated an all-optical signal quality monitoring system (SQMS) working at 10 Gb/s utilizing the mutual injection locking property in two Fabry Perot laser diodes (FP-LDs). The SQMS is capable of detecting errors due to amplitude jitters.

8.2 Future Work

During the course of this research work, some promising directions have been identified but could not be followed due to time limitation. We suggest the following future works.

1. All-optical signal quality monitoring system can work at 10 Gb/s. In future all optical networks the data rate will reach 40 Gb/s and hence will require high speed all-optical logic gates.
2. Two FP-LDs could be integrated in a planar lightwave circuit which would make the proposed size of SQMS very compact.
3. All-optical on-off switch has been demonstrated at 10 Gb/s. However, in principle it would work at higher bit rate due to instantaneous response of fiber.